Nonsingular Bouncing Cosmology

BingKan Xue

A Dissertation
Presented to the Faculty
of Princeton University
in Candidacy for the Degree
of Doctor of Philosophy

Recommended for Acceptance
by the Department of
Physics
Adviser: Professor Paul J. Steinhardt

September 2013

Abstract

This thesis studies the cosmological theory in which the universe transitions from a contraction phase into an expansion phase through a big bounce. Primordial fluctuations that seed structure formation in the expansion phase arise from adiabatic perturbations in the preceding contraction phase. The purpose of this study is to understand how the properties of the adiabatic perturbations are affected by the bounce. In particular, a nonsingular type of bounce is considered in which the universe ceases contraction and reverses to expansion at a finite size, fully described by known theories of classical gravity and effective field theory. Two major aspects of such a nonsingular bounce are studied – the stability of the bounce against inhomogeneities, and the power spectrum of adiabatic perturbations after the bounce. Results show that a class of bouncing models based on ghost condensation are subject to unstable growth of curvature and anisotropy, which alters the adiabatic perturbations and disrupts the nonsingular bounce. Another class of models with a ghost field are shown to have limited instability, though the contraction phase requires fine-tuning; sufficiently small perturbations can pass through the bounce and maintain a nearly scale-invariant power spectrum, consistent with observational constraints. Incorporating features of both models and resolving their problems, an ekpyrotic nonsingular bounce is proposed to support stable contraction and bouncing phases yet produce scale-invariant perturbations. Thus the nonsingular bouncing cosmology provides a possible explanation for the early universe.

Acknowledgements

I wish to thank my advisor Paul Steinhardt for his insightful guidance and vigorous encouragement over the years. I have especially benefited from his broad views in theoretical sciences and an open mind for diverse interests. I also thank Frans Pretorius and David Garfinkle for close collaboration and kind help on numerical computations. I would like to thank the Princeton Cosmology and Gravity Group with whom I enjoyed numerous lunches and discussions.

I am grateful to William Bialek who introduced me to the interesting field of biophysics and kindly advised my erratic efforts on the subject. I am also happy to thank Joshua Shaevitz and his lab members with whom I spent a wonderful summer and had a unique experience with biophysical experiments.

I hope to thank my senior colleagues from whom I learned great ideas and received excellent suggestions, including Jean-Luc Lehners, Thorsten Battefeld, Daniel Baumann, Adam Brown, Alex Dahlen, Enrico Pajer, and Daan Meerburg, as well as Aleksandra Walczak, Thierry Mora, and Jeremy England.

My time in Princeton could not have been so precious without the company of my dear friends. In particular, I am lucky to have shared an office with Arijeet Pal, Hans Bantilan, and Miroslav Hejna, who became my closest friends and have always been there for me.

Lastly, I owe my gratitude to my parents and grandparents who constantly provide me with love and support despite the distance between us.

To my parents and grandparents.

Contents

Chapter 1

Introduction

The Universe has been expanding and cooling for the past 14 billion years. The light from the stars and galaxies that we see in the sky has traveled a long distance and time to reach us – the further away the stars, the more ancient and red-shifted their images appear. The first galaxies formed more than 13 billion years ago inside the clumps of dark matter that condensed under gravitational self-attraction. These dark matter halos formed in the dense regions of the Universe where the primordial density fluctuations reached large amplitudes. Therefore, the large scale structure (LSS) of the galaxies and their clusters observed today reflects the statistical properties of the primordial fluctuations in the very early Universe.

Further back in time, the Universe was composed of a hot dense plasma of photons, electrons, and protons that constantly scattered off one another. The primordial density fluctuations induced small differences in the temperature of the plasma at different locations and angles. The Universe was essentially opaque to electromagnetic waves until it expanded and cooled to the point when electrons and protons recombined to form neutral hydrogen atoms. Photons then decoupled from matter and traveled freely through space, with their wavelengths being stretched by the cosmic expansion. The cosmic microwave background (CMB) that we observe today are the photons from the last scattering surface. The small anisotropies in their temperature and polarization carry important information about the nature of the primordial density fluctuations.

Current observations of CMB and LSS reveal that our Universe is extremely homogeneous, flat, and isotropic at large distances ranging from galactic scales to the entire visible Universe. Moreover, the power spectrum of the primordial density fluctuations on such large scales is measured to be nearly scale-invariant [69, 1]. The puzzle is, the regions of the Universe that are separated by such large distances became visible to us only very recently after the lights traveled over billions of years. In the far past, those regions would be way beyond the horizon from one another, having had no means of interaction to balance the local amplitude of fluctuations between them. Hence it poses a crucial challenge for models of the early Universe to explain the extreme homogeneity on the large scales – this is the *horizon problem* [126, 143, 113].

The horizon problem, together with the homogeneity, flatness, and isotropy of the Universe, are first explained by the inflation model [62, 104, 3]. In this scenario, the Universe went through an exponentially fast expansion phase after the big bang and before the nucleosynthesis. The fast expansion, i.e. *inflation*, stretched tiny regions of the space to enormous sizes that were many numbers of e-folds bigger than their original sizes. As a result, the local amount of inhomogeneity, curvature, and anisotropy was effectively smoothed out and became naturally small. The horizon problem is resolved since the separate regions of the Universe that were thought to be causally disconnected used to be much closer together and in causal contact before inflation. In addition, the quantum fluctuations within tiny regions of space smaller than a horizon size were stretched and amplified during inflation to give rise to the primordial density fluctuations, which turns out to acquire a nearly scale-invariant power spectrum that matches the observations [66, 130, 64, 13].

Despite the above notions that made it an appealing model of the early Universe, inflation has been found to suffer from serious drawbacks [73]. First, for inflation to happen, there must be a small patch of the universe that is relatively smooth over the size of a Hubble radius at the time when the density of the universe is near the Planck scale [105]. This is a strong assumption, especially for models with scalar fields that need to start with a large potential energy but a small kinetic energy and spatial gradient, or otherwise the kinetic energy and spatial gradient would grow faster and dominate over the potential energy to block inflation from happening [58]. A second problem is that almost all inflation models lead to *eternal inflation* which creates a whole spectrum of bubble universes with different physical properties [134, 140]. In such a *multiverse*, "everything happens an infinite number of times" [63], rendering the theory completely unpredictive since a meaningful measure has yet to be found despite many unsuccessful attempts [49]. Moreover, each single patch of the universe must exit the inflation process after an appropriate amount of time in order for the standard expansion phase to start. The amount of inflation predicted by a generic model is biased and disfavors the amount required to fit observations [50, 57, 2, 73]. All these problems would defy the inflation model as a complete solution to the puzzles of the early Universe.

Yet another issue about the early Universe that begs the question is whether the big bang is the beginning of time. In the standard big bang cosmology, the Universe is assumed to emerge from a big bang explosion, which is considered as a singularity of the spacetime. Inflation, as a modification to the timeline of the Universe between the big bang and the nucleosynthesis, does not change the assumption about the singularity [22]. Therefore it does not address the question about the beginning of time. Besides, restricting models of the early Universe to the period after the big bang is limiting the scope of possibilities.

The logical alternative, then, is to consider a scenario in which the Universe existed even before the big bang. In particular, the big bang may represent a transition from a preceding cosmic contraction phase to the current expansion phase – a "big bounce". The idea that the expansion phase is preceded by a contraction phase opens up a new avenue for modeling the early Universe. Problems of the standard big bang cosmology may find solutions in the contraction phase before the bounce. The horizon problem,

for example, is immediately resolved if the far separated regions of the Universe today were in causal contact during the previous contraction phase. Similarly, the homogeneity, flatness, and isotropy of the Universe may also be addressed by having a smoothing mechanism in the contraction phase.

Before exploring the possibilities that a bouncing model offers, it is interesting to note that the notion of a bouncing universe has appeared and persevered in human knowledge long before the modern cosmological studies [90, 133, 76]. The big bounce has often been speculated to be part of a cyclic process in which the bounce is repeated indefinitely, extending from the infinite past to the infinite future. An important aspect has been whether any influence is passed from the previous contraction phase to the following expansion phase, i.e. from cycle to cycle. A similar question will be the main concern of this thesis. It is therefore instructive to review some relevant history and development of bouncing cosmologies.

1.1 A historical account

The idea of a cyclic universe can be traced back to early mythologies [90, 89, 76]. In ancient philosophy, a future catastrophe is imagined to end the world, and out of the ashes a new world will be born; the process of creation and annihilation repeats itself to form an endless universe. Notably, the Stoics in ancient Greece conceived the world as a gigantic sphere undergoing cycles of expansion and contraction, ending and being reborn each cycle in an *ekpyrosis* – "out of fire" [133].

This "cyclic" view is contrasted with the "created" view that the Universe came into being a finite time ago and the "static" view that the Universe remains unchanged forever [133]. Distinctions should also be drawn with the narrow view of a bouncing universe in which only one bounce occurs and never repeats [89]. In principle, the big bang picture does not exclude the possibility of having a preexisting period before the bang. After all, the different views of the early Universe are merely philosophical speculations or aesthetic preferences without scientific evidence.

Modern scientific models of the Universe came after Einstein's theory of *general relativity*, which allows the spacetime of the Universe to be dynamically described by geometrical quantities that obey the laws of gravitation. Einstein in 1917 looked for a static solution in which the universe neither expands nor contracts [42]. His "static universe" was ruled out after Hubble discovered the cosmic expansion in 1929 [71]. The other two possibilities, "created" and "cyclic", were formulated around the same time and coexisted since then.

In 1922 Friedmann analyzed solutions to Einstein's equations that describe a homogeneous expanding universe with matter and a cosmological constant [51]. Three kinds of solutions were obtained that correspond to *open*, *flat*, and *closed* universes depending on the amount of matter and the value of the cosmological constant. Besides the first two solutions that start from a big bang singularity and expand forever, the third solution, with a sufficient matter density and a small or negative cosmological constant, would eventually stop expanding and recollapse to a big crunch in finite time. He termed the last solution a "periodic world", indicating that the process

could repeat infinitely. Similar models were studied more carefully by Lemaitre in 1927 [100], and by Einstein in 1931 in which he abandoned the cosmological constant to embrace the observed expansion of the Universe [43, 41].

The cyclic model was scrutinized over the next few decades and received several major criticisms that diminished its popularity. One problem, noted by Tolman in 1931, is that the duration of the cycles would increase over time due to the increase of *entropy* [138, 137]. Extrapolating backwards, the cycle shrinks and reaches zero within a finite time – the beginning of time exists just like in the "created" universe. This realization deprived the cyclic model of its original intent to depict an eternal universe, raising a strong argument against it. Tolman also knew about the existence of the spacetime singularity at each bounce, but he considered it as a mathematical artifact that would disappear in a realistic treatment.

Another important issue was investigated by Belinskii, Khalatnikov, and Lifshitz (BKL) in 1960s concerning the stability of the universe as it contracts towards the big crunch [101, 18]. They found that during contraction tiny amounts of anisotropy would be rapidly amplified, together with spatial curvature, leading to a chaotic process in which the space contracts along two directions and expands along the third, switching directions randomly every once in a while. This behavior, known as the "mixmaster" [112], would render the universe extremely inhomogeneous before the bounce, making it impossible to emerge with highly uniform matter and energy densities.

Worse still, by 1970 Hawking and Penrose proved a theorem that, under certain *energy condition*, a spacetime singularity is unavoidable in a gravitational collapse [68]. Accordingly, a contracting universe must reach a big crunch. In light of the chaotic mixmaster behavior, the bouncing model seemed to have failed badly.

The cyclic idea came back to attention again only about a decade ago with the effort of Steinhardt and Turok [132, 135]. Several innovations were made to overcome the difficulties of the bouncing model. In particular, inspired by the *M theory* and extra dimensions, the bounce was considered as the collision of two three-dimensional branes, on one of which our world lies. The branes keep stretching out along the three dimensions, but their distance in the extra dimension varies periodically, shrinking to zero at the beginning and end of every cycle. From the perspective of the three-dimensional space on the brane, however, the universe expands and contracts in volume during each cycle, and undergoes a big crunch/bang between the cycles that produces huge amounts of matter and radiation. This "ekpyrotic model" [80], named after the ancient Greek conception, brought new solutions to the issues facing the bouncing model.

As for Tolman's entropy problem, the increasingly longer cycles he found are in fact caused by the increase of the entropy density instead of the total entropy. In the new cyclic model, more entropy is still being produced at the bounce in the form of matter and radiation, but their density is diluted after each cycle due to the stretching of the branes. This allows the entropy density to remain the same, hence the cycling process can continue endlessly.

The solution to the chaotic mixmaster problem is more surprising. It turns out that BKL's calculation only considered a universe in which the pressure is smaller than

the energy density. However, in the colliding brane picture, high pressure naturally arises in the contraction phase before the bounce to squelch the mixmaster behavior and smooth out the branes. Enlightened by this result, it was soon realized that the chaotic mixmaster can be prevented as long as the universe has an energy component with a super-stiff equation of state, i.e. with pressure higher than the energy density [47, 53]. A contraction phase with such a super-stiff equation of state has come to be called an "ekpyrotic phase".

To be a successful model of the early Universe, the new cyclic model must also generate nearly scale-invariant primordial fluctuations before the expansion phase. Originally, it was imagined that the quantum vibrations of the branes cause them to ripple, which in turn perturbs their collision time and cause density variations in the matter and radiation produced at the collision [80]. This approach relies on the specific way the perturbations in the brane are matched on to the density fluctuations after the collision [136], which was later shown to be non-generic [33]. From the three-dimensional perspective, a more effective way is to have two scalar fields producing *entropic* perturbations between them, which then convert to *adiabatic* density fluctuations before the bounce [88, 98, 26, 34].

It gradually became clear that almost all essential features of the ekpyrotic/cyclic model can be described in a purely three-dimensional perspective, without having to invoke the extra dimensional interpretation in terms of the branes. The remaining issue is the bounce itself, which had been treated as the momentary vanishing of the extra dimension – a pretty mild type of spacetime singularity. In a purely three-dimensional model, however, the bounce still corresponds to a classical singularity at which the size of the universe shrinks to zero. It may be expected that the singularity would be resolved by unknown quantum gravity effects that can create a transition from contraction to expansion. The brane picture certainly provides some insight as to how the bouncing process might look like and how the influence of the previous cycle can be passed on to the next.

Some other approaches for having a bouncing universe have also been pursued. In *loop quantum cosmology*, quantum geometry effects arise when the spacetime curvature reaches the Planck regime, resolving the big bang singularity by a quantum bounce [10, 21]. Another approach, based on the *de Broglie-Bohm quantum theory*, uses the wavefunction of the universe to determine a quantum trajectory of the universe through a bounce [118, 122]. More radically, the *conformal cyclic cosmology* depicts the universe as undergoing repeated cycles of expansion with no contraction phases in between but a conformal geometrical structure instead [117].

A more immediate and perhaps bold approach, however, is to bypass the singularity within classical gravity theory and let the universe bounce at a finite size. This will be the approach taken in the current thesis, as explained in the next section.

1.2 The present study

The new approach that has been pursued in recent years is to achieve the bounce in a *nonsingular* way without involving quantum gravity [119, 4, 29, 26, 34, 102, 124,

40, 27]. In this approach the universe stops contraction and reverses to expansion at a finite size, such that the energy density remains sub-Planckian and the physical process stays within the validity of classical gravity. To evade the singularity theorem, there has to be a sustained period of "bouncing phase" that violates the *null energy condition* (NEC). This can be achieved by having particular types of matter or fields with large negative pressure, which would become substantial near the end of the contraction phase and induce a nonsingular bounce. In that case, the bouncing process can be completely described by general relativity and effective field theory. Unlike the singular bounce that often relies on certain matching conditions derived from the analyticity and unitarity of the quantum process [75, 72, 37, 48, 39, 14], the cosmological evolution through a nonsingular bounce can be followed directly by solving classical equations of motion.

It is tempting to consider the nonsingular bounce as an effective description of the singular bounce, for the convenience of studying the impact of the bounce on the cosmological perturbations. The intuition is that the physics at high energy density that is responsible for the bounce may decouple from the low energy physics that governs the cosmological perturbations on large length scales. If the properties of the primordial fluctuations on large scales do not depend sensitively on the details of the bouncing process, then the outcome of the bounce can be effectively studied by using a nonsingular bouncing model. Therefore, a rigorous analysis of a nonsingular bounce would help display properties and build intuition about the bouncing scenario in general.

The goal of the bouncing model is to account for the observed properties of the Universe, including the homogeneous, flat, and isotropic background, and the nearly scale-invariant primordial fluctuations. As mentioned above, the homogeneity, flatness, and isotropy can be achieved by an ekpyrotic mechanism during the contraction, whereas scale-invariant perturbations can be generated by an entropic mechanism with two scalar fields [88, 98, 26, 34]. Another variation, the *adiabatic ekpyrotic model* [82, 83], can generate scale-invariant adiabatic perturbations with just one scalar field. Other mechanisms to produce scale invariant perturbations include having a matter-like contraction phase as in the matter bounce model [141, 48], and using a curvaton field as in the pre-big bang model [54, 55, 46, 108]. The question, however, is whether the scale-invariant perturbations can pass through the bounce as desired.

Indeed, a nonsingular bounce involves several specific problems. First, the violation of the NEC may impair the *stability* of the bounce [147, 148]. As mentioned before, a contracting universe is subject to the growth of spatial curvature and anisotropy unless the contraction is ekpyrotic. But such ekpyrotic contraction would stop when the nonsingular bouncing phase begins. Thus, a sustained period of bouncing phase may become unstable against the growth of curvature and anisotropy. Their growth could potentially drag the universe into chaotic mixmaster behavior that disrupts the bounce altogether. It is therefore important to determine if the instability can be kept at a finite level during the bounce.

Moreover, the evolution of the adiabatic perturbations during the bouncing phase may alter the *power spectrum* of the primordial fluctuations [147, 148]. Since the Hubble scale becomes infinite at the nonsingular bounce, it appears that even the

adiabatic perturbations with long wavelengths would reenter the horizon near the bounce. If the amplitude of these adiabatic perturbations grows during the bounce and the growth varies with wavelength, then the power spectrum would be distorted away from scale invariance. Meanwhile, the divergence of the Hubble scale also signifies the *strong coupling* of the adiabatic perturbations [16]. At the classical level, it implies that their evolution would become nonlinear, causing a mixing of modes and a large non-Gaussianity. This problem must be avoided in order for the bouncing model to be compatible with observations.

In this thesis, we study the above two aspects of the nonsingular bounce by calculating the evolution of adiabatic perturbations through the bounce. Both perturbative analytic calculations and nonperturbative numerical computations are used to address these issues. We show that the adiabatic perturbations would become nonlinear if there is unstable growth of inhomogeneity and anisotropy during the bounce. On the other hand, if nonlinearity is suppressed during the bounce, then the adiabatic perturbations would pass through the bounce while maintaining a nearly scale-invariant power spectrum.

The thesis is organized as follows. Chapter 2 describes the background evolution of a homogeneous universe during contraction, bounce, and expansion. The Friedmann equations are used to show that an ekpyrotic contraction phase is stable against curvature and anisotropy, but a nonsingular bouncing phase is not. Several bouncing models are presented, including the ghost condensation model and the ghost field model. Chapter 3 introduces the theory of cosmological perturbations. Linear perturbation theory is used to calculate small perturbations, whereas the covariant formalism is used to compute nonlinear perturbations. The initial conditions for adiabatic perturbations are derived from quantum perturbations. Chapter 4 analyzes a bouncing model that connects an ekpyrotic contraction with a nonsingular bounce by means of a ghost condensation model. Through perturbative calculations, unstable growth of curvature and anisotropy is found to spoil the power spectrum and disrupt the nonsingular bounce. Chapter 5 uses numerical methods to study a nonsingular bounce based on a ghost field model. Nonlinear perturbations and the consequent disruption of the bounce are captured in regions with large inhomogeneity and anisotropy; on the other hand, sufficiently small perturbations are shown to pass through the bounce without altering the power spectrum. Chapter 6 presents an ekpyrotic nonsingular bouncing model that creates a stable nonsingular bounce and produces scale-invariant perturbations without fine-tuning. Chapter 7 concludes with a summary of the current study and an outlook on future works. In addition, Appendix A presents a classification of all single field cosmological models that can produce a scale-invariant power spectrum.

Chapter 2

Homogeneous Universe

According to the *cosmological principle*, the Universe is roughly homogeneous on large scales, so that it looks the same to observers everywhere – our position in the Universe is nowhere special. This assumption has been verified by astronomical observations, and will serve as the starting point of our study. Under this approximation, the background evolution of the Universe can be described by the time variation of a homogeneous space.

We will first derive the Friedmann equations that determine the dynamics of a homogeneous universe. We use these equations to show that a contraction phase is stable only if it is ekpyrotic. We then discuss the possibility of connecting the contraction phase to a nonsingular bounce. The nonsingular bouncing phase must violate the NEC, which brings about potential issues with stability against curvature and anisotropy.

2.1 Friedmann equations

According to the theory of general relativity, spacetime is described by a metric that interacts gravitationally with matter. A homogeneous, flat, and isotropic universe can be described by the simple metric

$$ds^2 = -dt^2 + a(t)^2 d\mathbf{x}^2, \tag{2.1}$$

where t and $\mathbf{x} = (x^1, x^2, x^3)$ are the time and spatial coordinates, and $a(t)$ is the *scale factor* of the universe. The expansion (contraction) rate of the universe is given by the *Hubble parameter*,

$$H \equiv \frac{\dot{a}}{a}, \tag{2.2}$$

where $\dot{}$ denotes the time derivative with respect to t. We use reduced Planck units with $c = \hbar = 8\pi G = 1$.

Assume that the universe is filled with one or more perfect fluids that have total energy density ρ and pressure p. The Einstein equations for the metric (2.1) reduce

to two *Friedmann equations*,

$$H^2 = \frac{\dot{a}^2}{a^2} = \frac{1}{3}\rho\,, \tag{2.3}$$

$$\dot{H} = \frac{\ddot{a}}{a} - \frac{\dot{a}^2}{a^2} = -\frac{1}{2}(\rho + p)\,. \tag{2.4}$$

The stress-energy conservation for each energy component is given by the equation

$$\dot{\rho} + 3\frac{\dot{a}}{a}(\rho + p) = 0, \tag{2.5}$$

which is consistent with the Friedmann equations. These equations need to be supplemented by the relation between ρ and p, which for a single fluid is characterized by the *equation of state*,

$$w \equiv \frac{p}{\rho}\,. \tag{2.6}$$

Pressureless matter has $w = 0$, radiation $w = \frac{1}{3}$, and a cosmological constant $w = -1$. For a constant equation of state, Eq. (2.5) implies

$$\rho \propto \frac{1}{a^{3(1+w)}}\,. \tag{2.7}$$

The NEC requires $\rho + p \geq 0$ for a perfect fluid, or equivalently $w > -1$ for a positive ρ. Define the parameter

$$\epsilon \equiv \frac{-\dot{H}}{H^2}, \tag{2.8}$$

which would be equal to $\frac{3}{2}(1 + w)$ if the universe is dominated by one fluid with an equation of state w. Alternative, we may consider $\frac{2\epsilon}{3} - 1$ as the overall equation of state of the universe.

In a more general case, the homogeneous space can have a uniform curvature. This case is described by the Friedmann-Lemaître-Robertson-Walker (FLRW) metric in reduced-circumference polar coordinates,

$$ds^2 = -dt^2 + a(t)^2\left(\frac{dr^2}{1 - Kr^2} + r^2 d\Omega^2\right), \tag{2.9}$$

where $K < 0$, $K = 0$, $K > 0$ represent negative, zero, and positive curvature respectively. For this metric the scale factor a satisfies the equations

$$H^2 = \frac{1}{3}\rho - \frac{K}{a^2}\,, \tag{2.10}$$

$$\dot{H} = -\frac{1}{2}(\rho + p) + \frac{K}{a^2}\,. \tag{2.11}$$

From the right hand side it can be seen that the curvature term K/a^2 acts like an energy component with an equation of state $w = -\frac{1}{3}$.

Friedmann originally studied the above equation with matter and a cosmological constant, for which $\rho = \rho_{\mathrm{m}0}/a^3 + \Lambda$ [51]. There are three types of solutions corresponding to *open*, *flat*, and *closed* universes respectively. The *closed* solution, with $K > 0$ and $\Lambda < 4K^3/\rho_{\mathrm{m}0}^2$, describes a universe that expands from a big bang and later contracts to a big crunch, which was considered as a candidate for constructing a cyclic universe.

In the absence of spatial curvature, anisotropy can be introduced into the homogeneous universe by generalizing Eq. (2.1) to a Kasner-like metric,

$$ds^2 = -dt^2 + a(t)^2\Big(e^{2\beta_1(t)}(dx^1)^2 + e^{2\beta_2(t)}(dx^2)^2 + e^{2\beta_3(t)}(dx^3)^2\Big), \tag{2.12}$$

where the exponents are chosen to satisfy $\beta_1+\beta_2+\beta_3 = 0$ so that a is the average scale factor. When these exponents are not equal, the space is expanding or contracting at different rates in different directions. In this case one finds, similar to Eqs. (2.3, 2.4),

$$\frac{\dot{a}^2}{a^2} - \frac{1}{6}\big(\dot{\beta}_1^2 + \dot{\beta}_2^2 + \dot{\beta}_3^2\big) = \frac{1}{3}\rho\,, \tag{2.13}$$

$$\frac{\ddot{a}}{a} - \frac{\dot{a}^2}{a^2} + \frac{1}{2}\big(\dot{\beta}_1^2 + \dot{\beta}_2^2 + \dot{\beta}_3^2\big) = -\frac{1}{2}(\rho + p)\,, \tag{2.14}$$

plus another equation for β_i,

$$\ddot{\beta}_i + 3\,\frac{\dot{a}}{a}\,\dot{\beta}_i = 0\,. \tag{2.15}$$

The last equation implies $\dot{\beta}_i = b_i/a^3$, where b_i are constants; let $\sigma_0^2 = \frac{1}{2}(b_1^2 + b_2^2 + b_3^2)$, then the first two equations become

$$H^2 = \frac{1}{3}\left(\rho + \frac{\sigma_0^2}{a^6}\right), \tag{2.16}$$

$$\dot{H} = -\frac{1}{2}(\rho + p) - \frac{\sigma_0^2}{a^6}\,. \tag{2.17}$$

The term σ_0^2/a^6, compared to Eq. (2.7), shows that the anisotropy contribution has an effective equation of state $w = 1$.

In a contracting universe, if the energy density ρ follows Eq. (2.7) with $w < 1$, then anisotropy would eventually come to dominate. Neglecting ρ in the above equations, the scale factor is solved to be $a \sim (-t)^{1/3}$, where t is negative and increasing. Using that in Eq. (2.15) gives $a^2 e^{2\beta_i} = (-t)^{2p_i}$, which recovers the Kasner metric with constant exponents $p_i = \frac{1}{3} + \frac{b_i}{\sqrt{3}\sigma_0}$. Since these exponents satisfy $p_1 + p_2 + p_3 = p_1^2+p_2^2+p_3^2 = 1$, it must be that two of them are positive and the third is negative. This solution describes exactly the BKL result in which two spatial dimensions contract while the third expands as $t \to 0^-$ [101, 18]. The chaotic switching of directions occurs if there is spatial curvature, in which case a Kasner solution works as an approximation during each epoch between consecutive switches.

All together, the most general Friedmann equations, including contributions from matter, radiation, cosmological constant, spatial curvature, anisotropy, and an additional component with equation of state w, can be written as

$$H^2 = \frac{1}{3}\left(\frac{\rho_{\rm m0}}{a^3} + \frac{\rho_{\rm r0}}{a^4} + \Lambda - \frac{3K}{a^2} + \frac{\sigma_0^2}{a^6} + \frac{\rho_0}{a^{3(1+w)}}\right), \tag{2.18}$$

$$\dot{H} = -\frac{1}{2}\frac{\rho_{\rm m0}}{a^3} - \frac{2}{3}\frac{\rho_{\rm r0}}{a^4} + \frac{K}{a^2} - \frac{\sigma_0^2}{a^6} - \frac{(1+w)}{2}\frac{\rho_0}{a^{3(1+w)}}\,. \tag{2.19}$$

In an expanding universe where a increases with time, the component with the smallest equation of state grows fastest. Conversely, in a contracting universe where a decreases, the component with the largest equation of state comes to dominate.

Therefore, in order that a contracting universe does not become dominated by anisotropy that leads to a chaotic mixmaster, there has to be an energy component with an equation of state $w > 1$. When this component grows to dominate the total energy density, the curvature and anisotropy are relatively diluted away. This is precisely the idea behind the ekpyrotic mechanism, as described below.

2.2 Ekpyrotic contraction

For the ekpyrotic mechanism to efficiently smooth out spatial curvature and anisotropy during a contraction phase, the dominant energy component needs to have a super stiff equation of state, $w \gg 1$. This can be implemented by having a scalar field ϕ rolling down a steep negative potential. Specifically, consider the Lagrangian

$$\mathcal{L}[\phi] = -\tfrac{1}{2}(\partial\phi)^2 - V(\phi), \tag{2.20}$$

where the potential can be partly approximated by $V(\phi) = V_0\, e^{-c\,\phi}$ with $V_0 < 0$ and $c \gg 1$, as shown in Fig. 2.1. In the homogeneous case, the energy density and pressure of the scalar field are given by

$$\rho = \tfrac{1}{2}\dot{\phi}^2 + V, \quad p = \tfrac{1}{2}\dot{\phi}^2 - V. \tag{2.21}$$

Therefore, since $\rho > 0$ and $V < 0$, the equation of state satisfies $w = p/\rho > 1$. The equation of motion,

$$\ddot{\phi} + 3H\dot{\phi} + V_{,\phi} = 0\,, \tag{2.22}$$

and the Friedmann equations (2.3, 2.4) have an *attractor* solution,

$$a \sim (-t)^{1/\epsilon}, \quad H = \frac{1}{\epsilon\, t}, \quad \phi = \sqrt{\tfrac{2}{\epsilon}}\,\log\left(\sqrt{\tfrac{-\epsilon^2 V_0}{\epsilon-3}}\,(-t)\right), \tag{2.23}$$

where $\epsilon = c^2/2 \gg 1$. This solution satisfies the scaling relation

$$H^2 = \frac{-1}{\epsilon - 3}V = \frac{1}{2\epsilon}\dot{\phi}^2 \propto \frac{1}{a^{3(1+w)}}, \tag{2.24}$$

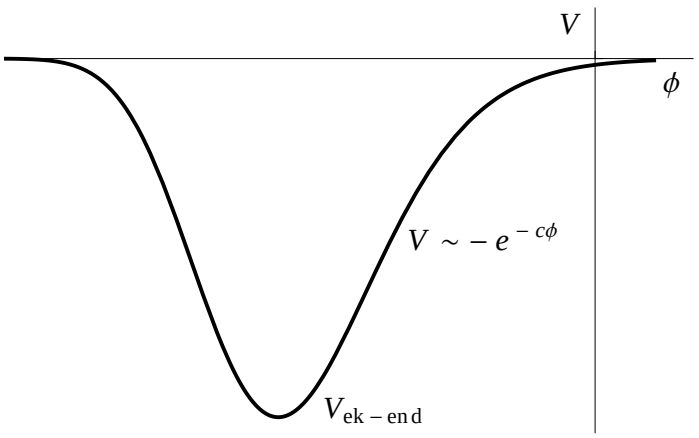

Figure 2.1: The potential $V(\phi)$ in the cyclic model.

where the equation of state w is constant,

$$w = \frac{2\epsilon}{3} - 1 = \frac{c^2}{3} - 1 \ , \tag{2.25}$$

which ensures $w \gg 1$ as desired.

During such ekpyrotic contraction, as t increases towards 0^-, the scale factor a decreases slowly while the Hubble parameter H grows rapidly in magnitude. This picture is dramatically different from the inflation process in which H remains nearly constant but a grows exponentially. However, in both cases the comoving horizon size, given by $1/|aH|$, shrinks rapidly so that Fourier modes with long wavelengths would exit the horizon (see Chapter 3). The total number of e-folds of modes that cross the horizon during the ekpyrotic phase is given by [84]

$$e^N \equiv \frac{(aH)_{\text{ek-end}}}{(aH)_{\text{ek-beg}}}, \tag{2.26}$$

where the subscripts denote the beginning and end of the ekpyrotic phase.

Assume that there exist small amounts of spatial curvature and anisotropy, which scale as $\sim 1/a^2$ and $1/a^6$ respectively. Then the ratio between these contributions and the scalar field energy density scales as

$$\frac{\rho_{K,\sigma^2}}{\rho_\phi} = \frac{a^{-2,-6}}{a^{-3(1+w)}} \approx a^{2\epsilon} \propto \frac{1}{H^2}. \tag{2.27}$$

Since $2\epsilon \gg 1$, this ratio decreases rapidly as the scale factor a contracts, hence any remaining curvature and anisotropy would soon become negligible. If the ekpyrotic phase lasts for N e-folds, then the initial amount of curvature and anisotropy would be suppressed by a factor $\approx e^{-2N}$, making the universe extremely flat and isotropic before the bounce.

In the new cyclic model, the ekpyrotic phase ends when the scalar field potential bottoms out at a depth $V_{\text{ek-end}}$, as shown in Fig. 2.1. The full potential can be writ-

ten as $V(\phi) = V_0 e^{-c\phi} F(\phi)$, where the factor $F(\phi) \sim e^{-1/g_s(\phi)}$ vanishes as $\phi \to -\infty$ because the string coupling $g_s \sim e^{\gamma\phi}$ diminishes [132]. The energy scale $V_{\text{ek-end}}$ determines the amplitude of primordial density fluctuations (see Chapter 4). After the field passes through the minimum, the potential energy quickly diminishes and converts into kinetic energy. From the three-dimensional perspective, the universe contracts towards a big crunch – a singular bounce. The bouncing process cannot be resolved in the three-dimensional description without resorting to the extra dimensional picture. For our study, however, we wish to replace the singular bounce by a nonsingular one that can be completely described within the framework of three spatial dimensions.

2.3 Nonsingular bounce

In a nonsingular bounce the contraction of the universe must come to a halt at a point when the scale factor a is still finite but the Hubble parameter H vanishes. Since H is negative during the contraction and positive after the bounce, $\dot{H}$ must be positive for a sustained period near the bounce. This is no trivial task because, according to Eq. (2.4), the energy density and pressure have to satisfy $\rho + p < 0$, which violates the NEC. In the following we present several approaches for accomplishing a nonsingular bounce.

2.3.1 Ghost condensation

Typically the violation of NEC would result in a gradient or ghost instability [70, 38]. There are however certain effective field theories with a stable violation of the NEC. One widely used approach is the "ghost condensation" [6]. In this approach, a scalar field is assumed to have a noncanonical Lagrangian that allows it to have $w < -1$.

Consider a scalar field ϕ with the Lagrangian

$$\mathcal{L}[\phi] = P(X, \phi), \quad X \equiv -\tfrac{1}{2}(\partial\phi)^2. \tag{2.28}$$

The energy density and pressure of this scalar field is given by (see Section 3.2)

$$\rho = 2XP_{,X} - P\,, \quad p = P\,, \tag{2.29}$$

where in the homogeneous case $X = \frac{1}{2}\dot{\phi}^2$. Therefore the Friedmann equations become

$$H^2 = \tfrac{1}{3}\big(2XP_{,X} - P\big)\,, \tag{2.30}$$

$$\dot{H} = -XP_{,X}\,. \tag{2.31}$$

The NEC is violated if $\rho + p = 2XP_{,X} < 0$, i.e. if the function $P(X, \phi)$ satisfies $P_{,X} < 0$, in certain regions of X, ϕ. Assuming that the energy density is positive, $\rho > 0$, then the scalar field would have an equation of state $w < -1$. Note that a canonical Lagrangian, $P(X, \phi) = X - V(\phi)$, would not satisfy such conditions.

The noncanonical Lagrangian also allows the energy density of the scalar field to become negative. The negative energy density does not cause a *ghost instability* as

long as $\rho_{,X} = 2XP_{,XX} + P_{,X}$ is positive [6]. On the other hand, the squared speed of sound,

$$c_s^2 = \frac{P_{,X}}{\rho_{,X}} = \frac{P_{,X}}{2XP_{,XX} + P_{,X}} \ , \tag{2.32}$$

becomes negative when $P_{,X} < 0$, indicating a *gradient instability*. It causes the equation of motion to change from being hyperbolic to elliptical and hence unstable [5, 91]. This problem can be controlled by assuming additional higher spatial derivative terms in the Lagrangian that modify the dispersion relation at large wavenumbers [6, 32], e.g. $\omega^2 = c_s^2 k^2 + \mathcal{O}(k^4)$. But such terms are not defined covariantly [5], hence hard to implement in a relativistic computation.

2.3.2 Ghost field

Another approach is to completely remove the gradient instability at the cost of having an explicit ghost instability. Consider a scalar field χ minimally coupled to gravity through the Lagrangian

$$\mathcal{L} = \tfrac{1}{2}(\partial\chi)^2 - W(\chi) \ . \tag{2.33}$$

The χ field has a canonical kinetic term except a wrong sign, hence it is a *ghost field*. For simplicity, assume that the potential $W(\chi)$ is absent. Then in the homogeneous case, the energy density and pressure of the χ field are given by

$$\rho = -\tfrac{1}{2}\dot{\chi}^2, \quad p = -\tfrac{1}{2}\dot{\chi}^2. \tag{2.34}$$

Therefore it has negative energy density and a constant equation of state, $w = 1$. This provides a new way of violating the NEC, $\rho + p = \rho(1 + w) < 0$, since here $w > -1$ but $\rho < 0$. Because the total energy density of the universe must be non-negative, there have to be another component with positive energy density, such as a normal scalar field. Let the other energy density and pressure be $\rho_{\rm o}$ and $p_{\rm o}$, then the Friedmann equations are given by

$$H^2 = \tfrac{1}{3}\big(\rho_{\rm o} - \tfrac{1}{2}\dot{\chi}^2\big) \ , \tag{2.35}$$

$$\dot{H} = -\tfrac{1}{2}(\rho_{\rm o} + p_{\rm o}) + \tfrac{1}{2}\dot{\chi}^2 \ . \tag{2.36}$$

Note that this bouncing mechanism only works if the other energy component has $w < 1$, so that the negative energy density of the χ field grows faster during contraction and eventually matches the other energy density to create a bounce [119, 4, 28].

Since the χ field has a unit speed of sound, the gradient instability is absent and the classical equation of motion is well-behaved. However, the ghost instability would lead to unstable quantum excitations of negative energy when the ghost field is coupled to other fields and gravity. It must be stabilized by some unknown UV-completion mechanism which is not considered here. Nevertheless, this model can serve as an effective bouncing mechanism for studying adiabatic perturbations on superhorizon scales that evolve classically. For these classical perturbations, without worrying

about the quantum instability, the cosmological evolution can be followed through the bounce by solving the classical equations of motion. This setup is especially convenient for nonperturbative relativistic computations since the equations of motion can be written in a covariant form.

2.3.3 Other models

The above two bouncing models will be the main subjects of our study. Another bouncing mechanism that is worth mentioning here is the recently proposed *Galileon* model [116, 35, 36]. This model contains the most general terms in a scalar field Lagrangian that keep the equation of motion second order in derivatives. As a generalization to the ghost condensation model, the advantage of the Galileon model is that the gradient instability may be absent within certain parameter range. However, the behavior of the bouncing process is similar to the above models [124, 40, 27].

Therefore, without loss of generality, we shall consider the two bouncing models presented above. To analyze the stability of the bounce and the properties of the primordial fluctuations, let us first develop the formalism for calculating the cosmological perturbations that represent the inhomogeneities in the universe.

Chapter 3

Cosmological Perturbations

In the real universe, there exist deviations from the homogeneous background. On large scales, the deviations can be studied by applying the theory of general relativity to an inhomogeneous spacetime. This is more complicated since the time and spatial coordinates are no longer separately and uniquely chosen. However, with a well-defined gauge choice, it is possible to perform a 3+1 decomposition, which gives a set of generalized Friedmann equations that characterize the evolution of an inhomogeneous universe with curvature and anisotropy [148].

For small perturbations, we will derive the linear perturbation theory in some commonly used gauges, and define some gauge-invariant quantities that are convenient for calculations. More generally, we will introduce the covariant formalism for calculating large perturbations beyond the linear approximation. These methods will be used in later chapters for analyzing the stability and power spectrum of the adiabatic perturbations. The amplitude of the adiabatic perturbations are initially fixed by quantum fluctuations when the modes are deep inside the horizon.

3.1 Generalized Friedmann equations

3.1.1 3+1 decomposition

The spacetime can be sliced by spatial hypersurfaces of constant time coordinate τ; the spatial hypersurfaces are then threaded by lines of constant spatial coordinates x^i. The *lapse function* α, defined as $\alpha \equiv \big(-(\partial\tau)^2 \big)^{-1/2}$, measures the ratio between the proper time and the coordinate time along the normal vector to the spatial hypersurface. Note that the normal vector does not have to coincide with the *time vector* ∂_τ tangent to the threading lines. Their difference is given by the *shift vector* β^i. In terms of α and β^i, the metric can be written as

$$ds^2 = -\alpha^2 d\tau^2 + \gamma_{ij}(dx^i + \beta^i d\tau)(dx^j + \beta^j d\tau), \tag{3.1}$$

where γ_{ij} is the *spatial metric* of the constant time hypersurface. In matrix form, the full metric and its inverse can be written as

$$g_{\mu\nu} = \begin{pmatrix} g_{00} & g_{0j} \\ g_{i0} & g_{ij} \end{pmatrix} = \begin{pmatrix} -\alpha^2 + \beta_k\beta^k & \beta_j \\ \beta_i & \gamma_{ij} \end{pmatrix}, \tag{3.2}$$

$$g^{\mu\nu} = \begin{pmatrix} g^{00} & g^{0j} \\ g^{i0} & g^{ij} \end{pmatrix} = \begin{pmatrix} -\frac{1}{\alpha^2} & \frac{\beta^j}{\alpha^2} \\ \frac{\beta^i}{\alpha^2} & \gamma^{ij} - \frac{\beta^i\beta^j}{\alpha^2} \end{pmatrix}, \tag{3.3}$$

where $\beta_i = \gamma_{ij}\beta^j$, and γ^{ij} is the inverse of $\gamma_{k\ell}$.

In a 3+1 decomposition [61], physical quantities are projected onto and perpendicular to the spatial hypersurface by using the unit normal vector

$$n_\mu = (-\alpha, \vec{0}), \quad n^\mu = \Big(\frac{1}{\alpha}, -\frac{\beta^i}{\alpha}\Big), \tag{3.4}$$

and the projection tensor

$$\gamma_{\mu\nu} \equiv g_{\mu\nu} + n_\mu n_\nu \ . \tag{3.5}$$

The geometry of the spacetime can be described by the intrinsic and extrinsic curvature of the spatial hypersurface. The intrinsic curvature of the hypersurface is given by the Ricci tensor ${}^{(3)}R_{ij}$ associated with the spatial metric γ_{ij} on the hypersurface. The extrinsic curvature of the hypersurface is given by

$$K_{\mu\nu} \equiv -\gamma^\kappa{}_\mu \gamma^\lambda{}_\nu \nabla_\kappa n_\lambda \ , \tag{3.6}$$

where ∇_μ denotes the covariant derivative associated with the metric $g_{\mu\nu}$. It can be shown that $K_{\mu\nu}$ is symmetric, $K_{\mu\nu} = K_{\nu\mu}$, and tangent to the hypersurface, $K_{\mu\nu}n^\nu = 0$. The mean curvature of the hypersurface is one third of the trace $K \equiv K^\mu{}_\mu = K^i{}_i$.

The Einstein equations can be written in the trace reversed form as

$$R_{\mu\nu} = \overline{T}_{\mu\nu} \equiv T_{\mu\nu} - \tfrac{1}{2} g_{\mu\nu} T \ . \tag{3.7}$$

Both sides can be decomposed by various contractions with n^μ and $\gamma^\mu{}_\nu$. The contraction of the 4-dimensional Riemann tensor $R^\mu{}_{\lambda\nu\kappa}$ gives rise to a set of Gauss-Codazzi relations [61], especially,

$$\gamma^\mu{}_\alpha \gamma^\nu{}_\beta R_{\mu\lambda\nu\kappa} n^\lambda n^\kappa + \gamma^\mu{}_\alpha \gamma^\nu{}_\beta R_{\mu\nu} = {}^{(3)}R_{\alpha\beta} + K K_{\alpha\beta} - K_{\alpha\mu} K^\mu{}_\beta \ , \tag{3.8}$$

$$2R_{\mu\nu}n^\mu n^\nu + R = {}^{(3)}R + K^2 - K^{ij}K_{ij} \ , \tag{3.9}$$

$$R_{\mu\nu} n^\mu \gamma^\nu{}_\alpha = -D_\alpha K + D_\mu K^\mu{}_\alpha \ , \tag{3.10}$$

where $D_\mu \equiv \gamma_\mu{}^\nu \nabla_\nu$. It can be shown that D_i is equal to the covariant derivative associated with the spatial metric γ_{ij} [61].

For a perfect fluid the stress-energy tensor is given by

$$T_{\mu\nu} = (\rho + p) u_\mu u_\nu + p\, g_{\mu\nu} \ , \tag{3.11}$$

where ρ and p are the rest energy density and pressure, and u^μ is the 4-velocity of the fluid. Projections of $\overline{T}_{\mu\nu} = T_{\mu\nu} - \frac{1}{2} g_{\mu\nu} T$ give

$$\overline{T}_{\mu\nu} n^\mu n^\nu = E + \tfrac{1}{2}(-\rho + 3p) \ , \tag{3.12}$$

$$\overline{T}_{\mu\nu} n^\mu \gamma^\nu{}_i = -p_i = -(E+p) U_i \ , \tag{3.13}$$

$$\overline{T}_{\mu\nu} \gamma^{\mu i} \gamma^\nu{}_j = (E+p) U^i U_j + \tfrac{1}{2} \gamma^i{}_j \rho \ . \tag{3.14}$$

Here U^μ is the fluid velocity relative to the Eulerian observer (see below),

$$U^\mu \equiv \frac{u^\mu}{\Gamma} - n^\mu \ , \tag{3.15}$$

which has a Lorentz factor

$$\Gamma = -n^\mu u_\mu = (1 - U^\mu U_\mu)^{-1/2}, \tag{3.16}$$

whereas E and P_α are the energy and momentum density as measured by the Eulerian observer,

$$E \equiv T_{\mu\nu} n^\mu n^\nu = \Gamma^2 (\rho + p) - p \ , \tag{3.17}$$

$$P_\alpha \equiv -T_{\mu\nu} n^\mu \gamma^\nu{}_\alpha = (E+p) U_\alpha \ . \tag{3.18}$$

3.1.2 Eulerian observer

The timelike unit vector n^μ can be regarded as the 4-velocity of a fiducial *Eulerian observer* [61], for whom the spatial hypersurface of constant time coordinate is truly synchronous. Therefore the spacetime as decomposed in a particular 3+1 slicing describes the cosmic evolution as measured by the corresponding Eulerian observer. The worldline of the Eulerian observer is the integral curve of the normal vector n^μ. The dynamics of the spacetime can be characterized by studying the congruence of those worldlines.

Since the worldline is not necessarily a geodesic, the acceleration of the Eulerian observer is given by

$$a_\mu \equiv \dot{n}_\mu \ . \tag{3.19}$$

Here $\dot{}$ denotes $n^\mu \nabla_\mu$, the covariant derivative along the normal vector. The *expansion tensor* $\theta_{\mu\nu} \equiv n_{\mu;\nu} + a_\mu n_\nu$ can be shown to be symmetric and equal to $-K_{\mu\nu}$ [30]. Decomposing $\theta_{\mu\nu}$ further into the trace and the traceless parts, we have

$$\nabla_\nu n_\mu = \tfrac{1}{3} \theta \gamma_{\mu\nu} + \sigma_{\mu\nu} - a_\mu n_\nu \ , \tag{3.20}$$

where θ is the *volume expansion*,

$$\theta \equiv \nabla_\mu n^\mu = -K \ , \tag{3.21}$$

and $\sigma_{\mu\nu}$ is the *shear tensor*,

$$\sigma_{\mu\nu} = \tfrac{1}{3} K \gamma_{\mu\nu} - K_{\mu\nu} \ . \tag{3.22}$$

Both $\sigma_{\mu\nu}$ and a_μ are tangent to the hypersurface, $\sigma_{\mu\nu} n^\nu = a_\nu n^\nu = 0$.

The kinematics of the congruence of the worldlines can be described by using the *Fermi derivative*[1] $\frac{D_F}{ds}$ along the integral curve of n^ν [67]. The Fermi derivative of the expansion tensor $\theta_{\mu\nu}$ is given by

$$\frac{D_F}{ds}\theta_{\mu\nu} = -R_{\mu\lambda\nu\kappa} n^\lambda n^\kappa - \theta_{\mu\lambda}\theta^\lambda{}_\nu - 2 n_{(\mu}\theta_{\nu)\lambda} a^\lambda + \gamma^\lambda{}_\mu \gamma^\kappa{}_\nu \nabla_{(\lambda} a_{\kappa)} + a_\mu a_\nu \ . \tag{3.23}$$

The trace of this equation gives the Raychaudhuri equation,

$$\dot\theta = -R_{\lambda\kappa} n^\lambda n^\kappa - \tfrac{1}{3}\theta^2 - 2\sigma^2 + \nabla_\mu a^\mu, \tag{3.24}$$

and the traceless part of the equation gives, using Eqs. (3.8, 3.9),

$$\begin{aligned} \frac{D_F}{ds}\sigma^i{}_j = {} & \gamma^{\mu i}\gamma^\nu{}_j R_{\mu\nu} - {}^{(3)}R^i{}_j - \theta\sigma^i{}_j - n^i \sigma_{jk} a^k - \tfrac{1}{3}\theta n^i a_j + D_j a^i \\ & + a^i a_j + \dot a^i n_j - \tfrac{1}{3}\gamma^i{}_j (R + R_{\mu\nu} n^\mu n^\nu - {}^{(3)}R + D_i a^i). \end{aligned} \tag{3.25}$$

Finally, using the Einstein equations (3.7) and the projections (3.12, 3.13, 3.14), equations (3.9), (3.24), (3.10) and (3.25) can be written as

$$(\tfrac{1}{3}\theta)^2 = \tfrac{1}{3}\big(E - \tfrac{1}{2}{}^{(3)}R + \sigma^2\big) \ , \tag{3.26}$$

$$\tfrac{1}{3}\dot\theta = -\tfrac{1}{2}\big(\tfrac{4E-\rho}{3} + P\big) + \tfrac{1}{6}{}^{(3)}R - \sigma^2 + \tfrac{1}{3} D_i a^i \ , \tag{3.27}$$

$$\tfrac{1}{3} D_i \theta = \tfrac{1}{2}\big(E + P\big) U_i + \tfrac{1}{2} D_j \sigma^j{}_i \ , \tag{3.28}$$

$$\begin{aligned} \tfrac{D_F}{ds}\sigma^i{}_j = {} & (E+P) U^i U_j - {}^{(3)}R^i{}_j - \theta\sigma^i{}_j - n^i \sigma_{jk} a^k - \tfrac{1}{3}\theta n^i a_j \\ & + D_j a^i + a^i a_j + \dot a^i n_j - \tfrac{1}{3}\delta^i{}_j (E - \rho - {}^{(3)}R + D_i a^i). \end{aligned} \tag{3.29}$$

Eqs. (3.26) and (3.28) are equivalent to the $\binom{0}{0}$ and $\binom{0}{i}$ components of the Einstein equations; Eq. (3.27) corresponds to the trace of the $\binom{i}{j}$ components, whereas Eq. (3.29) corresponds to the traceless part.

[1] The Fermi derivative is defined with respect to a timelike vector V^ν such that it is propagated along its integral curve, $\frac{D_F}{ds} V^\nu \equiv 0$. The Fermi derivative of a vector field X^μ with respect to V^ν is defined as

$$\frac{D_F}{ds} X^\mu \equiv \dot X^\mu - V^\mu \dot V_\nu X^\nu + \dot V^\mu V_\nu X^\nu,$$

whereas for a covector ω_μ,

$$\frac{D_F}{ds} \omega_\mu \equiv \dot\omega_\mu - V_\mu \dot V^\nu \omega_\nu + \dot V_\mu V^\nu \omega_\nu,$$

and similarly for tensors. It reduces to the covariant derivative along V^ν if the integral curve of V^ν is a geodesic, i.e. $\frac{D_F}{ds} X^\mu = \dot X^\mu \equiv V^\nu \nabla_\nu X^\mu$ if $\dot V^\nu = 0$.

These equations are generalizations of the Friedmann equations for a homogeneous universe. Indeed, in the homogeneous case, Eqs. (3.26, 3.27) reduce to

$$(\tfrac{1}{3}\theta)^2 = \tfrac{1}{3}\big(\rho - \tfrac{1}{2}{}^{(3)}\!R + \sigma^2\big)\ , \tag{3.30}$$

$$\tfrac{1}{3}\dot{\theta} = -\tfrac{1}{2}\big(\rho + p\big) + \tfrac{1}{6}{}^{(3)}\!R - \sigma^2\ , \tag{3.31}$$

Eq. (3.28) vanishes identically, and Eq. (3.29) simplifies to

$$\dot{\sigma}^i{}_j = -\theta\sigma^i{}_j - {}^{(3)}\!R^i{}_j + \tfrac{1}{3}\delta^i{}_j{}^{(3)}\!R\ . \tag{3.32}$$

In comparison to Eqs. (2.18, 2.19), the expansion θ can be considered as three times the local Hubble parameter in an inhomogeneous universe [106]. In the absence of spatial curvature, Eq. (3.32) implies

$$\sigma^i{}_j \propto \frac{1}{a^3}\ , \quad \sigma^2 \propto \frac{1}{a^6}\ . \tag{3.33}$$

Thus the anisotropy term in Eqs. (2.18, 2.19) is precisely the squared shear σ^2.

3.2 Linear perturbation theory

For small perturbations, the metric (3.1) can be expanded about the background (2.1) to linear order,

$$\begin{aligned} ds^2 = a(\eta)^2\Big[&-(1+2A)d\eta^2 + 2(B_{,i} + S_i)d\eta dx^i \\ &+ \big((1-2\psi)\delta_{ij} + 2E_{,ij} + 2F_{(i,j)} + 2h_{ij}\big)dx^i dx^j\Big], \end{aligned} \tag{3.34}$$

where η is the conformal time defined by $dt = a\,d\eta$. We use $'$ to denote time derivative with respect to η, and $_{,i}$ to denote spatial derivative with respect to x^i. Here A, B, ψ and E represent the scalar perturbations; S_i and F_i, with $S^i{}_{,i} = F^i{}_{,i} = 0$, represent the vector perturbations; and h_{ij}, with $h^i{}_i = h^i{}_{j,i} = 0$, represent the tensor perturbations [114]. Comparing the metric to (3.1), the lapse, shift and spatial metric are found to be, to linear order,

$$\alpha = a\,(1+A), \tag{3.35}$$

$$\beta_i = a^2(B_{,i} + S_i), \tag{3.36}$$

$$\gamma_{ij} = a^2\big((1-2\psi)\delta_{ij} + 2E_{,ij} + 2F_{(i,j)} + 2h_{ij}\big). \tag{3.37}$$

Accordingly, the normal vector to the constant time hypersurface is

$$n_\mu = (-a(1+A), \mathbf{0}\,)\ . \tag{3.38}$$

The intrinsic curvature of the hypersurface is given by, to linear order,

$$ {}^{(3)}R = \frac{4}{a^2}\nabla^2\psi \ , \tag{3.39} $$

hence the variable ψ is referred to as the *curvature perturbation*. The expansion θ and the shear σ_{ij} are given by

$$ \theta = \frac{1}{a}\big[3\mathcal{H}(1-A) - 3\psi' + \nabla^2(E'-B)\big], \tag{3.40} $$

$$ \begin{aligned} \sigma_{ij} &= a\big((E'_{,ij} - B_{,ij}) - \tfrac{1}{3}\delta_{ij}\nabla^2(E'-B)\big) + a\big(F'_{(i,j)} - S_{(i,j)}\big) \\ &\equiv a\big(\sigma^{\rm S}_{,ij} - \tfrac{1}{3}\delta_{ij}\nabla^2\sigma^{\rm S}\big) + a\,\sigma^{\rm V}_{(i,j)} \ , \end{aligned} \tag{3.41} $$

where $\sigma^{\rm S} \equiv E' - B$ is the *scalar shear perturbation*, and $\sigma^{\rm V}_i \equiv F'_i - S_i$ is the *vector shear perturbation*. Here $\mathcal{H} \equiv a'/a = aH$ is the *conformal Hubble parameter*.

Consider a scalar field ϕ with a general Lagrangian $\mathcal{L} = P(\phi, X)$, where $X = -\frac{1}{2}(\partial\phi)^2$. The corresponding stress-energy tensor is

$$ T_{\mu\nu} = P_{,X}\,\partial_\mu\phi\,\partial_\nu\phi + P\,g_{\mu\nu} \ , \tag{3.42} $$

which takes the form of a perfect fluid (3.11) with pressure $p = P$, energy density $\rho = 2XP_{,X} - P$, and velocity $u_\mu = \partial_\mu\phi/\sqrt{2X}$ (here we assume $\phi' < 0$ as in our models). At the background level, $\phi = \phi(\eta)$, $X = \frac{1}{2a^2}\phi'^2$, and $u_\mu = (-a, \mathbf{0})$. For a small perturbation $\delta\phi(\eta, \mathbf{x})$, and accordingly $\delta X = 2X(-A + \frac{\delta\phi'}{\phi'})$, the changes in the velocity, energy density, and pressure are given by, to linear order,

$$ \delta u_0 = -aA \ , \quad \delta u_i = a\,\delta u_{,i} \ , \quad \delta u \equiv \Big(\frac{\delta\phi}{-\phi'}\Big) \ , \tag{3.43} $$

$$ \delta\rho = \frac{2}{a^2}(\mathcal{H}'-\mathcal{H}^2)\Big[\,\frac{1}{c_s^2}\big(\delta u' + \mathcal{H}\delta u + A\big) - 3\mathcal{H}\delta u\Big], \tag{3.44} $$

$$ \delta p = \frac{2}{a^2}(\mathcal{H}'-\mathcal{H}^2)\Big[\,\delta u' + \Big(2\mathcal{H} + \frac{(\mathcal{H}'-\mathcal{H}^2)'}{(\mathcal{H}'-\mathcal{H}^2)}\Big)\delta u + A\Big], \tag{3.45} $$

where the speed of sound is $c_s^2 = \frac{P_{,X}}{\rho_{,X}}$, which only needs to be kept to zeroth order.

The equations of motion for the linear perturbations are given by the perturbed Einstein equations, $\delta G^\mu_{\ \nu} = \delta T^\mu_{\ \nu}$. At linear order, the scalar, vector, and tensor perturbations evolve independently and can be treated separately.

3.2.1 scalar perturbations

The $\binom{0}{0}$, $\binom{0}{i}$, traceless $\binom{i}{j}$, and trace $\binom{i}{i}$ components of the Einstein equations give

$$ \frac{2}{a^2}\Big[3\mathcal{H}(\psi'+\mathcal{H}A) - \nabla^2\big(\psi + \mathcal{H}(E'-B)\big)\Big] = -\delta\rho, \tag{3.46} $$

$$ \frac{2}{a^2}\Big[\,-(\psi'+\mathcal{H}A)\Big] = (\rho+P)\delta u \ , \tag{3.47} $$

$$\frac{2}{a^2}\Big[\psi - A + (E'-B)' + 2\mathcal{H}(E'-B)\Big] = 0\,, \tag{3.48}$$

$$\frac{2}{a^2}\Big[(\psi'+\mathcal{H}A)' + 2\mathcal{H}(\psi'+\mathcal{H}A) + (\mathcal{H}'-\mathcal{H}^2)A\Big] = \delta p\,, \tag{3.49}$$

where $\delta\rho$, δu, and δp are given in terms of $\delta\phi$ by Eqs. (3.43 - 3.45). For those matter perturbations, one of the equations in (3.46) $\sim$ (3.49) is redundant. Using the background equations (2.3, 2.4, 2.22) and simplifying, we obtain three equations

$$(\mathcal{H}' - \mathcal{H}^2)A - c_s^2\nabla^2\psi - \mathcal{H}c_s^2\nabla^2(E' - B) = -\tfrac{1}{2}\phi'\delta\phi' - \tfrac{3}{2}\mathcal{H}\phi'\delta\phi - \tfrac{1}{2}V_\phi\delta\phi\,, \tag{3.50}$$

$$\psi' + \mathcal{H}A = \tfrac{1}{2}\phi'\delta\phi\,, \tag{3.51}$$

$$\psi - A + (E' - B)' + 2\mathcal{H}(E' - B) = 0\,. \tag{3.52}$$

The first and second equations are the *Hamiltonian* and *momentum constraints* at linear order.

There are 5 unknown variables, namely A, B, ψ, E, and $\delta\phi$; but they are not all independent since there exists *gauge freedom*. Consider the infinitesimal coordinate transformation

$$x^\mu \to x^\mu + \xi^\mu\,, \tag{3.53}$$

given by two functions $\xi^0(x^\mu)$ and $\xi(x^\mu)$, where $\xi_i \equiv \xi_{,i}$. The scalar perturbations transform as

$$A \to A - \tfrac{1}{a}(a\,\xi^0)'\,, \tag{3.54}$$

$$B \to B + \xi^0 - \xi'\,, \tag{3.55}$$

$$\psi \to \psi + \mathcal{H}\,\xi^0\,, \tag{3.56}$$

$$E \to E - \xi\,, \tag{3.57}$$

$$\delta\phi \to \delta\phi - \phi'\,\xi^0\,. \tag{3.58}$$

To fix the gauge, one has to specify the time slicing by choosing ξ^0 and the spatial coordinates by choosing ξ. In particular, some commonly used slicing conditions are [87]: the synchronous gauge in which one sets $A = 0$; the flat gauge in which $\psi = 0$; the Newtonian gauge in which $\sigma^{\rm S} = 0$; the comoving gauge in which $\delta u = 0$, or in our case $\delta\phi = 0$; the uniform density gauge in which $\delta\rho = 0$; and the uniform Hubble gauge in which $\delta\mathcal{H} \equiv \frac{a}{3}\theta - \mathcal{H} = 0$. Below we describe these gauges (which are to be further supplemented by a choice of spatial coordinates).

Comoving gauge: $\delta u = \delta\phi = 0$**.** This gauge is defined only for $\phi' \neq 0$. The variables measured in this gauge can be given by the quantities

$$A_{\rm c} \equiv A + \frac{1}{a}(a\,\delta u)' = A + \frac{1}{a}\Big(a\,\frac{\delta\phi}{-\phi'}\Big)'\,, \tag{3.59}$$

$$\mathcal{R} \equiv \psi - \mathcal{H}\,\delta u = \psi - \mathcal{H}\Big(\frac{\delta\phi}{-\phi'}\Big)\,, \tag{3.60}$$

$$\sigma_{\rm c} \equiv \sigma^{\rm S} + \delta u = \sigma^{\rm S} + \left(\frac{\delta\phi}{-\phi'}\right) . \tag{3.61}$$

Note that each quantity is *gauge-invariant* under the coordinate transformation [12], so they can be evaluated in any other gauges as well. In particular, the *comoving curvature perturbation* $\mathcal{R}$ is a convenient quantity for our study because it is conserved on superhorizon scales during expansion, and hence determines the power spectrum of primordial fluctuations. In this gauge, Eqs. (3.50 - 3.52) simplify to

$$(\mathcal{H}'-\mathcal{H}^2)A_{\rm c} - c_s^2\nabla^2\mathcal{R} - \mathcal{H}c_s^2\nabla^2\sigma_{\rm c} = 0 , \tag{3.62}$$

$$\mathcal{R}' + \mathcal{H}A_{\rm c} = 0 , \tag{3.63}$$

$$\mathcal{R} - A_{\rm c} + \sigma_{\rm c}' + 2\mathcal{H}\sigma_{\rm c} = 0 . \tag{3.64}$$

Eliminating $A_{\rm c}$ and $\sigma_{\rm c}$, one obtains a simple equation for $\mathcal{R}$ alone,

$$\mathcal{R}'' + 2\,\frac{z'}{z}\mathcal{R}' - c_s^2\,\nabla^2\mathcal{R} = 0, \tag{3.65}$$

where $z \equiv a\sqrt{2\epsilon/c_s^2} = a\sqrt{-2(\mathcal{H}'-\mathcal{H}^2)/c_s^2\mathcal{H}^2}$.

Newtonian gauge: $\sigma^{\rm S} = E' - B = 0$. Perturbations in this gauge are represented by the gauge-invariant quantities

$$\Phi \equiv A - \tfrac{1}{a}(a\,\sigma^{\rm S})' , \tag{3.66}$$

$$\Psi \equiv \psi + \mathcal{H}\,\sigma^{\rm S} , \tag{3.67}$$

$$\overline{\delta\phi} \equiv \delta\phi - \phi'\,\sigma^{\rm S} . \tag{3.68}$$

Φ is referred to as the *Newtonian potential* [12]. Equations (3.50 - 3.52) become

$$(\mathcal{H}' - \mathcal{H}^2)\Phi - c_s^2\nabla^2\Psi = -\tfrac{1}{2}\phi'\overline{\delta\phi}' - \tfrac{3}{2}\mathcal{H}\phi'\overline{\delta\phi} - \tfrac{1}{2}V_\phi\overline{\delta\phi} , \tag{3.69}$$

$$\Psi' + \mathcal{H}\Phi = \tfrac{1}{2}\phi'\overline{\delta\phi} , \tag{3.70}$$

$$\Psi - \Phi = 0 . \tag{3.71}$$

A single equation can be obtained for Φ after replacing Ψ by Φ and eliminating $\delta\phi$, similar to (3.65),

$$\left(\frac{a^2}{\mathcal{H}}\Phi\right)'' + 2\,\frac{\theta'}{\theta}\left(\frac{a^2}{\mathcal{H}}\Phi\right)' - c_s^2\,\nabla^2\left(\frac{a^2}{\mathcal{H}}\Phi\right) = 0, \tag{3.72}$$

where $\theta \equiv 1/a\sqrt{2\epsilon} = \sqrt{\mathcal{H}^2/2a^2(-\mathcal{H}' + \mathcal{H}^2)}$. The perturbations in the Newtonian gauge can be related to that in the comoving gauge. In particular, by Eq. (3.68), the

velocity perturbation is

$$\overline{\delta u} \equiv \frac{\overline{\delta\phi}}{-\phi'} = \Big(\frac{\delta\phi}{-\phi'}\Big) + \sigma^{\rm S} = \sigma_{\rm c} \,, \tag{3.73}$$

and similarly, by Eqs. (3.67), (3.62) and (3.63),

$$\Psi = \mathcal{R} + \mathcal{H}\,\sigma_{\rm c} = -\frac{\mathcal{H}'-\mathcal{H}^2}{\mathcal{H}\,c_s^2}\,\nabla^{-2}\,\mathcal{R}' \,. \tag{3.74}$$

Flat gauge: $\psi = 0$**.** This gauge is defined for $\mathcal{H} \neq 0$. Perturbations in this gauge are given by the following gauge-invariant quantities,

$$A_\psi \equiv A + \frac{1}{a}\Big(\frac{a}{\mathcal{H}}\psi\Big)' \,, \tag{3.75}$$

$$\sigma_\psi \equiv \sigma^{\rm S} + \frac{1}{\mathcal{H}}\psi \,, \tag{3.76}$$

$$\delta\phi_\psi \equiv \delta\phi + \frac{\phi'}{\mathcal{H}}\psi \,. \tag{3.77}$$

By Eq. (3.60), the scalar field perturbation $\delta\phi_\psi$ is related to the comoving curvature perturbation $\mathcal{R}$ by

$$\delta\phi_\psi = \frac{\phi'}{\mathcal{H}}\mathcal{R} \,. \tag{3.78}$$

Synchronous gauge: $A = 0$**.** This gauge has a residual gauge freedom, $\xi^0 = C(\mathbf{x})/a$, where $C(\mathbf{x})$ is an arbitrary function of spatial coordinates. The perturbations in this gauge can be represented by the following quantities,

$$\psi_{\rm s} \equiv \psi + \frac{\mathcal{H}}{a}\int^\eta a A d\eta' \,, \tag{3.79}$$

$$\sigma_{\rm s} \equiv \sigma^{\rm S} - \frac{1}{a}\int^\eta a A d\eta' \,, \tag{3.80}$$

$$\delta\phi_{\rm s} \equiv \delta\phi - \frac{\phi'}{a}\int^\eta a A d\eta' \,, \tag{3.81}$$

which are invariant up to the residual gauge freedom, absorbed into the constant of integration. By Eqs. (3.79) and (3.63), $\psi_{\rm s}$ can be related to the comoving curvature perturbation $\mathcal{R}$ through

$$\psi_{\rm s} = \mathcal{R} + \frac{\mathcal{H}}{a}\int^\eta a A_{\rm c} d\eta' = \mathcal{R} - \frac{\mathcal{H}}{a}\int^\eta \frac{a}{\mathcal{H}}\,\mathcal{R}' d\eta' \,. \tag{3.82}$$

Similarly, by Eqs. (3.80) and (3.63), $\sigma_{\rm s}$ can be expressed in the comoving gauge as

$$\sigma_{\rm s} = \sigma_{\rm c} - \frac{1}{a}\int^\eta a A_{\rm c} d\eta' = \sigma_{\rm c} + \frac{1}{a}\int^\eta \frac{a}{\mathcal{H}}\,\mathcal{R}' d\eta' \,. \tag{3.83}$$

Uniform density gauge: $\delta\rho = 0$**.** This gauge is only defined for $\rho' \neq 0$, since under the coordinate transformation (3.53), the density perturbation $\delta\rho$ transforms as

$$\delta\rho \to \delta\rho - \rho'\xi^0 \ . \tag{3.84}$$

Some gauge-invariant quantities for this gauge are

$$A_\rho \equiv A - \frac{1}{a}\Big(\frac{a}{\rho'}\delta\rho\Big)' \ , \tag{3.85}$$

$$\zeta \equiv -\psi - \frac{\mathcal{H}}{\rho'}\delta\rho \ , \tag{3.86}$$

$$\sigma_\rho \equiv \sigma^{\rm S} - \frac{\delta\rho}{\rho'} \ , \tag{3.87}$$

$$\delta p_\rho \equiv \delta p - \frac{p'}{\rho'}\,\delta\rho \ . \tag{3.88}$$

Note that even for a single scalar field, this gauge is not equal to the comoving gauge where $\delta\phi = 0$. But the curvature perturbation on uniform density slices is very close to the comoving curvature perturbation; their difference,

$$\zeta + \mathcal{R} = -\frac{1}{3(\mathcal{H}' - \mathcal{H}^2)}\,\nabla^2\Phi \ , \tag{3.89}$$

vanishes on superhorizon scales. ζ satisfies the equation

$$\zeta' = \frac{a^2\mathcal{H}}{2(\mathcal{H}' - \mathcal{H}^2)}\,\delta p_\rho - \frac{1}{3}\nabla^2(\sigma_\rho + \delta u_\rho) \ , \tag{3.90}$$

which implies that ζ is conserved on superhorizon scales provided that *non-adiabatic perturbation* δp_ρ is absent; and so is $\mathcal{R}$.

Uniform Hubble gauge: $\delta\mathcal{H} \equiv \frac{a}{3}\theta - \mathcal{H} = 0$**.** By Eq. (3.40), the perturbation in the local conformal Hubble parameter at linear order is

$$\delta\mathcal{H} \equiv \frac{a}{3}\theta - \mathcal{H} = -\mathcal{H}A - \psi' + \frac{1}{3}\nabla^2\sigma^{\rm S} \ , \tag{3.91}$$

which transforms as

$$\delta\mathcal{H} \to \delta\mathcal{H} - (\mathcal{H}' - \mathcal{H}^2)\xi^0 - \frac{1}{3}\nabla^2\xi^0 \tag{3.92}$$

under the coordinate transformation (3.53). Therefore, we can define the following gauge-invariant quantities to represent the perturbations in this gauge,

$$A_{\rm H} \equiv A - \frac{1}{a}\bigg(\frac{a}{(\mathcal{H}' - \mathcal{H}^2) + \frac{1}{3}\nabla^2}\,\delta\mathcal{H}\bigg)' \ , \tag{3.93}$$

$$\psi_{\rm H} \equiv \psi + \frac{\mathcal{H}}{(\mathcal{H}'-\mathcal{H}^2)+\frac{1}{3}\nabla^2}\,\delta\mathcal{H}\ , \tag{3.94}$$

$$\sigma_{\rm H} \equiv \sigma^{\rm S} - \frac{1}{(\mathcal{H}'-\mathcal{H}^2)+\frac{1}{3}\nabla^2}\,\delta\mathcal{H}\ , \tag{3.95}$$

$$\delta\phi_{\rm H} \equiv \delta\phi - \frac{\phi'}{(\mathcal{H}'-\mathcal{H}^2)+\frac{1}{3}\nabla^2}\,\delta\mathcal{H}\ . \tag{3.96}$$

The quantities $\psi_{\rm H}$ and $\sigma_{\rm H}$ can be expressed in the comoving gauge as

$$\psi_{\rm H} = \frac{(\mathcal{H}'-\mathcal{H}^2)}{(\mathcal{H}'-\mathcal{H}^2)+\frac{1}{3}\nabla^2}\Big(-\frac{\mathcal{R}'}{3c_s^2\mathcal{H}}+\mathcal{R}\Big)\ , \tag{3.97}$$

$$\sigma_{\rm H} = \frac{(\mathcal{H}'-\mathcal{H}^2)}{(\mathcal{H}'-\mathcal{H}^2)+\frac{1}{3}\nabla^2}\,\sigma_{\rm c}\ . \tag{3.98}$$

3.2.2 vector perturbations

The scalar field has no vector contribution to the stress-energy tensor. Hence the $\binom{0}{i}$ and $\binom{i}{j}$ components of the Einstein equations lead to

$$\frac{1}{2a^2}\,\nabla^2(F_i'-S_i)=0\ , \tag{3.99}$$

$$\frac{1}{a^2}\Big[(F'_{(i,j)}-S_{(i,j)})'+2\mathcal{H}(F'_{(i,j)}-S_{(i,j)})\Big]=0\ . \tag{3.100}$$

Under the coordinate transformation

$$x^i \to x^i+\hat{\xi}^i\ , \tag{3.101}$$

where $\hat{\xi}^i{}_{,i}=0$, the combination $\sigma_i^{\rm V}\equiv F_i'-S_i$ is invariant by itself. Therefore the vector shear perturbation $\sigma_i^{\rm V}$ is the one and only gauge-invariant quantity, which obeys the equations

$$\nabla^2\sigma_i^{\rm V}=0\ , \tag{3.102}$$

$$\sigma_i^{\rm V\prime}+2\mathcal{H}\,\sigma_i^{\rm V}=0\ . \tag{3.103}$$

3.2.3 tensor perturbations

The tensor perturbation h_{ij} is invariant under coordinate transformations. Since the scalar field has no tensor contribution to the stress-energy tensor either, the $\binom{i}{j}$ component of the Einstein equations gives

$$h^i{}_j{}'' + 2\mathcal{H}h^i{}_j{}' - \nabla^2 h^i{}_j = 0\ . \tag{3.104}$$

3.3 Nonlinear perturbations

The amplitude of curvature and shear perturbations grow during the contraction and bouncing phases, and may become nonlinear. To calculate nonlinear perturbations, we follow the *covariant formalism* [65, 45, 25, 94, 95]. In this approach, the cosmological perturbations are defined in a geometrical way without referring to specific coordinates. Such covariant variables are interpreted as perturbations because they vanish identically in a homogeneous, flat, and isotropic background; but they are fully nonperturbative quantities not restricted to linear order in a perturbative expansion. This approach is closely related to the δN *formalism* for calculating the curvature perturbation on superhorizon scales [131, 127, 128, 106, 107].

Consider again the unit normal vector n_μ to the spatial hypersurfaces of constant time. The congruence of its integral curves has a volume expansion $\theta \equiv \nabla_\mu n^\mu$. Define the *integrated expansion* to be

$$\mathcal{N} \equiv \int \frac{\theta}{3}\, dt\,, \tag{3.105}$$

where the integration is along the integral curve of n^μ, and t is the proper time given by the lapse function α through $dt = \alpha\, d\tau$. The integrated expansion $\mathcal{N}$ is defined up to an integration constant for each worldline, and can be considered as the *local number of e-folds* of the Hubble expansion[2]. It is a covariant quantity that satisfies the equation

$$\dot{\mathcal{N}} = \frac{\theta}{3}\,, \quad \text{i.e.} \quad n^\mu \partial_\mu \mathcal{N} = \frac{1}{3}\,\nabla_\mu n^\mu\,. \tag{3.106}$$

Note that this quantity $\mathcal{N}$ depends on the choice of the spacetime slicing through the normal vector n^μ. (Recall from Section 3.1.2 that choosing a slicing is equivalent to picking a locally non-rotating Eulerian observer with 4-velocity n^μ.)

In the covariant formalism, $\mathcal{N}$ is used to define a covector [94]

$$\zeta_\mu \equiv \partial_\mu \mathcal{N} - \frac{\dot{\mathcal{N}}}{\dot{\rho}} \partial_\mu \rho\,, \tag{3.107}$$

whose components ζ_i describe the spatial gradient of $\mathcal{N}$ on the uniform density slice where $\rho = \text{const}$. This covector ζ_μ vanishes in a homogeneous background, and in that sense defines a true perturbation that is fully nonperturbative. It is a generalization of the linear perturbation ζ from Eq. (3.86), which describes the curvature perturbation ψ in the uniform density gauge where $\delta\rho = 0$.

More generally, the nonlinear curvature perturbation in a particular gauge with normal vector n_μ can be described by the covector

$$-\psi_\mu \equiv D_\mu \mathcal{N} = \partial_\mu \mathcal{N} - \dot{\mathcal{N}} n_\mu\,, \tag{3.108}$$

where the integrated expansion $\mathcal{N}$ is defined with respect to the same vector n^μ. Note that $-\psi_i = \partial_i \mathcal{N}$ in the coordinates adapted to the slicing, since the spatial components n_i vanish identically. In general, at linear order, ψ_i reduces to the gradient

[2] $\mathcal{N}$ is equal to the logarithm of the *local scale factor*, $\ln \mathsf{a} \equiv \frac{1}{6} \ln(\det \gamma_{ij})$, if the shift β^i is zero.

of the linear curvature perturbation ψ in the same gauge [94]. Therefore, the negative integrated expansion $-\mathcal{N}$ is a covariant and nonlinear generalization of the linear curvature perturbation ψ.

Indeed, the homogeneous part of $\mathcal{N}$ equals the number of e-folds N in the homogeneous background,

$$N = \int H\, dt = \ln a\,, \tag{3.109}$$

where the scale factor a is set to be 1 initially. At linear order, the inhomogeneous part of $\mathcal{N}$ is given by, up to an integration constant, [95]

$$\mathcal{N}^{(1)} = -\psi + \frac{1}{3}\int \nabla^2\sigma\, d\eta\,. \tag{3.110}$$

On superhorizon scales, neglecting the gradient term, the inhomogeneous part of $\mathcal{N}$ then becomes

$$\delta N \equiv \mathcal{N} - N \approx -\psi\,, \tag{3.111}$$

provided that $\mathcal{N} = -\psi$ on the initial time slice. This is the δN formula for computing the curvature perturbation ψ on superhorizon scales [128, 106]. In practice, $\mathcal{N}$ is often calculated by making the separate universe approximation [142, 125] that $\mathcal{N}(t, x^i) \approx N(\phi^I(t_0, x^i))$, where $N(\phi^I(t_0, x^i))$ is the homogeneous number of e-folds as a function of the scalar fields ϕ^I on different patches of the initial time slice [128, 106, 107].

Instead of using the δN formalism, we can solve for $\mathcal{N}$ directly from Eq. (3.106). To calculate the perturbation in a particular gauge, n_μ should be chosen as the unit normal vector to the corresponding time slices. For example, the generalization of the comoving curvature perturbation $\mathcal{R}$ can be calculated by using $n_\mu^{(\phi)} = \partial_\mu\phi/\sqrt{-(\partial\phi)^2}$, which is the normal vector to the constant ϕ hypersurfaces. Since $\mathcal{N}$ is covariantly defined, the calculation can be done in any coordinates given the values of $n_\mu^{(\phi)}$ in that coordinates. This situation is exactly the same as for the gauge-invariant variable $\mathcal{R}$, which is defined as the linear curvature perturbation in the comoving gauge but can be evaluated in any other gauges.

We will use the above approach to compute the adiabatic perturbations during the nonsingular bounce. So far our calculations are for classical perturbations that evolve according to their equations of motion. There are however quantum perturbations that can arise from vacuum fluctuations of the spacetime at wavelengths much smaller than the horizon size. Those quantum perturbations are amplified during the contraction phase and provide initial values for the classical perturbations.

3.4 Quantum perturbations

The adiabatic perturbations arise from quantum fluctuations in the early contraction phase when the modes are deep inside the horizon. Since the wavelength is much smaller than the curvature radius of the space ($\sim$ horizon size), these modes are essentially in the ground state of a Minkowski vacuum. As the horizon scale shrinks during the contraction phase, the quantum perturbations are amplified and become

classical. Therefore the amplitude of the final adiabatic perturbations is determined by their initial state in the Minkowski vacuum. In this Section we derive the initial values for the adiabatic perturbations that are used for later calculations.

3.4.1 metric perturbations

Consider the universe filled with a single canonical scalar field ϕ. We start by writing the action for the metric perturbations in the gauge where $\delta\phi = E = 0$. Using the variables from the linear perturbation theory and expanding to quadratic order, the Einstein action can be written as

$$S_2 = \int d\eta\, d^3x\, a^2 \Big[-(\mathcal{H}' + 2\mathcal{H}^2)A^2 - 6\mathcal{H}A\psi' + 2A\nabla^2\psi - 2\mathcal{H}A\nabla^2 B - 3\psi'^2 + (\partial_i\psi)^2 - 2\psi'\nabla^2 B \Big]. \tag{3.112}$$

The lapse and shift variables A, B can be considered as Lagrange multipliers [110] and eliminated by using the Hamiltonian and momentum constraints (3.50, 3.51); then the action is expressed only in terms of ψ, or $\mathcal{R}$ as denoted in the comoving gauge. After integration by parts, the quadratic action becomes

$$S_2 = \int d\eta\, d^3x\, \frac{z^2}{2} \Big[\mathcal{R}'^2 - (\partial_i \mathcal{R})^2 \Big], \tag{3.113}$$

where $z^2 = 2a^2(\mathcal{H}^2 - \mathcal{H}')/\mathcal{H}^2$.

Introducing the Mukhanov variable $v \equiv z\,\mathcal{R}$ [114], the quadratic action takes the canonical form

$$S_2 = \int d\eta\, d^3x\, \frac{1}{2} \Big[(v')^2 - (\partial_i v)^2 + \frac{z''}{z} v^2 \Big]. \tag{3.114}$$

The variable v can be Fourier transformed as

$$v(\eta, \mathbf{x}) = \int \frac{d^3\mathbf{k}}{(2\pi)^3}\, v_{\mathbf{k}}(\eta) e^{i\mathbf{k}\cdot\mathbf{x}}. \tag{3.115}$$

The Fourier mode $v_{\mathbf{k}}$ satisfies the equation of motion

$$v_{\mathbf{k}}'' + k^2 v_{\mathbf{k}} - \frac{z''}{z}\, v_{\mathbf{k}} = 0, \tag{3.116}$$

which describes a harmonic oscillator with a time-dependent mass $\omega_k^2 = k^2 - z''/z$. Since $v_{\mathbf{k}}$ only depends on the magnitude $k = |\mathbf{k}|$, we will write it as v_k below.

The canonical momentum conjugate to v is $\pi = v'$. To quantize the action [114], first promote v and π to quantum operators,

$$\hat{v}(\eta, \mathbf{x}) = \int \frac{d^3\mathbf{k}}{(2\pi)^3} \Big(v_k(\eta) \hat{a}_{\mathbf{k}} e^{i\mathbf{k}\cdot\mathbf{x}} + v_k^*(\eta) \hat{a}_{\mathbf{k}}^\dagger e^{-i\mathbf{k}\cdot\mathbf{x}} \Big), \tag{3.117}$$

$$\hat{\pi}(\eta, \mathbf{x}) = \int \frac{d^3\mathbf{k}}{(2\pi)^3} \Big(v_k'(\eta) \hat{a}_{\mathbf{k}} e^{i\mathbf{k}\cdot\mathbf{x}} + v_k^{*\prime}(\eta) \hat{a}_{\mathbf{k}}^\dagger e^{-i\mathbf{k}\cdot\mathbf{x}} \Big). \tag{3.118}$$

Here the *mode function* v_k satisfies the equation of motion (3.116), and the creation and annihilation operators $\hat{a}^\dagger_{\mathbf{k}}$ and $\hat{a}_{\mathbf{k}}$ satisfy the usual commutation relations

$$[\hat{a}_{\mathbf{k}}, \hat{a}_{\mathbf{k}'}] = [\hat{a}^\dagger_{\mathbf{k}}, \hat{a}^\dagger_{\mathbf{k}'}] = 0 \,, \quad [\hat{a}_{\mathbf{k}}, \hat{a}^\dagger_{\mathbf{k}'}] = (2\pi)^3 \delta^3(\mathbf{k} - \mathbf{k}'). \tag{3.119}$$

In order for $\hat{v}$ and $\hat{\pi}$ to satisfy the canonical commutation relation

$$[\hat{v}(\eta, \mathbf{x}), \hat{\pi}(\eta, \mathbf{x}')] = i\, \delta^3(\mathbf{x} - \mathbf{x}') \,, \tag{3.120}$$

the Wronskian of v_k and v_k^* must be normalized such that

$$v_k v_k^{*\prime} - v_k^* v_k' = i \,. \tag{3.121}$$

The vacuum state is defined to be annihilated by $\hat{a}_{\mathbf{k}}$,

$$\hat{a}_{\mathbf{k}} |0\rangle = 0 \,. \tag{3.122}$$

In general, the solution of v_k to Eq. (3.116), under the constraint (3.121), can be the sum of a positive and a negative frequency mode $\sim e^{\pm i\omega_k \eta}$. Choosing a different combination corresponds to a Bogoliubov transformation of the operators $\hat{a}_{\mathbf{k}}$ and $\hat{a}^\dagger_{\mathbf{k}}$, hence a different vacuum state [114, 15]. By convention, we choose the *Bunch-Davies vacuum state* [20] which contains only the positive frequency mode,

$$v_k(\eta) \sim \frac{1}{\sqrt{2\omega_k}}\, e^{-i\omega_k \eta} \,. \tag{3.123}$$

Consider the case in which the background evolution is given by a power law, $a \sim (-\tau)^p \sim (-\eta)^{\frac{p}{1-p}}$, so that

$$\frac{z''}{z} = \frac{p\,(2p-1)}{(1-p)^2\, \eta^2} \,. \tag{3.124}$$

Then the solution to Eq. (3.116) is given by the Hankel functions,

$$v_k(\eta) = \sqrt{-\eta}\big[v_1 H^{(1)}_\nu(-k\eta) + v_2 H^{(2)}_\nu(-k\eta)\big] \,, \tag{3.125}$$

where $\nu = \frac{1}{2} - \frac{p}{1-p}$. The constants v_1, v_2 can be fixed by the initial conditions. At early times the mode is deep inside the horizon, $k/|\mathcal{H}| \sim k(-\eta) \gg 1$, so $\omega_k \approx k$; the solution should match the Bunch-Davies vacuum state,

$$v_k \to \frac{1}{\sqrt{2k}}\, e^{-ik\eta}. \tag{3.126}$$

Using the asymptotic behavior of the Hankel functions, $H^{(1,2)}_\nu(x) \to \sqrt{\frac{2}{\pi x}}\, e^{\pm i(x - \frac{\nu\pi}{2} - \frac{\pi}{4})}$ for $x \to \infty$, the solution is fixed to be

$$v_k(\eta) = \frac{\sqrt{\pi(-\eta)}}{2}\, H^{(1)}_\nu(-k\eta)\, e^{i(\frac{\nu\pi}{2} + \frac{\pi}{4})}. \tag{3.127}$$

After the mode exits the horizon, $k(-\eta) \ll 1$; neglecting the constant phase factor and using the expansion of the Hankel function $H_\nu^{(1)}(x)$ for $x \to 0$, the solution can be approximated by

$$v_k(\eta) \approx \frac{\sqrt{\pi(-\eta)}}{2}\bigg[-i\,\frac{2^\nu\Gamma(\nu)}{\pi(-k\eta)^\nu}+\bigg(\frac{1}{2^\nu\Gamma(1+\nu)}-i\,\frac{\cos(\nu\pi)\Gamma(-\nu)}{2^\nu\pi}\bigg)(-k\eta)^\nu+\mathcal{O}(k^2)\bigg]. \tag{3.128}$$

The expectation value for the variance of $\hat{v}(\eta,\mathbf{x})$ is given by

$$\langle 0|\hat{v}(\eta,\mathbf{x})^2|0\rangle = \int d(\log k)\,\frac{k^3}{2\pi^2}\,|v_k|^2\ . \tag{3.129}$$

The quantum operator $\hat{v}$ would behave like a classical variable after the mode exits the horizon. This can be seen, e.g. from Eq. (3.121), by which the commutator becomes much smaller than the expectation value [92]. Therefore, after horizon crossing, we may treat v as a classical random field whose Fourier transform is given by (3.115), and whose variance $\langle v(\eta,\mathbf{x})^2\rangle$ is given by (3.129).

Similarly, we can calculate the power spectrum of the comoving curvature perturbation $\mathcal{R}$. Since $\mathcal{R} = v/z$, the mode function for $\mathcal{R}$ is given by the leading terms

$$\mathcal{R}_k \approx \sqrt{\frac{\pi p}{8}}\frac{(-\eta)^\nu}{(1-p)^{\frac{p}{1-p}}a_0^{\frac{1}{1-p}}}\bigg[-i\,\frac{2^\nu\Gamma(\nu)}{\pi(-k\eta)^\nu}+\bigg(\frac{1}{2^\nu\Gamma(1+\nu)}-i\,\frac{\cos(\nu\pi)\Gamma(-\nu)}{2^\nu\pi}\bigg)(-k\eta)^\nu\bigg]\ , \tag{3.130}$$

where a_0 is the proportionality constant in $a = a_0(-\tau)^p$. Then the correlation function of $\mathcal{R}$ is given by

$$\langle \mathcal{R}(\eta,\mathbf{x})^2\rangle = \int d(\log k)\,\frac{k^3}{2\pi^2}\,|\mathcal{R}_k|^2\ . \tag{3.131}$$

The *power spectrum* is defined as

$$\Delta^2_{\mathcal{R}} \equiv \frac{k^3}{2\pi^2}\,|\mathcal{R}_k|^2\,, \tag{3.132}$$

and the *spectral index* (or *tilt*) and its *running* are defined by

$$n_{\rm s} - 1 \equiv \frac{d\ln\Delta^2_{\mathcal{R}}}{d\ln k}\ , \quad r \equiv \frac{d\,n_{\rm s}}{d\ln k}\ . \tag{3.133}$$

Therefore, a scale-invariant power spectrum ($n_{\rm s} = 1$) means $\mathcal{R}_k \sim k^{-3/2}$. Comparing to Eq. (3.130), it implies $\nu = \pm\frac{3}{2}$; see Appendix A for a category of single-field cosmological models with a scale-invariant power spectrum. The observed primordial density fluctuations indicate that the power spectrum is nearly scale-invariant, with an amplitude $\Delta^2_{\mathcal{R}} \approx 2.4\times10^{-9}$ [69, 1].

3.4.2 scalar field perturbations

Another way to quantize the perturbations is to use the flat gauge in which $\psi = E = 0$. After eliminating the lapse and shift variables A, B by the Hamiltonian and momentum constraints, the quadratic action can be expressed solely in terms of the scalar field perturbation $\delta\phi$,

$$S_2 = \int d\eta\, d^3x\, \frac{a^2}{2}\Big[\delta\phi'^2 - (\partial_i\delta\phi)^2\Big]\,. \tag{3.134}$$

Introduce the variable $u \equiv a\,\delta\phi$, whose Fourier transform u_k satisfies the equation

$$u_k'' + k^2 u_k - \frac{a''}{a}\,u_k = 0\,. \tag{3.135}$$

Without going through the canonical quantization again, the bottom line is to solve for the mode function u_k that matches the initial condition

$$u_k \to \frac{1}{\sqrt{2k}}\,e^{-ik\eta} \tag{3.136}$$

when the mode is deep inside the horizon, $k(-\eta) \gg 1$, at early times.

For the power law background, $a \sim (-\eta)^{\frac{p}{1-p}}$, the solution is given by

$$u_k = \frac{\sqrt{\pi(-\eta)}}{2}\,H_\nu^{(1)}(-k\eta)\,e^{i(\frac{\nu\pi}{2}+\frac{\pi}{4})}, \tag{3.137}$$

where $\nu = \frac{1}{2} - \frac{p}{1-p}$. In fact this solution is exactly the same as (3.127), since for the power law background we have $z = a\sqrt{2/p}$, hence $a''/a = z''/z$. Therefore the amplitude of u_k after horizon crossing is the same as (3.128). Then the scalar field perturbation $\delta\phi$ in the flat gauge can be found by $\delta\phi_\psi = u_k/a$.

Note that for a single scalar field, by Eq. (3.78), the comoving curvature perturbation $\mathcal{R}$ can be related to the scalar field perturbation $\delta\phi_\psi$ through $\mathcal{R} = \frac{\mathcal{H}}{\phi'}\,\delta\phi_\psi$. Using the background equation (2.4), one finds $\mathcal{H}/a\phi' = 1/z$, hence u and v are the same variable. But the calculation in the flat gauge can be easily extended to more than one scalar field. For the two scalar fields ϕ and χ in Section 2.3.2, for example, the comoving curvature perturbation would be defined as [4]

$$\mathcal{R} \equiv \psi + \mathcal{H}\Big(\frac{\phi'\delta\phi - \chi'\delta\chi}{\phi'^2 - \chi'^2}\Big)\,. \tag{3.138}$$

It would be much easier to calculate the amplitude of $\mathcal{R}$ in the flat gauge.

We will take Eq. (3.130) to be the amplitude of the curvature perturbation on superhorizon scales near the end of the contraction phase. In the following Sections, we will calculate the further evolution of this amplitude during the bouncing phase, in order to analyze the stability of the bounce and the scale dependence of the power spectrum.

Chapter 4

Perturbative Analysis

In this Chapter we consider a bouncing model that smoothly connects an ekpyrotic contraction to a nonsingular bounce. The ekpyrotic phase serves to homogenize, flatten, and isotropize the universe before the bounce. The transition into the bouncing phase is triggered by the ghost condensation mechanism described in Section 2.3.1. We will show that an unexpected huge growth of curvature perturbation occurs during the transition, enough to break the homogeneity and flatness and spoil the power spectrum [147]. Furthermore, shear perturbation also grows rapidly during the bouncing phase, creating an overwhelming amount of anisotropy that disrupts the bounce altogether [148]. We study how these problems are related to the specific bouncing mechanism, as a guide for making improved models in later Chapters.

4.1 Ekpyrotic contraction and nonsingular bounce

The model is constructed in such a way that both the ekpyrotic contraction and the nonsingular bounce are driven by the same scalar field. The field has a noncanonical Lagrangian that allows it to undergo ghost condensation after the ekpyrotic phase. The motivation for this setup is that, in general, it is hard to achieve a nonsingular bounce by combining two independent components with $w > 1$ and $w < -1$ respectively. Otherwise, the $w > 1$ component would come to dominate during the ekpyrotic phase, so the $w < -1$ component would become too insignificant to induce the bounce. Therefore it requires less fine-tuning to have the $w > 1$ component itself turn into $w < -1$ after the ekpyrotic phase.

This framework is described in the "new ekpyrotic model" [26] (cf. [34, 102]) by the Lagrangian

$$\mathcal{L} = P(X) - V(\phi), \quad X \equiv -\tfrac{1}{2}(\partial\phi)^2 .$$

Specifically, the kinetic function $P(X)$ is canonical for large X, $P(X) \approx X$, but has a minimum at a low energy scale X_c where the ghost condensation takes place, as shown in Fig. 4.1. The potential function $V(\phi)$ is approximated by a negative exponential on the right side, $V(\phi) \approx V_0\, e^{-c\phi}$, and it bottoms out and rises sharply on the left, as shown in Fig. 4.2. The Universe evolves through the ekpyrotic phase ($w \gg 1$) to the

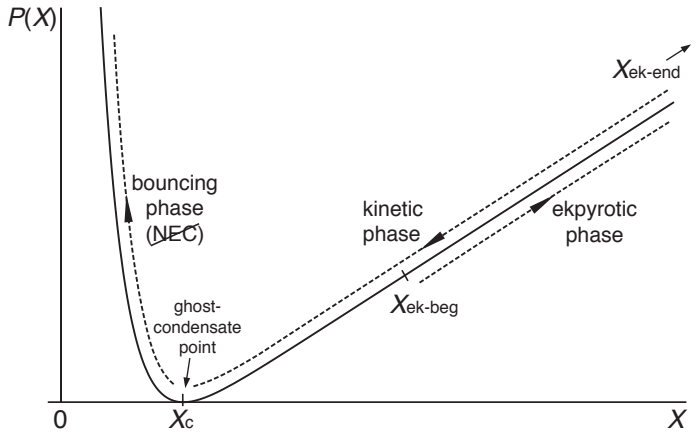

Figure 4.1: The kinetic term $P(X)$ versus $X \equiv \frac{1}{2}(\partial\phi)^2$ in the effective Lagrangian for the scalar field ϕ. During the ekpyrotic phase, X is in the linear region $X \gg X_{\rm c}$ and increases by a factor e^{2N}. In the transition to the bouncing phase, X decreases by an even greater factor to reach $X = X_{\rm c}$. During the bouncing phase, X further decreases to $X < X_{\rm c}$ where NEC is violated.

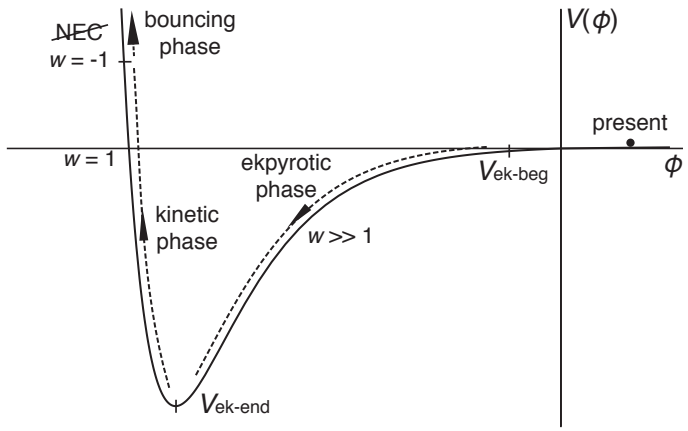

Figure 4.2: The potential term $V(\phi)$ in the effective Lagrangian for the scalar field ϕ. The ekpyrotic phase corresponds to the exponential decline from $V_{\text{ek-beg}}$ to $V_{\text{ek-end}}$ near the minimum of the potential. The kinetic phase refers to the quick rise from $V_{\text{ek-end}}$ to $V_{\rm c} \approx 3p\,|V_{\text{ek-end}}|$. The nonsingular bouncing phase occurs at $V > V_{\rm c}$.

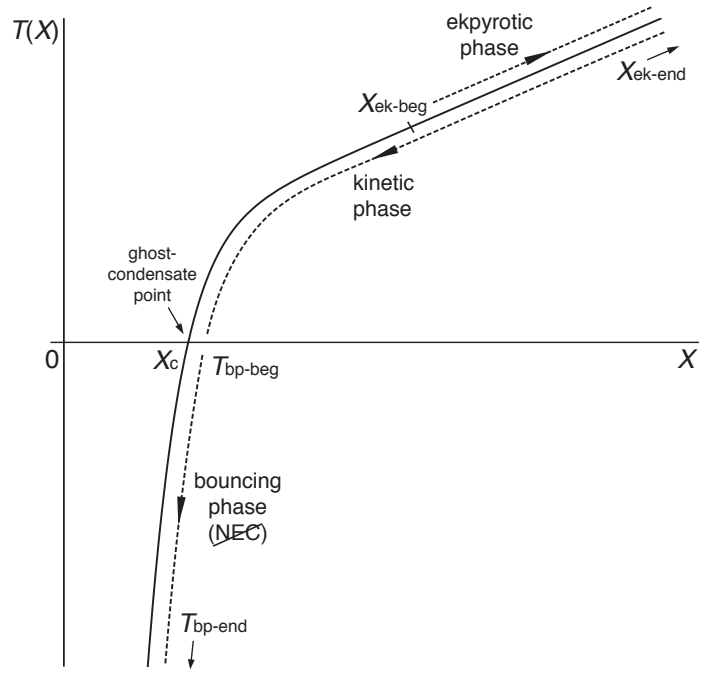

Figure 4.3: The kinetic energy $T(X) = 2XP_{,X} - P$ for the scalar field ϕ. It is a linear function of X in the region $X \gg X_{\rm c}$, but becomes negative at $X < X_{\rm c}$.

bouncing phase ($w < -1$), with a transient kinetic energy dominated phase ($w \sim 1$) in between, as indicated in the figures.

The ekpyrotic phase is described by the attractor solution (2.23) and the scaling relation (2.24), presented in Section 2.2. During the ekpyrotic phase, the kinetic energy of the ϕ field increases from $X_{\text{ek-beg}}$ to $X_{\text{ek-end}}$. Since the field is assumed to be nearly canonical during the ekpyrotic phase, the energy scales should satisfy $X_{\rm c} < X_{\text{ek-beg}}$, as shown in the figures. This implies the relation

$$\frac{X_{\rm c}}{X_{\text{ek-end}}} < \frac{X_{\text{ek-beg}}}{X_{\text{ek-end}}} = \frac{(H^2)_{\text{ek-beg}}}{(H^2)_{\text{ek-end}}} \approx e^{-2N}, \tag{4.1}$$

where we used the scaling relation (2.24) and the ratio (2.26).

After the ekpyrotic phase, the potential $V(\phi)$ rises sharply so the ϕ field slows down and X reduces from $X_{\text{ek-end}}$ to $X_{\rm c}$. This transient "kinetic phase" lasts much shorter than a Hubble time, during which the total energy is almost conserved. Let $V_{\rm c}$ be the value of the potential when X reaches $X_{\rm c}$, then

$$V_{\rm c} = 3H_{\rm c}^2 \approx 3H_{\text{ek-end}}^2 \approx \tfrac{3}{\epsilon}\,|V_{\text{ek-end}}|, \tag{4.2}$$

where $\epsilon = \frac{c^2}{3} - 1 \gg 1$, as in (2.23). The bouncing phase begins when X further decreases to less than $X_{\rm c}$. Then $\dot{H} = -XP_{,X}$ becomes positive and the kinetic energy of the scalar field $T \equiv 2XP_{,X} - P$ becomes negative, as shown in Fig. 4.3. The bounce occurs when X reaches a point where the negative kinetic energy T

cancels the positive potential energy V, so that H vanishes. The universe then starts to expand afterwards.

To avoid the ghost instability, i.e. to have $T_{,X} = 2XP_{,XX} + P_{,X} > 0$, we assume that the function $P(X)$ increases quickly as X decreases, in particular,

$$|XP_{,X}| \gg P \ , \text{ and } XP_{,XX} \gg |P_{,X}| \ , \quad \text{for } X < X_{\rm c} \ . \tag{4.3}$$

In that case $T(X)$ drops rapidly to large and negative values, so the bounce would happen at an X very close to the ghost condensation point $X_{\rm c}$. By Eq. (2.32), condition (4.3) also implies $|c_s^2| \ll 1$ during the bouncing phase, which limits the amount of gradient instability for specific modes of interest, as discussed below in Section 4.2. To limit the gradient instability, it is commonly assumed that the bouncing phase lasts as short as a few Hubble times. In the contrary, we will show that the bouncing phase cannot be arbitrarily short. Indeed, by the end of the ekpyrotic phase H is negative and exponentially large, so there must be a long period of $\dot{H} > 0$ for H to increase to zero.

To determine how long the bouncing phase really lasts, we solve the equation of motion for the scalar field (cf. Eq. (5.33)),

$$T_{,X}\, \dot{X} + 6HP_{,X}\, X + V_{,\phi}\, \dot{\phi} = 0. \tag{4.4}$$

A general solution to Eq. (4.4) can be found by using the approximation (4.3). Since $|XP_{,X}| \gg P$ for $X < X_{\rm c}$, the kinetic energy can be approximate by

$$T(X) = 2XP_{,X} - P \approx 2XP_{,X} \ . \tag{4.5}$$

The potential energy and its gradient are nearly constant during the bouncing phase,

$$V(\phi) \approx V_{\rm c} \ , \quad V_{,\phi} \approx V_{,\phi_{\rm c}} \ , \tag{4.6}$$

as can be seen from the estimation

$$\frac{\Delta V}{V_{\rm c}} \approx \Big(\frac{-V_{,\phi_{\rm c}}}{V_{\rm c}}\Big)\Delta\phi \approx \Big(\frac{-V_{,\phi_{\rm c}}}{V_{\rm c}}\Big)\sqrt{2X_{\rm c}}\,\Delta t_{\rm bp} \lesssim N\, e^{-N}, \tag{4.7}$$

where $\Delta t_{\rm bp} \approx N/3|H_{\rm c}|$ as found below; and similarly for $V_{,\phi}$. The factors $\big(\frac{-V_{,\phi_{\rm c}}}{V_{\rm c}}\big)$ and $\big(\frac{V_{,\phi_{\rm c}\phi_{\rm c}}}{V_{\rm c}}\big)$ are taken to be large yet much less than e^N; otherwise one has to fine-tune the steepness of the potential to super Planckian scales, making quantum gravity effects unavoidable.

Under the above approximations, Eq. (4.4) becomes

$$\dot{T} + 3HT + V_{,\phi_{\rm c}}\, \dot{\phi} = 0. \tag{4.8}$$

The solution can be described in three stages according to whether the Hubble friction or the potential gradient term dominates. According to Fig. 4.3, at the very beginning of the bouncing phase, $|H| \approx |H_{\rm c}| = \sqrt{V_{\rm c}/3}$ but $|T|$ is small, hence the friction term is negligible. Next, the negative kinetic energy $|T|$ increases and the friction term

overtakes the gradient term. Finally, very close to the bounce, $T \approx -V_{\rm c}$ but $|H|$ becomes small, so the friction term is again subdominant to the gradient term. The transitions between these stages are given by the estimate $3HT \sim V_{,\phi_{\rm c}}\dot\phi$. Denote

$$T_{\text{bp-beg}} \equiv \left.\frac{V_{,\phi_{\rm c}}\,\dot\phi}{3H}\right|_{\text{bp-beg}} \approx \Big(\frac{-V_{,\phi_{\rm c}}}{V_{\rm c}}\Big)\sqrt{\tfrac{2}{3}X_{\rm c}V_{\rm c}}\ , \tag{4.9}$$

$$H_{\text{bp-end}} \equiv \left.\frac{V_{,\phi_{\rm c}}\,\dot\phi}{3T}\right|_{\text{bp-end}} \approx \Big(\frac{-V_{,\phi_{\rm c}}}{V_{\rm c}}\Big)\sqrt{2X_{\rm c}}\ , \tag{4.10}$$

$$T_{\text{bp-end}} \equiv -V_{\rm c} + 3H^2_{\text{bp-end}} \approx -V_{\rm c}\ , \tag{4.11}$$

where "bp-beg" and "bp-end" refer to the beginning and end of the middle stage. The first and the last stages are both very short and uninteresting. Indeed, since the friction and the gradient terms are both positive during the bouncing phase, Eq. (4.8) implies

$$|\dot T| \geq V_{,\phi}\,\dot\phi \approx (-V_{,\phi_{\rm c}})\sqrt{2X_{\rm c}}\ . \tag{4.12}$$

The first stage goes from $T = 0$ until $T \approx T_{\text{bp-beg}}$, which lasts less than a Hubble time,

$$t_{\text{bp-beg}} - t_{\rm c} \sim \frac{|T_{\text{bp-beg}}|}{|\dot T|} \lesssim \frac{(-V_{,\phi_{\rm c}})\sqrt{2X_{\rm c}/3V_{\rm c}}}{(-V_{,\phi_{\rm c}})\sqrt{2X_{\rm c}}} \approx \frac{1}{3|H_{\rm c}|}\ , \tag{4.13}$$

hence the scale factor does not change much, $a_{\text{bp-beg}} \approx a_{\rm c} \approx a_{\text{ek-end}}$. Similarly, the third stage begins from $T_{\text{bp-end}}$ and reaches the bounce at $T = -V_{\rm c}$, so the time it takes can be bounded by

$$t_{\rm b} - t_{\text{bp-end}} \approx \frac{3H^2_{\text{bp-end}}}{|\dot T|} \lesssim \frac{(-V_{,\phi_{\rm c}}/V_{\rm c})^2\,6X_{\rm c}}{(-V_{,\phi_{\rm c}})\sqrt{2X_{\rm c}}} \approx \Big(\frac{-V_{,\phi_{\rm c}}}{V_{\rm c}}\Big)\sqrt{\frac{2\epsilon X_{\rm c}}{X_{\text{ek-end}}}}\frac{1}{|H_{\rm c}|} \lesssim \frac{e^{-N}}{|H_{\rm c}|}\ , \tag{4.14}$$

which is much less than a Hubble time, implying $a_{\rm b} \approx a_{\text{bp-end}}$. Finite factors like ϵ and $\big(\frac{-V_{,\phi_{\rm c}}}{V_{\rm c}}\big)$ are neglected in these estimates.

Therefore the bouncing phase mainly consists of the middle stage during which the friction term dominates and the gradient is negligible. Under this condition, the equation of motion simplifies to

$$\dot T + 3HT = 0, \quad \text{with } H^2 = \tfrac{1}{3}(T + V_{\rm c}). \tag{4.15}$$

The bouncing solution is given by

$$T = \frac{-V_{\rm c}}{\cosh^2\big(\frac{3}{2}|H_{\rm c}|(t-t_0)\big)}\ , \tag{4.16}$$

$$H = |H_{\rm c}|\,\tanh\big(\tfrac{3}{2}|H_{\rm c}|(t-t_0)\big)\ , \tag{4.17}$$

where t_0 is formally the time of the bounce. This solution is valid between the moments $t_{\text{bp-beg}}$ and $t_{\text{bp-end}}$, which correspond to $T \approx T_{\text{bp-beg}}$ and $H \approx H_{\text{bp-end}}$ respec-

tively. Equating (4.9) and Eq. (4.16) gives

$$\cosh^{-2}\left(\tfrac{3}{2}|H_{\rm c}|(t_{\text{bp-beg}}-t_0)\right)\approx\left(\frac{-V_{,\phi_{\rm c}}}{V_{\rm c}}\right)\sqrt{\frac{X_{\rm c}}{X_{\text{ek-end}}}}\sim e^{-N}, \tag{4.18}$$

hence

$$t_0-t_{\text{bp-beg}}\approx\frac{N}{3|H_{\rm c}|}\,. \tag{4.19}$$

Similarly, comparing (4.10) and Eq. (4.17) gives

$$\left|\tanh\left(\tfrac{3}{2}|H_{\rm c}|(t_{\text{bp-end}}-t_0)\right)\right|\approx\left(\frac{-V_{,\phi_{\rm c}}}{V_{\rm c}}\right)\sqrt{\frac{X_{\rm c}}{X_{\text{ek-end}}}}\sim e^{-N}, \tag{4.20}$$

hence

$$t_0-t_{\text{bp-end}}\approx\frac{2e^{-N}}{3|H_{\rm c}|}\,. \tag{4.21}$$

Therefore the bouncing phase approximately lasts for a period

$$\Delta t_{\rm bp}\approx t_{\text{bp-end}}-t_{\text{bp-beg}}\approx\frac{N}{3}\frac{1}{|H_{\rm c}|}\,, \tag{4.22}$$

which is a large number of Hubble times.

This long duration of the bouncing phase allows anisotropy to grow significantly. From Eq. (4.15), the scale factor $a(t)$ scales as

$$a\propto\cosh^{2/3}\left(\tfrac{3}{2}|H_{\rm c}|(t-t_0)\right)\propto|T|^{-1/3}. \tag{4.23}$$

Before the end of the bouncing phase, it contracts by a factor

$$\frac{a_{\text{bp-end}}}{a_{\text{bp-beg}}}=\left|\frac{T_{\text{bp-end}}}{T_{\text{bp-beg}}}\right|^{-\frac{1}{3}}\approx\left(\frac{-V_{,\phi_{\rm c}}}{V_{\rm c}}\right)^{\frac{1}{3}}\left(\frac{X_{\rm c}}{X_{\text{ek-end}}}\right)^{\frac{1}{6}}\lesssim e^{-\frac{1}{3}N}. \tag{4.24}$$

Therefore, the anisotropy term in the Friedmann equation (2.18) would increase by a factor

$$\frac{(\sigma^2)_{\text{bp-end}}}{(\sigma^2)_{\text{bp-beg}}}=\left(\frac{a_{\text{bp-end}}}{a_{\text{bp-beg}}}\right)^{-6}\sim\frac{X_{\text{ek-end}}}{X_{\rm c}}\gtrsim e^{2N}, \tag{4.25}$$

which cancels the suppression (2.27) it has experienced during the ekpyrotic phase. More precisely, during the ekpyrotic phase, the anisotropy term remains almost constant by itself, while the scalar field energy increases by an exponential factor e^{2N}. In the bouncing phase, however, the anisotropy term grows by the same factor e^{2N}, while the scalar field energy decreases towards zero. The nonsingular bounce would not happen if the anisotropy term overtakes the scalar field energy before the bounce.

To derive a general condition for the nonsingular bounce to happen, suppose that there is some initial anisotropy $\sigma^2_{\text{ek-beg}}$ at the beginning of the ekpyrotic phase. Including the anisotropy term in the Friedmann equations (2.30, 2.31) and using the

approximations (4.5) and (4.6), we have

$$3H^2 = T + V + \sigma^2 \approx T + V_{\rm c} + \sigma^2, \tag{4.26}$$

$$\dot{H} = -XP_{,X} - \sigma^2 \approx \frac{-T}{2} - \sigma^2. \tag{4.27}$$

In order to reach a nonsingular bounce, the scalar field energy density $\rho = T+V$ must decrease to a negative value to cancel σ^2 in (4.26). Meanwhile, $\dot{H}$ must stay positive before H reaches zero, hence T has to be sufficiently negative so that $|T| > 2\sigma^2$ in (4.27). We show that a nonsingular bounce is guaranteed if these conditions are valid up to $t_{\text{bp-end}}$. Introduce the variable $q \equiv \left(\frac{a_{\text{bp-end}}}{a}\right)^3$, which equals 1 at $t_{\text{bp-end}}$ and increases as a further decreases. Since $\sigma^2 \propto a^{-6} \propto q^2$, we have

$$\frac{d\sigma^2}{dq} = \sigma^2_{\text{bp-end}} \cdot 2q. \tag{4.28}$$

By Eq. (4.8), the scalar field obeys $\dot{\rho} + 3HT = 0$, and hence

$$\frac{d\rho}{dq} = \frac{T}{q} \leq \frac{T_{\text{bp-end}}}{q}, \tag{4.29}$$

since T is monotonically decreasing. Therefore, Eq. (4.26) satisfies

$$\frac{d(3H^2)}{dq} \leq -\frac{|T_{\text{bp-end}}|}{q} + 2\sigma^2_{\text{bp-end}}\, q, \tag{4.30}$$

which integrates to give

$$3H^2 \leq 3H^2_{\text{bp-end}} - |T_{\text{bp-end}}|\, \log q + \sigma^2_{\text{bp-end}}(q^2 - 1). \tag{4.31}$$

To have a bounce at a finite a, a sufficient condition is if the right hand side has a root in $\{q > 1\}$. At $q^2 = |T_{\text{bp-end}}|/2\sigma^2_{\text{bp-end}}$, the right hand side reaches a minimum value

$$3H^2_{\text{bp-end}} - \frac{|T_{\text{bp-end}}|}{2} \log \frac{|T_{\text{bp-end}}|}{2\sigma^2_{\text{bp-end}}} + \sigma^2_{\text{bp-end}} \left(\frac{|T_{\text{bp-end}}|}{2\sigma^2_{\text{bp-end}}} - 1 \right) = V_{\rm c} - \frac{|T_{\text{bp-end}}|}{2} \left(1 + \log \frac{|T_{\text{bp-end}}|}{2\sigma^2_{\text{bp-end}}} \right), \tag{4.32}$$

where we used (4.26). Requiring this to be less than 0 gives the condition

$$\sigma^2_{\text{bp-end}} \leq \frac{|T_{\text{bp-end}}|}{2}\, e^{1 - 2V_{\rm c}/|T_{\text{bp-end}}|} \approx \frac{V_{\rm c}}{2e} \sim V_{\rm c}. \tag{4.33}$$

Extrapolating back to the beginning of the bouncing phase by using Eqs. (4.24) and (4.2), the condition becomes

$$\sigma^2_{\text{bp-beg}} \lesssim \frac{a^6_{\text{bp-end}}}{a^6_{\text{bp-beg}}}\, V_{\rm c} \approx \left(\frac{-V_{,\phi_{\rm c}}}{V_{\rm c}} \right)^2 \left(\frac{X_{\rm c}}{X_{\text{ek-end}}} \right) \frac{3}{\epsilon} V_{\text{ek-end}} \sim X_{\rm c}\,. \tag{4.34}$$

Since σ^2 is nearly constant through the ekpyrotic phase, $\sigma^2_{\text{ek-beg}}$ is finally given by

$$\sigma^2_{\text{ek-beg}} \approx \sigma^2_{\text{bp-beg}} \lesssim X_{\text{c}} \ . \tag{4.35}$$

Therefore, to prevent the anisotropy from becoming a problem during the bouncing phase, the initial condition must be fine-tuned so that the ekpyrotic phase is highly isotropic to begin with.

4.2 Curvature perturbation and power spectrum

It is known that the ekpyrotic phase produces an adiabatic contribution to the curvature perturbation that carries a blue spectrum [33]. In order to match the observations, several mechanisms have been proposed to produce an extra scale-invariant contribution, such as the entropic mechanism [98, 26] and the adiabatic ekpyrotic mechanism [82, 83] (see Appendix A). The scale-invariant contribution dominate over the adiabatic contribution, and are conserved on superhorizon scales. However, in the transition from the ekpyrotic phase to the bouncing phase, it happens that an adiabatic contribution grows exponentially and surpasses the scale-invariant contribution even on large scales.

To see this problem, consider the comoving curvature perturbation $\mathcal{R}$, whose Fourier modes obey the equation (3.65),

$$\mathcal{R}_k'' + 2\frac{z'}{z}\mathcal{R}_k' + c_s^2 k^2 \mathcal{R}_k = 0, \tag{4.36}$$

where $z = a\sqrt{-2\dot{H}/c_s^2 H^2}$. After the mode exits the horizon, the k^2 term can be treated perturbatively, and the equation is formally solved by an expansion in k^2,

$$\mathcal{R}_k = \mathcal{R}_k^{(0)} - k^2 \int \frac{d\eta}{z^2} \int d\eta \, c_s^2 z^2 \mathcal{R}_k \ . \tag{4.37}$$

The leading order $\mathcal{R}_k^{(0)}$ is the solution to the equation without the k^2 term, which contains two general solutions,

$$\mathcal{R}_k^{(0)} = C_1(k) + C_2(k) \int \frac{d\eta}{z^2} \equiv \mathcal{R}_k^{\text{const}} + \mathcal{R}_k^{\text{int}} \ . \tag{4.38}$$

These two terms are the leading adiabatic contributions to the curvature perturbation; the k-dependence of the dominant term determines the spectral index of the adiabatic perturbations on large scales.

The k-dependence of the constants C_1, C_2 can be found by matching the amplitude of $\mathcal{R}_k$ from Eq. (3.130). Since the ekpyrotic contraction is given by a power law (2.23),

$a \sim (-t)^{1/\epsilon}$ with $\epsilon \gg 1$, Eq. (3.130) can be approximated by

$$\mathcal{R}_k \approx \frac{-i}{2\sqrt{\epsilon} a_0^{\frac{\epsilon}{\epsilon-1}}} k^{-\frac{1}{2}+\frac{1}{\epsilon-1}} + \frac{1}{2\sqrt{\epsilon} a_0^{\frac{\epsilon}{\epsilon-1}}} k^{\frac{1}{2}-\frac{1}{\epsilon-1}} (-\eta)^{\frac{\epsilon-3}{\epsilon-1}}. \tag{4.39}$$

Meanwhile, the leading terms in the solution (4.38) can be evaluated to be

$$\mathcal{R}_k^{\rm const} + \mathcal{R}_k^{\rm int} = C_1(k) + C_2(k) \frac{a_0^{\frac{-2\epsilon}{\epsilon-1}}}{2\epsilon - 6} \Big(\frac{\epsilon - 1}{\epsilon} (-\eta) \Big)^{\frac{\epsilon-3}{\epsilon-1}}. \tag{4.40}$$

Comparing the coefficients, one finds

$$C_1(k) \approx \frac{-i}{\sqrt{\epsilon} 2 a_0^{\frac{\epsilon}{\epsilon-1}}} \, k^{-\frac{1}{2}+\frac{1}{\epsilon-1}} \sim \frac{1}{\sqrt{k}} \, , \tag{4.41}$$

$$C_2(k) \approx \sqrt{\epsilon} a_0^{\frac{\epsilon}{\epsilon-1}} \, k^{\frac{1}{2}-\frac{1}{\epsilon-1}} \sim \sqrt{k} \, . \tag{4.42}$$

Therefore

$$\mathcal{R}_k^{\rm const}\big|_{\text{ek-end}} = C_1(k), \tag{4.43}$$

$$\mathcal{R}_k^{\rm int}\big|_{\text{ek-end}} \approx \frac{C_2(k)}{2\epsilon^2 (a^3 H)_{\text{ek-end}}} \approx \frac{C_2(k)}{2 a^3_{\text{ek-end}}} \frac{1}{\sqrt{\epsilon^3 X_{\text{ek-end}}}} \, . \tag{4.44}$$

Since $k^{3/2}|C_1(k)| \sim k$, and $k^{3/2}|C_2(k)| \sim k^2$, both $\mathcal{R}_k^{\rm const}$ and $\mathcal{R}_k^{\rm int}$ terms have *blue* spectral indices, as stated above.

Suppose an independent scale-invariant contribution $\mathcal{R}_k^{\text{sc-inv}} \sim k^{-3/2}$ is generated by certain mechanism at the end of the ekpyrotic phase. Then the total curvature perturbation is the sum of the terms,

$$\mathcal{R}_k^{\rm tot} \approx \mathcal{R}_k^{\text{sc-inv}} + \mathcal{R}_k^{\rm const} + \mathcal{R}_k^{\rm int}. \tag{4.45}$$

By the end of the ekpyrotic phase, the integral term $\mathcal{R}_k^{\rm int}$ is suppressed relative to $\mathcal{R}_k^{\rm const}$ by a factor

$$\left| \frac{\mathcal{R}_k^{\rm int}}{\mathcal{R}_k^{\rm const}} \right|_{\text{ek-end}} \approx \frac{1}{\epsilon} \left| \frac{k}{(aH)_{\text{ek-end}}} \right| \approx \sqrt{\frac{X_k}{X_{\text{ek-end}}}} \equiv e^{-N_k}, \tag{4.46}$$

where X_k is the kinetic energy at horizon crossing, and N_k is the *remaining* number of e-folds of the ekpyrotic phase after the k-mode exits the horizon. Due to its blue spectrum, the constant term $\mathcal{R}_k^{\rm const}$ is in turn suppressed with respect to the scale-invariant term $\mathcal{R}_k^{\text{sc-inv}}$ by a factor

$$\left| \frac{\mathcal{R}_k^{\rm const}}{\mathcal{R}_k^{\text{sc-inv}}} \right|_{\text{ek-end}} \sim \left| \frac{k}{(aH)_{\text{ek-end}}} \right| \approx \sqrt{\frac{X_k}{X_{\text{ek}-\text{end}}}} = e^{-N_k}. \tag{4.47}$$

Hence the integral term is *sub-subdominant*,

$$\left|\frac{\mathcal{R}_k^{\rm int}}{\mathcal{R}_k^{\text{sc-inv}}}\right|_{\text{ek-end}} \sim \left|\frac{k}{(aH)_{\text{ek-end}}}\right|^2 \approx \frac{X_k}{X_{\text{ek}-\text{end}}} = e^{-2N_k}. \tag{4.48}$$

Therefore, the total curvature perturbation right after the ekpyrotic phase is

$$\mathcal{R}_k^{\rm tot}\Big|_{\text{ek-end}} \approx \mathcal{R}_k^{\text{sc-inv}} \sim \frac{1}{k^{3/2}}\,, \tag{4.49}$$

which ensures a scale-invariant power spectrum. Note that $\mathcal{R}_k^{\text{sc-inv}}$ and $\mathcal{R}_k^{\rm const}$ remain constant, but the integral term $\mathcal{R}_k^{\rm int}$ is time-varying even on superhorizon scales. The total curvature perturbation $\mathcal{R}_k$ is conserved and scale-invariant only if the time-varying piece remains negligible.

We now demonstrate that, in fact, $\mathcal{R}_k^{\rm int}$ grows rapidly during the transition from the ekpyrotic phase to the bouncing phase when the equation of state w drops from $\gg 1$ to -1. Indeed, from Eqs. (2.31) and (2.32), the integral term can be written as

$$\mathcal{R}_k^{\rm int} = C_2(k)\int \frac{c_s^2}{a^3}\frac{H^2}{-2\dot H}dt = C_2(k)\int \frac{1}{a^3}\frac{H^2}{2XT_{,X}}\frac{dX}{\dot X}\,. \tag{4.50}$$

In Figs. 4.2 and 4.1, as the field passes the bottom of the potential and climbs up the left side, its kinetic energy quickly decreases to $X \approx X_{\rm c}$. During this period the Hubble friction term in Eq. (4.4) can be neglected, hence

$$\mathcal{R}_k^{\rm int}\Big|_{w\to-1} \approx C_2(k)\int \frac{1}{a^3}\frac{H^2}{2X}\frac{dX}{V_{,\phi}\sqrt{2X}} \approx \frac{C_2(k)}{2a_{\rm c}^3}\Big(\frac{H_{\rm c}^2}{V_{,\phi_{\rm c}}}\Big)\int^{X_{\rm c}}\frac{dX}{\sqrt{2X^3}} \approx \frac{C_2(k)}{3a_{\text{ek-end}}^3}\Big(\frac{V_{\rm c}}{-V_{,\phi_{\rm c}}}\Big)\frac{1}{\sqrt{2X_{\rm c}}}, \tag{4.51}$$

where the integral in the first line is dominated by contributions from near the upper limit, so we approximated the slowly varying quantities by their values there. Compared to the value in (4.44) at the end of the ekpyrotic phase, the integral term has grown exponentially,

$$\frac{|\mathcal{R}_k^{\rm int}|_{w\to-1}}{|\mathcal{R}_k^{\rm int}|_{\text{ek-end}}} \approx \Big(\frac{V_{\rm c}}{-V_{,\phi_{\rm c}}}\Big)\sqrt{\frac{X_{\text{ek-end}}}{X_{\rm c}}} \gtrsim e^N. \tag{4.52}$$

It exceeds the scale-invariant term by a ratio

$$\left|\frac{\mathcal{R}_k^{\rm int}}{\mathcal{R}_k^{\text{sc-inv}}}\right|_{w\to-1} \sim \frac{X_k}{X_{\text{ek-end}}}\sqrt{\frac{X_{\text{ek-end}}}{X_{\rm c}}} \gtrsim e^{N-2N_k}, \tag{4.53}$$

which is exponentially large for a wide range of modes with $N_k < N/2$.

Thus, modes that exit the horizon in the second half of the ekpyrotic phase, including all modes within current observable horizon, become dominated by the

integral term which carries a blue spectrum,

$$\mathcal{R}_k^{\rm tot}\Big|_{w\to-1} \approx \mathcal{R}_k^{\rm int} \sim \sqrt{k}\,, \tag{4.54}$$

in contradiction to observations. Moreover, assuming that the amplitude of the scale-invariant modes in (4.53) matches the measured amplitude, $\Delta^2_{\mathcal{R}^{\rm sc\text{-}inv}} = \frac{k^3}{2\pi^2}|\mathcal{R}_k^{\rm sc\text{-}inv}|^2 \approx 2.4\ \times\ 10^{-9}$, then the blue modes would have an amplitude $\Delta^2_{\mathcal{R}} \approx e^{2N-4N_k}\Delta^2_{\mathcal{R}^{\rm sc\text{-}inv}}$, which indicates a nonlinearity for modes with $N_k < N/2 - 5$.

It remains to show that the dominantly blue curvature perturbation persists through the bouncing phase without significant changes. By Eq. (4.50), the change in the integral term is

$$\Delta\mathcal{R}_k^{\rm int} = C_2(k)\int_{\rm bp\text{-}beg}^{\rm bp\text{-}end} \frac{H^2}{2a^3\dot{T}}\frac{dX}{X}\,. \tag{4.55}$$

During the bouncing phase the following relation holds due to Eq. (4.15) and (4.23),

$$\frac{H}{a^3\dot{T}} \le \frac{H}{a^3\dot{T}}\Big|_{\rm bp\text{-}beg} \approx \frac{1}{3a^3_{\rm ek\text{-}end}}\Big(\frac{V_{\rm c}}{-V_{,\phi_{\rm c}}}\Big)\frac{1}{|H_{\rm c}|\sqrt{2X_{\rm c}}}\,; \tag{4.56}$$

this inequality is also true in the short stages before $t_{\rm bp\text{-}beg}$ and after $t_{\rm bp\text{-}end}$ as a result of Eq. (4.12). Therefore we can estimate Eq. (4.55) as

$$\Delta\mathcal{R}_k^{\rm int} \lesssim \frac{C_2(k)}{6a^3_{\rm ek\text{-}end}}\Big(\frac{V_{\rm c}}{-V_{,\phi_{\rm c}}}\Big)\frac{1}{\sqrt{2X_{\rm c}}}\int\frac{H}{|H_{\rm c}|}\frac{dX}{X} \lesssim \frac{C_2(k)}{3a^3_{\rm ek\text{-}end}}\Big(\frac{V_{\rm c}}{-V_{,\phi_{\rm c}}}\Big)\frac{1}{\sqrt{2X_{\rm c}}}\Big|\frac{\Delta X}{2X_{\rm c}}\Big|\,, \tag{4.57}$$

where we used $|H| \le |H_{\rm c}|$ and assumed $\Delta X \ll X_{\rm c}$ in the bouncing phase. Hence the total change of the integral term is much less than the value (4.51) right before the bouncing phase.

Our analysis differs in an important way from [34, 102], which considered similar models and concluded that the comoving curvature perturbation changes negligibly near the bounce. In their analysis, the Hubble parameter is assumed to vary approximately linearly with time during the bounce. From our bouncing solution (4.17), this corresponds to the period when $|t - t_0| \ll 1/|H_{\rm c}|$, so that

$$H \approx \tfrac{3}{2}H_{\rm c}^2(t-t_0), \quad \dot{H} \approx \tfrac{3}{2}H_{\rm c}^2. \tag{4.58}$$

This is within the last e-fold of the bouncing phase, where $|c_s^2| \ll 1$ and $a \approx a_{\rm bp\text{-}end}$ as given in Eq. (4.24). During this linear regime the curvature perturbation changes by

$$\begin{aligned}\Delta\mathcal{R}_k^{\rm int} &\approx C_2(k)\int\frac{c_s^2}{a^3_{\rm bp\text{-}end}}\frac{H^2}{-2\dot{H}}dt \ll \frac{C_2(k)}{a^3_{\rm bp\text{-}end}}\int\frac{3}{4}H_{\rm c}^2(t-t_0)^2dt \\ &\ll \frac{C_2(k)}{a^3_{\rm ek\text{-}end}}\Big(\frac{V_{\rm c}}{-V_{,\phi_{\rm c}}}\Big)\sqrt{\frac{X_{\rm ek\text{-}end}}{X_{\rm c}}}\,\frac{1}{4|H_{\rm c}|} \sim \frac{C_2(k)}{a^3_{\rm ek\text{-}end}}\Big(\frac{V_{\rm c}}{-V_{,\phi_{\rm c}}}\Big)\frac{1}{\sqrt{2X_{\rm c}}}\,.\end{aligned} \tag{4.59}$$

Thus, as found by [34, 102], $\mathcal{R}$ changes very little as compared to its value (4.51) at the beginning of the bouncing phase. However, we emphasize that the comoving curvature perturbation grows large at a much earlier stage, just before the bouncing phase begins. This period was ignored in previous studies, and so the problem with the blue spectrum was missed.

Let us also comment on the gradient instability in the bouncing phase when $c_s^2 < 0$. According to the dispersion relation $\omega_k^2 = c_s^2 k^2$, all modes would grow exponentially instead of undergoing oscillations. As discussed in Section 2.3.1, the instability may be cut off by certain higher derivative terms at large k. Consider only the N e-folds of modes that exit the horizon during the ekpyrotic phase. Since the rate of exponential growth is proportional to $|c_s|k$, the gradient instability could be tamed if $|c_s^2|$ is small given the duration of the bouncing phase. Specifically, converting $\Delta t_{\rm bp}$ to conformal time, one finds

$$|c_s|k\Delta\eta_{\rm bp} \sim |c_s|\, e^{\frac{N}{3}-N_k}, \tag{4.60}$$

which could be large for modes with $N_k < N/3$. To avoid the gradient instability, the speed of sound has to be

$$|c_s^2| \lesssim e^{-\frac{2}{3}N}. \tag{4.61}$$

This is the same condition under which the leading term (4.38) dominates the expansion in Eq. (4.37) so that our computations are valid. Note that the unstable growth of the curvature perturbation $\mathcal{R}$ occurs before c_s^2 becomes negative, hence is a separate problem from the gradient instability.

Having analyzed the curvature perturbation in the comoving gauge, let us consider the results in other gauges. According to Eq. (3.56), the curvature perturbation is gauge-invariant at the nonsingular bounce when $H = 0$; hence the results computed in different gauges must agree near the bounce. However, the growth pattern of the curvature perturbation in different gauges can be quite different. For example, in the Newtonian gauge, the Newtonian potential Φ keeps growing during the ekpyrotic phase, but undergoes no abrupt change in the transitional kinetic phase, then grows further in the bouncing phase to reach the same value as $\mathcal{R}$ at the bounce. In the above analysis we chose to study the comoving curvature perturbation $\mathcal{R}$ because it is conserved outside the horizon in the expansion phase and therefore determines the density and temperature fluctuations observed in the LSS and CMB. It is also a convenient variable to study because it is almost conserved during both the ekpyrotic contraction and the nonsingular bouncing phases, whereas the exponential growth can be clearly traced to the transition between the two phases.

Since the comoving curvature perturbation $\mathcal{R}$ becomes exponentially large right before the bouncing phase, another concern is whether the perturbative computation breaks down at this point. We address this question by noting that the perturbation theory is valid if there exists one gauge in which the perturbation of all relevant physical quantities remain small; then the variables in other gauges can be formally defined through gauge transformations. In our case, it can be checked that, in the synchronous gauge, the physical quantities including the curvature perturbation $\psi_{\rm s}$, the shear perturbation $\sigma_{\rm s}$, and the matter perturbations $\delta\rho_{\rm s}$, $\delta p_{\rm s}$, $(\rho+p)\delta u_{\rm s}$, all remain finite during the transitional phase. In particular, the curvature perturbation $\psi_{\rm s}$ in

the synchronous gauge can be related to $\mathcal{R}$ through Eq. (3.82). After a mode exits the horizon, using Eq. (4.38), one finds

$$\psi_{\rm s} \approx C_1(k) + C_2(k) \int_0^t dt' \dot{H} \int_0^{t'} dt'' \frac{c_s^2 H}{2a^3 \dot{H}} \,. \tag{4.62}$$

Due to $\dot{H}$ in the outer integral, the second term remains small when $\dot{H} \to 0$, so $\psi_{\rm s}$ is well behaved when the equation of state w crosses -1. Nevertheless, $\psi_{\rm s}$ grows exponentially near the bounce to match the value of $\mathcal{R}$.

Specifically, Eq. (4.62) can be evaluated as follows. Denote

$$\psi_{\rm s}^{\rm const} + \psi_{\rm s}^{\rm int} \equiv C_1(k) + C_2(k) \int_0^t dt' \dot{H} \cdot I(t') \,, \tag{4.63}$$

where $I(t')$ is the inner integral in (4.62). In the kinetic phase, similar to Eq. (4.51), $I(t')$ can be computed as

$$I(t') \equiv \int_0^{t'} dt'' \frac{c_s^2 H}{2a^3 \dot{H}} \approx \frac{H_{\rm c}}{2a_{\rm c}^3} \int \frac{dX/X}{(-V_{,\phi})\sqrt{2X}} \xrightarrow{t' \to t_{\rm c}} \frac{1}{3a_{\text{ek-end}}^3} \Big(\frac{V_{\rm c}}{-V_{,\phi_{\rm c}}}\Big) \frac{1}{|H_{\rm c}|\sqrt{2X_{\rm c}}} \,. \tag{4.64}$$

But since $\dot{H} \to 0$ in the outer integral in (4.63), $\psi_{\rm s}^{\rm int}$ does not grow when $t' \to t_{\rm c}$. Then in the bouncing phase, as for Eqs. (4.55) and (4.57), $I(t')$ can be found to stay nearly constant,

$$\Delta I \approx \int_{X_{\rm c}}^{X} \frac{H}{2a^3 \dot{T}} \frac{dX}{X} \lesssim \frac{1}{3a_{\text{ek-end}}^3} \Big(\frac{V_{\rm c}}{-V_{,\phi_{\rm c}}}\Big) \frac{1}{|H_{\rm c}|\sqrt{2X_{\rm c}}} \Big|\frac{\Delta X}{2X_{\rm c}}\Big| \ll I(t_{\rm c}). \tag{4.65}$$

Therefore it contributes a constant factor to the outer integral in (4.63),

$$\psi_{\rm s}^{\rm int} \approx C_2(k) \int_0^t dt' \dot{H} \, \frac{1}{3a_{\text{ek-end}}^3} \Big(\frac{V_{\rm c}}{-V_{,\phi_{\rm c}}}\Big) \frac{1}{|H_{\rm c}|\sqrt{2X_{\rm c}}} \approx \frac{C_2(k)}{3a_{\text{ek-end}}^3} \Big(\frac{V_{\rm c}}{-V_{,\phi_{\rm c}}}\Big) \frac{1}{\sqrt{2X_{\rm c}}} \int_{H_{\rm c}}^{H} \frac{dH}{|H_{\rm c}|} \,. \tag{4.66}$$

Clearly when $H \to 0$ near the bounce, $\psi_{\rm s}^{\rm int}$ approaches the same value as $\mathcal{R}^{\rm int}$, given by Eq. (4.51), which is exponentially large and nonlinear for a wide range of k modes.

From the above derivation we see that $\psi_{\rm s}$ becomes exponentially large near the bounce when $|H| \ll |H_{\rm c}|$. This corresponds to $|t - t_0| \ll 1/|H_{\rm c}|$ in the bouncing solution (4.17), which is within the last e-fold before the bounce. We shall see below that by this time the anisotropy would have grown exponentially large as well.

4.3 Anisotropy and nonsingular bounce

As explained in Section 3.1.2, anisotropy is described by the shear tensor $\sigma^i{}_j$. In linear perturbation theory, the shear is given by Eq. (3.41), with both scalar and vector contributions. The vector shear perturbation $\sigma_i^{\rm V}$ is not sourced by the scalar

field, hence follows very simple behavior. By Eq. (3.103), one finds $\sigma_i^{\rm V} \propto \frac{1}{a^2}$, and hence $\sigma^{{\rm V}i}{}_j = \frac{1}{a^2}\,\sigma_{ij}^{\rm V} = \frac{1}{a}\,\sigma_{(i,j)}^{\rm V} \propto \frac{1}{a^3}$, in agreement with (3.33).

The scalar shear perturbation is given by $\sigma^{\rm S} \equiv E' - B$. In the comoving gauge, the shear perturbation $\sigma_{\rm c}$ can be obtained from the comoving curvature perturbation $\mathcal{R}$ through Eqs. (3.62, 3.63),

$$\sigma_{\rm c} = \frac{\mathcal{H}' - \mathcal{H}^2}{c_s^2 k^2 \mathcal{H}^2}\mathcal{R}' - \frac{\mathcal{R}}{\mathcal{H}}\,. \tag{4.67}$$

Since $\mathcal{R}$ undergoes exponential amplification right before the bouncing phase when w crosses -1, we expect the comoving shear perturbation $\sigma_{\rm c}$ to follow the same growth. Indeed, using Eqs. (4.38) and (4.37), one finds, up to order $\mathcal{O}(k^{1/2})$,

$$\sigma_{\rm c} = -\frac{C_2(k)}{2k^2a^2} - \frac{C_1(k)}{a^2}\int_0^t dt' a + \frac{C_2(k)}{a^2}\bigg(\frac{a}{H}\int_0^t dt' \frac{c_s^2 H^2}{2a^3\dot{H}} + \int_0^t dt' \frac{a\dot{H}}{H^2}\int_0^{t'} dt'' \frac{c_s^2 H^2}{2a^3\dot{H}}\bigg). \tag{4.68}$$

Along the same lines as for Eqs. (4.51) and (4.62), we see that the third term increases exponentially as $\dot{H} \to 0$, while the fourth and all higher order terms are well behaved and finite. Compared to the leading term, $\sigma_{\rm c}$ becomes dominated by the third term which surpasses the leading term by a factor

$$\frac{\sigma_{\rm c}|_{w\to -1}}{\sigma_{\rm c}|_{\text{ek-end}}} \approx \frac{2k^2}{3(aH)^2_{\text{ek-end}}}\Big(\frac{V_{\rm c}}{-V_{,\phi_{\rm c}}}\Big)\sqrt{\frac{X_{\text{ek-end}}}{2\epsilon X_{\rm c}}} \sim e^{N-2N_k}. \tag{4.69}$$

Note that this is the same exponential factor as in (4.53).

Like for $\mathcal{R}$, this huge growth factor does not imply the breakdown of perturbation theory at this point. Indeed, in the synchronous gauge, the shear perturbation $\sigma_{\rm s}$ remains small until near the bounce. $\sigma_{\rm s}$ can be related to the comoving shear perturbation $\sigma_{\rm c}$ through the gauge transformation (3.83). After the mode exits the horizon, using Eqs. (4.68), one finds

$$\begin{aligned}
\sigma_{\rm s} &= \sigma_{\rm c} - \frac{C_2(k)}{a}\int_0^t dt' \frac{c_s^2 H}{2a^3\dot{H}} \\
&= -\frac{C_2(k)}{2k^2a^2} - \frac{C_1(k)}{a^2}\int_0^t dt' a + \frac{C_2(k)}{a^2}\bigg(\int_0^t dt' \frac{a\dot{H}}{H^2}\int_0^{t'} dt'' \frac{c_s^2 H^2}{2a^3\dot{H}} - a\int_0^t dt' \frac{\dot{H}}{H^2}\int_0^{t'} dt'' \frac{c_s^2 H^2}{2a^3\dot{H}}\bigg) \\
&= -\frac{C_2(k)}{2k^2a^2} - \frac{C_1(k)}{a^2}\int_0^t dt' a - \frac{C_2(k)}{a^2}\int_0^t dt' aH \int_0^{t'} dt'' \frac{\dot{H}}{H^2}\int_0^{t''} dt''' \frac{c_s^2 H^2}{2a^3\dot{H}}\,.
\end{aligned} \tag{4.70}$$

From the first to the second line the growing (third) term in $\sigma_{\rm c}$ is absorbed by the gauge transformation term, leaving behind an integral that is well behaved as $\dot{H} \to 0$. In the bouncing phase, using similar calculations that lead to (4.66), $\sigma_{\rm s}$ can be evaluated as

$$\sigma_{\rm s} \approx -\frac{C_2(k)}{2k^2a^2} - \frac{C_1(k)}{a^2}\int_0^t dt' a - \frac{C_2(k)}{a^2}\int_0^t dt' aH \cdot \frac{1}{H}\frac{1}{3a^3_{\text{ek-end}}}\Big(\frac{V_{\rm c}}{-V_{,\phi_{\rm c}}}\Big)\frac{1}{\sqrt{2X_{\rm c}}}$$

$$\approx -\frac{C_2(k)}{2k^2a^2} - \left[C_1(k) + \frac{C_2(k)}{3a^3_{\text{ek-end}}}\frac{(-V_{\rm c}/V_{,\phi_{\rm c}})}{\sqrt{2X_{\rm c}}}\right]\frac{1}{a^2}\int_0^t dt' a$$
$$\approx -\frac{C_2(k)}{2k^2a^2} - \frac{C_1(k)}{a^2}\frac{a_{\text{bp-beg}}}{|H_{\rm c}|} - \frac{1}{a^2}\frac{C_2(k)}{3a^2_{\text{ek-end}}}\frac{(-V_{\rm c}/V_{,\phi_{\rm c}})}{|H_{\rm c}|\sqrt{2X_{\rm c}}}\,. \tag{4.71}$$

The integral in the second line is found by using (4.23), which rapidly converges to the constant value $\approx a_{\text{bp-beg}}/|H_{\rm c}|$. From the last line we see that all three terms scale equally as $1/a^2$ near the bounce, which leads to $\sigma_{\rm s}{}^i{}_j = \frac{1}{a}\big(\sigma_{{\rm s},ij} - \frac{1}{3}\delta_{ij}\nabla^2\sigma_{\rm s}\big) \propto \frac{1}{a^3}$, in agreement with (3.33). The third term in (4.71) dominates over the first (and second) term by a factor

$$\frac{2k^2}{3a^2_{\text{ek-end}}}\frac{(-V_{\rm c}/V_{,\phi_{\rm c}})}{|H_{\rm c}|\sqrt{2X_{\rm c}}} \sim \frac{k^2}{(aH)^2_{\text{ek-end}}}\sqrt{\frac{X_{\text{ek-end}}}{X_{\rm c}}} \sim e^{N-2N_k}, \tag{4.72}$$

similar to (4.69) but only at a much later time near the end of the bouncing phase.

To see whether the resulting anisotropy grows nonlinear, we estimate the size of the anisotropy by computing the auto-correlation function of the shear perturbation,

$$\langle(\sigma^{\rm S})^2\rangle = \langle\tfrac{1}{2}\,\sigma^{{\rm S}ij}(\vec{x})\,\sigma^{\rm S}_{ij}(\vec{x})\rangle = \int\frac{d^3k}{(2\pi)^3}\,\frac{1}{2a^2}\Big|\big(-k_ik_j+\tfrac{1}{3}\delta_{ij}k^2\big)\sigma^{\rm S}_k\Big|^2 = \int\frac{1}{6\pi^2a^2}\,|\sigma^{\rm S}_k|^2\,k^6dk. \tag{4.73}$$

The integration is carried over the modes that exit the horizon in the second half of the ekpyrotic phase, i.e. those with $0 < N_k < N/2$ that are dominated by the third term in (4.71). Modes with $N_k > N/2$ are negligible since the power spectrum of $\sigma^{\rm S}$ is very blue, whereas modes with $N_k < 0$ remain inside the horizon and have no classical contribution. Therefore, a lower estimate of the anisotropy is

$$\langle(\sigma^{\rm S})^2\rangle \gtrsim \int_{e^{-N/2}k_{\max}}^{k_{\max}}\frac{1}{6\pi^2a^6}\Big|\frac{C_2(k)}{3a^2_{\text{ek-end}}}\frac{(-V_{\rm c}/V_{,\phi_{\rm c}})}{|H_{\rm c}|\sqrt{2X_{\rm c}}}\Big|^2\,k^6dk \approx \frac{1}{108\pi^2a^6}\frac{(-V_{\rm c}/V_{,\phi_{\rm c}})^2}{a^4_{\text{ek-end}}H^2_{\rm c}X_{\rm c}}\int^{k_{\max}}|C_2(k)|^2k^6dk$$
$$\approx \frac{1}{108\pi^2a^6}\frac{(-V_{\rm c}/V_{,\phi_{\rm c}})^2}{a^4_{\text{ek-end}}H^2_{\text{ek-end}}X_{\rm c}}\,\epsilon a^2_{\text{ek-end}}\frac{(aH)^8_{\text{ek-end}}}{8} \sim \frac{a^6_{\text{ek-end}}}{a^6}\Big(\frac{V_{\rm c}}{-V_{,\phi_{\rm c}}}\Big)^2\frac{X_{\text{ek-end}}}{X_{\rm c}}H^4_{\text{ek-end}}, \tag{4.74}$$

where $k_{\max} \equiv (aH)_{\text{ek-end}}$, and we used the expression (4.42) for $C_2(k)$. Near the bounce, using Eq. (4.24), the above estimate becomes

$$\langle(\sigma^{\rm S})^2\rangle_{\text{bp-end}} \gtrsim \frac{a^6_{\text{bp-beg}}}{a^6_{\text{bp-end}}}\,e^{2N}\,H^4_{\text{ek-end}} \sim V_{\rm c}^2\,e^{4N}. \tag{4.75}$$

For anisotropy to not become a problem, condition (4.33) requires $\sigma^2_{\text{bp-end}} \lesssim V_{\rm c}$. This can be satisfied only if $V_{\rm c}^2\,e^{4N} \lesssim V_{\rm c}$, or $V_{\rm c} \lesssim e^{-4N}$ in reduced Planck units. However, in order for the primordial density fluctuation to match the observed amplitude, the bottom of the potential $V_{\text{ek-end}}$ needs to satisfy $\sqrt{2\epsilon V_{\text{ek-end}}} \sim 10^{-3}M^2_{\rm Pl}$ [98], which

implies $V_{\rm c} \approx \frac{3}{\epsilon} V_{\text{ek-end}} \sim 10^{-6}/\epsilon^2$. For a typical value of $\epsilon \sim 10^2$ [85], these conditions are far from being satisfied consistently.

Let us comment on the gauge choice for computing (4.74). Recall that condition (4.33) is obtained by using the Friedmann equations for a homogeneous universe. In the inhomogeneous case, the Friedmann equations are generalized to Eqs. (3.26, 3.27) for the local expansion $\theta/3$. In order to apply condition (4.33), it is preferable to use the uniform Hubble gauge in which $\theta/3$ is equal to H. The scalar shear perturbation in the uniform Hubble gauge can be computed through (3.98) and is of the same order of magnitude as the synchronous shear perturbation $\sigma_{\rm s}$. It is worth mentioning the Newtonian gauge in which the shear perturbation $\sigma^{\rm S}$ is set to zero identically. This does not mean that the bounce is free from problems. According to Eq. (3.91), the variation of the local Hubble parameter is given by

$$\delta\mathcal{H} = -(\mathcal{H}' - \mathcal{H}^2)\delta u + \tfrac{1}{3}\nabla^2\sigma^{\rm S} \,. \tag{4.76}$$

In the Newtonian gauge, though $\sigma^{\rm S} = 0$, the velocity perturbation $\overline{\delta u}$, given by Eq. (3.73), would grow exponentially due to Eq. (4.69). Therefore the local Hubble parameter is extremely inhomogeneous in space, which means the nonsingular bounce is not reached even though the background value H appears to vanish.

In a consistent perturbative analysis, the σ^2 term in the Friedmann equations should be negligible at linear order. The exponentially large $\langle(\sigma^{\rm S})^2\rangle$ in (4.74) indicates that the perturbation theory may become invalid. Once the anisotropy becomes nonlinear and dominates the total energy density, the universe would be driven to a chaotic mixmaster that ends up in an extremely inhomogeneous and anisotropic big crunch [112, 18].

4.4 Discussions

We have identified four different problems in this bouncing model that connects an ekpyrotic contraction to a nonsingular bounce by means of ghost condensation:

• Gradient instability is caused by $c_s^2 < 0$ in the bouncing phase. Fine-tuning is required to make c_s^2 exponentially small, as in (4.61). Alternatively, it has been proposed that generalizing the ghost condensation model to the galileon model [124, 40, 27] may remove this problem.

• Classical anisotropy that is suppressed during the ekpyrotic phase is exponentially amplified to an even greater amount during the bouncing phase. This creates a problem for the nonsingular bounce unless the initial anisotropy present before the ekpyrotic phase is fine-tuned to an extremely small value given by (4.35). This can be achieved by having a dark energy phase before the ekpyrotic phase, as in [132, 135].

• A sub-subdominant component of curvature perturbation generated from quantum fluctuations in the ekpyrotic phase grows exponentially when the equation of state w passes through -1. It dominates over the scale-invariant component and results in a blue power spectrum that is inconsistent with observations.

• The shear perturbation generated from quantum fluctuations in the ekpyrotic phase

grows exponentially during the bouncing phase and causes a large anisotropy that disrupts the nonsingular bounce. This problem is due to both the equation of state w dropping below -1 and the scale factor a decreasing exponentially in the bouncing phase.
It is worth noting that none of the above problems appear in a singular bounce, such as the cyclic model [132, 135], because c_s^2 is always positive and w remains greater than 1.

The problems of the nonsingular bounce considered here are mainly due to the clash between the high energy density near the end of the ekpyrotic phase and the low energy scale associated with the ghost condensation. Indeed, from Eqs. (4.52) and (4.69) it is clear that the growth of both curvature and anisotropy are proportional to the same factor $X_{\text{ek-end}}/X_{\text{c}}$. By Eq. (4.1), these energy scales have to satisfy the relation $X_{\text{ek-end}} \gg X_{\text{c}}$. Our calculation illustrates how this large factor shows up in relevant physical quantities and leads to the four problems listed above.

Therefore, it proves difficult to combine an ekpyrotic contraction phase with $w \gg 1$ and a nonsingular bouncing phase with $w < -1$ by a single scalar field. In the next Chapter, we consider another approach that uses a separate scalar field to induce the bounce. Such a setup would necessarily involve certain degree of fine-tuning during the contraction phase, as discussed at the beginning of Section 4.1. Nevertheless, our purpose is to first see if the bouncing phase can keep curvature and anisotropy from growing nonlinear.

Chapter 5

Numerical Computations

In this Chapter we study a nonsingular bounce based on the ghost field model described in Section 2.3.2. Nonperturbative numerical methods are used to compute the classical evolution of the universe from near the end of the contraction phase through the bounce into the expansion phase. The Einstein equations are solved by using harmonic coordinates, and the amplitude of adiabatic perturbations is calculated by using the covariant formalism. We show that the bounce is disrupted in regions of the universe with large inhomogeneity and anisotropy, but is achieved in regions that are relatively homogeneous and isotropic. Sufficiently small perturbations can pass through the nonsingular bounce with negligible nonlinearity. Despite the fine-tuning required to keep a stable contraction phase, the nonsingular bounce succeeds in maintaining a nearly scale-invariant power spectrum [146].

5.1 Matter-like contraction and nonsingular bounce

The nonsingular bounce is described by a model with a canonical scalar field ϕ and a ghost field χ,

$$\mathcal{L} = -\tfrac{1}{2}(\partial\phi)^2 - V(\phi) + \tfrac{1}{2}(\partial\chi)^2. \tag{5.1}$$

Here ϕ is a canonical scalar field with a potential $V(\phi) = V_0\, e^{-c\phi}$, whereas χ is a ghost field with a wrong-signed kinetic term. The conditions are chosen so that the universe is dominated by the normal scalar field ϕ during the contraction phase. Under such conditions, the ϕ field has a scaling solution given by Eqs. (2.23, 2.24), with a constant equation of state $w_\phi = \frac{c^2}{3} - 1$. For $c > \sqrt{6}$ and $V_0 < 0$, this solution is an ekpyrotic attractor with $w_\phi > 1$, as described in Section 2.2. Here we consider the other case with $c < \sqrt{6}$ and $V_0 > 0$, so that $w_\phi < 1$ and a nonsingular bounce can be obtained, as described in Section 2.3.2. In this case, the scaling solution is *not* an attractor – the initial condition must be fine-tuned in order to keep w_ϕ nearly constant for a sustained period.

Our computation starts near the end of the contraction phase, assuming that the ϕ field has w_ϕ given by the scaling solution and the χ field has negligible energy density. Since the χ field has an equation of state $w_\chi = 1$ that is greater than w_ϕ, the negative energy density of the χ field grows faster than the positive energy density of the ϕ

field during the contraction. Eventually the total energy density vanishes and causes a nonsingular bounce, at which point the contraction stops and the expansion begins. Then the energy density of the χ field quickly diminishes and becomes negligible again compared to that of the ϕ field.

In a homogeneous, flat, and isotropic background, the equations of motion for the scalar fields are

$$\phi'' + a^6 V_{,\phi} = 0, \tag{5.2}$$

$$\chi'' = 0. \tag{5.3}$$

Here $'$ denotes the derivative with respect to the *harmonic time* τ, related to the physical time t by $dt = a^3 d\tau$; it is chosen to satisfy the gauge condition (5.37), as introduced in Section 5.2 below. The Friedmann equations in the harmonic time are given by

$$\mathcal{H}^2 = \tfrac{1}{3}\big(\tfrac{1}{2}\phi'^2 + a^6 V - \tfrac{1}{2}\chi'^2\big), \tag{5.4}$$

$$\mathcal{H}' = a^6 V, \tag{5.5}$$

where the *harmonic Hubble parameter* $\mathcal{H}$ is defined as $\mathcal{H} \equiv a'/a$.

The background solution can be found by evolving Eqs. (5.2, 5.3, 5.5) and using (5.4) as a constraint. The initial values for ϕ, ϕ', χ, χ', a, and $\mathcal{H}$ are set by

$$\phi(0) \equiv \phi_0 = 0, \quad \phi'(0) \equiv a_0^3 \dot{\phi}_0 = -a_0^3 \sqrt{\frac{2c^2 V_0}{6 - c^2}}, \tag{5.6}$$

$$\chi(0) \equiv \chi_0 = 0, \quad \chi'(0) \equiv a_0^3 \dot{\chi}_0 = a_0^3 \sqrt{\frac{12 V_0}{(6 - c^2) r_0}}, \tag{5.7}$$

$$a(0) \equiv a_0 = 1, \quad \mathcal{H}(0) \equiv a_0^3 H_0 = -a_0^3 \sqrt{\frac{2V_0(r_0 - 1)}{(6 - c^2) r_0}}, \tag{5.8}$$

We choose $c = \sqrt{3}$ so that initially the ϕ field obeys the scaling relation (2.24) with a matter-like equation of state, $w_\phi = 0$; r_0 represents the initial value of the ratio between the energy density of the ϕ field and the χ field, $|\rho_\phi/\rho_\chi|$. For $V_0 = 0.1$ and $r_0 = 1000$, the bouncing solution for the scale factor a is shown in Fig. 5.1. The ratio between the energy density of the ϕ and χ fields is shown in Fig. 5.2, illustrating that the χ field is only significant near the bounce.

The ghost field χ must be stabilized by some mechanism at the quantum level, which will not be considered in this thesis. Here we only use its classical equation of motion to effectively describe the nonsingular bouncing process. This simple setup allows us to study the classical evolution of adiabatic modes that have left the horizon during the contraction phase. In particular, we will follow the amplitude of the curvature perturbation as it passes through the nonsingular bounce.

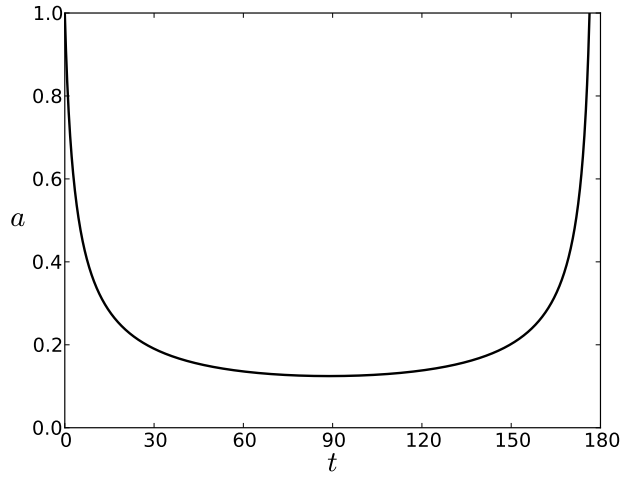

Figure 5.1: Background solution of the scale factor a as a function of harmonic time.

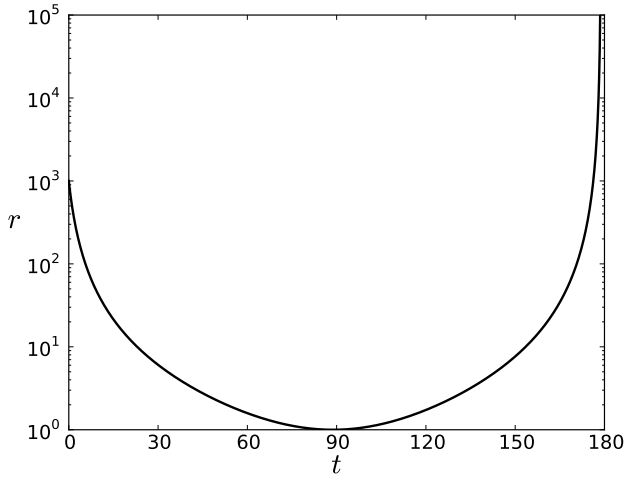

Figure 5.2: The ratio between the energy density of the scalar fields ϕ and χ. The χ field energy density is significant only near the bounce and otherwise negligible.

In the following we first present the calculation of the adiabatic perturbations using linear perturbation theory. This will serve as a comparison to our fully non-perturbative analysis presented in the later Sections. In particular, we introduce the *harmonic gauge* for linear perturbations, in accordance with the harmonic coordinates used in our numerical computations in Section 5.2.

In harmonic time τ, the metric (3.34) with scalar perturbations can be written as

$$ds^2 = -a^6(1+2A)d\tau^2 + 2a^4 B_{,i} d\tau dx^i + a^2\big((1-2\psi)\delta_{ij} + 2E_{,ij}\big)dx^i dx^j . \tag{5.9}$$

At linear order, the harmonic gauge condition (5.38) is given by

$$\mathcal{C}^0 \equiv A' + 3\psi' - \nabla^2(E' - a^2 B) = 0 , \tag{5.10}$$

$$\mathcal{C} \equiv (a^2 B)' + a^4(A - \psi - \nabla^2 E) = 0 . \tag{5.11}$$

Under the infinitesimal coordinate transformation (3.53), the constraints $\mathcal{C}^0, \mathcal{C}$ become

$$\mathcal{C}^0 \to \mathcal{C}^0 - (\xi^0)'' + a^4 \nabla^2 \xi^0 , \tag{5.12}$$

$$\mathcal{C} \to \mathcal{C} - \xi'' + a^4 \nabla^2 \xi . \tag{5.13}$$

Therefore, to transform into the harmonic gauge, one needs to solve a wave equation for each ξ^0 and ξ. Such solutions do exist for the bouncing background, hence the harmonic gauge is well defined throughout the bouncing phase. Note that the harmonic gauge has a residual gauge freedom allowed by homogeneous solutions to the wave equations for ξ^0 and ξ.

The linearized Einstein equations (3.46 - 3.49) become

$$3\mathcal{H}\psi' + \mathcal{H}' A - a^4 \nabla^2 \psi - \mathcal{H}\nabla^2(E' - a^2 B) = -\tfrac{1}{2}(\phi'\delta\phi' - \chi'\delta\chi') - \tfrac{1}{2}a^6 V_{,\phi}\delta\phi , \tag{5.14}$$

$$\psi' + \mathcal{H} A = \tfrac{1}{2}(\phi'\delta\phi - \chi'\delta\chi) , \tag{5.15}$$

$$a^4\psi - a^4 A + (E' - a^2 B)' = 0 , \tag{5.16}$$

$$\psi'' + \mathcal{H}A' + \mathcal{H}' A = \tfrac{1}{2}(\phi'\delta\phi' - \chi'\delta\chi') - \tfrac{1}{2}a^6 V_{,\phi}\delta\phi . \tag{5.17}$$

In addition, the equations of motion for the scalar field perturbations $\delta\phi$ and $\delta\chi$ are

$$\delta\phi'' - a^4\nabla^2\delta\phi + a^6 V_{,\phi\phi}\delta\phi + 2a^6 V_{,\phi} A - \phi'\big(A' + 3\psi' - \nabla^2(E' - a^2 B)\big) = 0 , \tag{5.18}$$

$$\delta\chi'' - a^4\nabla^2\delta\chi - \chi'\big(A' + 3\psi' - \nabla^2(E' - a^2 B)\big) = 0 . \tag{5.19}$$

Eq. (5.17) is redundant since it can be derived from (5.15). Eq. (5.14) serves as the Hamiltonian constraint, whereas Eq. (5.15) is the momentum constraint.

Specifying to the harmonic gauge, Eq. (5.10) becomes a dynamical equation for A, and Eq. (5.11) for B. The complete set of equations are then given by, for a single Fourier mode with wavenumber k,

$$A' + 3\psi' + k^2(E' - a^2 B) = 0 , \tag{5.20}$$

$$B' + 2\mathcal{H}B + a^2(A - \psi + k^2 E) = 0\,, \tag{5.21}$$

$$\psi' + \mathcal{H}A = \tfrac{1}{2}(\phi'\delta\phi - \chi'\delta\chi)\,, \tag{5.22}$$

$$E'' + a^4 k^2 E = 0\,, \tag{5.23}$$

$$\delta\phi'' + a^4 k^2 \delta\phi + a^6 V_{,\phi\phi}\delta\phi + 2a^6 V_{,\phi} A = 0\,, \tag{5.24}$$

$$\delta\chi'' + a^4 k^2 \delta\chi = 0\,, \tag{5.25}$$

with a constraint coming from Eqs. (5.14, 5.15),

$$-\tfrac{1}{2}(\phi'^2 - \chi'^2)A + a^4 k^2 \psi + \mathcal{H}k^2(E' - a^2 B) + \tfrac{1}{2}(\phi'\delta\phi' - \chi'\delta\chi') + \tfrac{3}{2}\mathcal{H}(\phi'\delta\phi - \chi'\delta\chi) + \tfrac{1}{2}a^6 V_{,\phi}\delta\phi = 0. \tag{5.26}$$

The initial values for $\delta\phi$, $\delta\phi'$, $\delta\chi$, $\delta\chi'$, A, B, ψ, E, and E' are chosen to agree with the initial data for our numerical computation in the next Section, Eqs. (5.61 - 5.70). At linear order,

$$A(0) = 0, \qquad B(0) = 0, \tag{5.27}$$

$$\psi(0) = -2\delta\Psi, \qquad E(0) = 0, \tag{5.28}$$

$$\delta\phi(0) = f_1, \qquad \delta\phi'(0) = a_0^3(f_0 - 6\dot{\phi}_0\delta\Psi), \tag{5.29}$$

$$\delta\chi(0) = f_3, \qquad \delta\chi'(0) = a_0^3(f_2 - 6\dot{\chi}_0\delta\Psi), \tag{5.30}$$

and $E'(0)$ is given by the constraint equation (5.26). Here $\delta\Psi$ is given by the conformal factor Ψ in Eq. (5.53) expanded to linear order,

$$\delta\Psi = \frac{\dot{\phi}_0 f_0 - \dot{\chi}_0 f_2 - cV_0 f_1}{4(9H_0^2 - 3V_0 + k^2/a_0^2)}\,, \tag{5.31}$$

and the parameters f_0 - f_3 are specified in the next Section. Note that the above initial values satisfy the relation

$$\psi(0) = -\frac{1}{2a_0 k^2}\big(\dot{\phi}_0\delta\phi'(0) - \dot{\chi}_0\delta\chi'(0) + a_0^3 V_0'\delta\phi(0)\big)\,, \tag{5.32}$$

which makes the initial time slice a constant mean curvature surface, as chosen in our numerical computations.

5.2 Inhomogeneity and anisotropy

To analyze the above nonsingular bouncing model nonperturbatively, we employ numerical methods to solve the equations for the spacetime metric and the scalar fields. Our methods allow a wide range of inhomogeneous, nonflat, and anisotropic initial conditions.

Consider a coordinate system $(x^\mu) = (\tau, x^i)$, where τ is a timelike coordinate and x^i are spacelike coordinates. The full set of equations include the Einstein equations

for the metric $g_{\mu\nu}$ and the equations of motion for the scalar fields ϕ and χ. From the Lagrangian (5.1) it follows that the ϕ and χ fields satisfy the equations

$$\nabla_\alpha \nabla^\alpha \phi = V'(\phi)\,, \tag{5.33}$$

$$\nabla_\alpha \nabla^\alpha \chi = 0\,, \tag{5.34}$$

where ∇_μ is the covariant derivative associated with $g_{\mu\nu}$. The total stress-energy tensor is given by

$$T_{\alpha\beta} = \nabla_\alpha\phi\,\nabla_\beta\phi - \nabla_\alpha\chi\,\nabla_\beta\chi - g_{\alpha\beta}\left(\tfrac{1}{2}\nabla^\gamma\phi\,\nabla_\gamma\phi + V - \tfrac{1}{2}\nabla^\gamma\chi\,\nabla_\gamma\chi\right). \tag{5.35}$$

Hence the Einstein equations can be written in the trace reversed form as

$$R_{\alpha\beta} = \nabla_\alpha\phi\,\nabla_\beta\phi - \nabla_\alpha\chi\,\nabla_\beta\chi + V g_{\alpha\beta}\,, \tag{5.36}$$

where we use reduced Planck units with $8\pi G \equiv 1$.

To solve the Einstein equations, one must first remove the diffeomorphic freedom in the coordinates by fixing a gauge. This involves choosing a set of time slices, such as the constant mean curvature slices used in simulating the ekpyrotic contraction phase [53]. However, the same method is not applicable to the bouncing phase. The mean curvature becomes non-monotonic in time when the universe enters the bouncing phase from the contraction phase, and when it exits the bouncing phase to enter the expansion phase. Consequently, in the presence of inhomogeneities, the constant mean curvature slices stop being spacelike during these transitions (see Section 5.3), rendering the numerical evolution ill-behaved. So instead, we shall use a different gauge that is well-defined throughout the entire cosmic transition from contraction to expansion – the *harmonic gauge* [52, 123, 103].

The harmonic coordinates are defined to satisfy the gauge condition

$$\nabla_\alpha \nabla^\alpha x^\mu = 0\,. \tag{5.37}$$

Consequently, the Christoffel symbols $\Gamma^\gamma{}_{\alpha\beta}$ must satisfy the condition

$$g^{\alpha\beta}\Gamma^\gamma{}_{\alpha\beta} = 0\,. \tag{5.38}$$

Under this condition, the Ricci tensor takes the form

$$R_{\alpha\beta} = -\tfrac{1}{2}g^{\gamma\sigma}\partial_\gamma\partial_\sigma g_{\alpha\beta} + g^{\lambda\mu}g^{\rho\nu}\partial_\mu g_{\nu(\alpha}\partial_{\beta)}g_{\lambda\rho} - \Gamma^\gamma{}_{\sigma\alpha}\Gamma^\sigma{}_{\gamma\beta}\,. \tag{5.39}$$

The first term controls the character of the equations, giving rise to hyperbolic differential equations for the metric components $g_{\alpha\beta}$. These 10 equations are subject to the 4 constraints given by (5.38).

To solve the equations numerically, we first reduce them to first order differential equations in time. Define the variables $P_{\alpha\beta}$, P_ϕ, and P_χ by

$$P_{\alpha\beta} \equiv \partial_0 g_{\alpha\beta}\,, \tag{5.40}$$

$$P_\phi \equiv \partial_0 \phi \,, \tag{5.41}$$

$$P_\chi \equiv \partial_0 \chi \,. \tag{5.42}$$

Then the Einstein equations (5.36) become

$$\begin{aligned} -g^{00}\partial_0 P_{\alpha\beta} = {} & 2g^{0k}\partial_k P_{\alpha\beta} + g^{ik}\partial_i\partial_k g_{\alpha\beta} - 2g^{\lambda\mu}g^{\rho\nu}\partial_\mu g_{\nu(\alpha}\partial_{\beta)}g_{\lambda\rho} \\ & + 2\Gamma^\gamma{}_{\sigma\alpha}\Gamma^\sigma{}_{\gamma\beta} + 2\left(\partial_\alpha\phi\partial_\beta\phi - \partial_\alpha\chi\partial_\beta\chi + V g_{\alpha\beta}\right) \,, \end{aligned} \tag{5.43}$$

and the equations (5.33, 5.34) for ϕ and χ become

$$-g^{00}\partial_0 P_\phi = 2g^{0k}\partial_k P_\phi + g^{ik}\partial_i\partial_k\phi - V'(\phi) \,, \tag{5.44}$$

$$-g^{00}\partial_0 P_\chi = 2g^{0k}\partial_k P_\chi + g^{ik}\partial_i\partial_k\chi \,. \tag{5.45}$$

To specify initial data, we choose the initial time slice to have constant mean curvature, $K = -3H_0$. The full metric $g_{\mu\nu}$ can be decomposed as

$$ds^2 = -\alpha^2 d\tau^2 + \gamma_{ij}(\beta^i d\tau + dx^i)(\beta^j d\tau + dx^j) \,, \tag{5.46}$$

where α, β^i are the lapse function and the shift vector, and γ_{ij} is the spatial metric on the constant time slice. We can freely choose the lapse and the shift to be $\alpha = 1$ and $\beta^i = 0$ initially, then the spatial metric γ_{ij} and its time derivative $\partial_0\gamma_{ij} = -2K_{ij}$ must satisfy the Hamiltonian and momentum constraints,

$${}^{(3)}R + K^2 - K^{ij}K_{ij} = \dot\phi^2 + D^i\phi\, D_i\phi + 2V - \dot\chi^2 - D^i\chi\, D_i\chi \,, \tag{5.47}$$

$$D_i K^i{}_j - D_j K = -\dot\phi\, D_j\phi + \dot\chi\, D_j\chi \,. \tag{5.48}$$

Here ${}^{(3)}R$ and K_{ij} are the intrinsic and extrinsic curvature; $\dot{}$ denotes the derivative along the normal vector to the time slice, and D_i is the covariant derivative associated with γ_{ij}. Once the above constraints are satisfied by the initial data, they will hold at all times as a result of the harmonic coordinate condition [103].

The constraint equations (5.47, 5.48) can be solved by using the York method [149, 60]. Specifically, we choose the spatial metric to be conformally flat, and decompose the extrinsic curvature into the trace (i.e. mean curvature) and the traceless parts,

$$\gamma_{ij} \equiv \Psi^4 \delta_{ij} \,, \tag{5.49}$$

$$K_{ij} \equiv \tfrac{1}{3} K \gamma_{ij} + \Psi^{-2} A_{ij} \,. \tag{5.50}$$

Define further the variables Q_ϕ and Q_χ by

$$Q_\phi \equiv \Psi^6 \dot\phi \,, \tag{5.51}$$

$$Q_\chi \equiv \Psi^6 \dot\chi \,. \tag{5.52}$$

The Hamiltonian and momentum constraints then become

$$\partial^i\partial_i\Psi = -\tfrac{1}{8}\big(A^{ij}A_{ij} + {Q_\phi}^2 - {Q_\chi}^2\big)\Psi^{-7} + \tfrac{1}{12}(K^2 - 3V)\Psi^5 - \tfrac{1}{8}\left(\partial^i\phi\,\partial_i\phi - \partial^i\chi\,\partial_i\chi\right)\Psi\,, \tag{5.53}$$

$$\partial^i A_{ij} = -Q_\phi\partial_j\phi + Q_\chi\partial_j\chi\,, \tag{5.54}$$

where the indices in these equations are raised and lowered with the flat metric δ_{ij}.

For simplicity, we restrict our computation to the case with inhomogeneity only along one spatial dimension (x) with periodic boundary conditions. Then Eq. (5.54) is solved by the following ansatz,

$$Q_\phi(x) = \dot\phi_0 + f_0\cos(mx)\,, \tag{5.55}$$

$$\phi(x) = \phi_0 + f_1\cos(mx)\,, \tag{5.56}$$

$$Q_\chi(x) = \dot\chi_0 + f_2\cos(mx)\,, \tag{5.57}$$

$$\chi(x) = \chi_0 + f_3\cos(mx)\,, \tag{5.58}$$

and the particular solution

$$A_{ij}(x) = \begin{pmatrix} A_{11}(x) & 0 & 0 \\ 0 & \lambda A_{11}(x) & 0 \\ 0 & 0 & -(1+\lambda)A_{11}(x) \end{pmatrix}\,, \tag{5.59}$$

where f_0, f_1, f_2, f_3, and λ are parameters to choose, and

$$A_{11}(x) = -\dot\phi_0 f_1\cos(mx) - \tfrac{1}{4}f_0 f_1\cos(2mx) + \dot\chi_0 f_3\cos(mx) + \tfrac{1}{4}f_2 f_3\cos(2mx)\,. \tag{5.60}$$

These expressions are then put into Eq. (5.53) to solve for $\Psi(x)$, using a relaxation method. The results are substituted into the expressions for γ_{ij} and its time derivative P_{ij}; the remaining components $g_{0\mu}$ are given by the lapse and the shift, and $P_{0\mu}$ are solved from the constraint (5.38).

Thus our initial data are specified as follows:

$$g_{00}(0,x) = -1\,, \tag{5.61}$$

$$g_{0i}(0,x) = g_{i0}(0,x) = 0\,, \tag{5.62}$$

$$g_{ij}(0,x) = \Psi(x)^4\delta_{ij}\,, \tag{5.63}$$

$$P_{00}(0,x) = 2K\,, \tag{5.64}$$

$$P_{0i}(0,x) = P_{i0}(0,x) = -2\Psi(x)^{-1}\partial_i\Psi(x)\,, \tag{5.65}$$

$$P_{ij}(0,x) = -\tfrac{2}{3}K\Psi(x)^4\delta_{ij} - 2\Psi(x)^{-2}A_{ij}(x)\,, \tag{5.66}$$

$$\phi(0,x) = \phi(x)\,, \tag{5.67}$$

$$P_\phi(0,x) = \Psi(x)^{-6}Q_\phi(x)\,, \tag{5.68}$$

$$\chi(0,x) = \chi(x)\,, \tag{5.69}$$

$$P_\chi(0,x) = \Psi(x)^{-6} Q_\chi(x)\,. \tag{5.70}$$

The parameters ϕ_0, $\dot\phi_0$, χ_0, $\dot\chi_0$ in (5.55 - 5.60) and $K = -3H_0$ are chosen to match the background values given in (5.6 - 5.8), whereas the parameters f_0, f_1, f_2, f_3, and λ will be set to incorporate different amounts of inhomogeneity in the initial data. In the limit of small inhomogeneities, our choice of initial data represents a single Fourier mode with comoving wavenumber $k = m$ (see Section 5.1). Notice however the terms with double wavenumber $k = 2m$ in Eq. (5.60), which represent small nonlinearities that are second order in f_i.

The ansatz (5.55 - 5.60) can also be generalized to include multiple modes. As an illustration, the ansatz for two Fourier modes $k = m_1$ and m_2 is given by

$$Q_\phi(x) = \dot\phi_0 + f_0 \cos(m_1 x + d_1) + g_0 \cos(m_2 x + d_2)\,, \tag{5.71}$$

$$\phi(x) = \phi_0 + f_1 \cos(m_1 x + d_1) + g_1 \cos(m_2 x + d_2)\,, \tag{5.72}$$

$$Q_\chi(x) = \dot\chi_0 + f_2 \cos(m_1 x + d_1) + g_2 \cos(m_2 x + d_2)\,, \tag{5.73}$$

$$\chi(x) = \chi_0 + f_3 \cos(m_1 x + d_1) + g_3 \cos(m_2 x + d_2)\,, \tag{5.74}$$

and

$$\begin{aligned} A_{11}(x) = &- \big(\dot\phi_0 f_1 - \dot\chi_0 f_3\big) \cos(m_1 x + d_1) - \tfrac{1}{4}\big(f_0 f_1 - f_2 f_3\big) \cos(2m_1 x + 2d_1) \\ &- \big(\dot\phi_0 g_1 - \dot\chi_0 g_3\big) \cos(m_2 x + d_2) - \tfrac{1}{4}\big(g_0 g_1 - g_2 g_3\big) \cos(2m_2 x + 2d_2) \\ &- \frac{(f_0 g_1 m_2 + f_1 g_0 m_1) - (f_2 g_3 m_2 + f_3 g_2 m_1)}{2(m_1 + m_2)} \cos\big((m_1 + m_2)x + (d_1 + d_2)\big) \\ &- \frac{(f_0 g_1 m_2 - f_1 g_0 m_1) - (f_2 g_3 m_2 - f_3 g_2 m_1)}{2(m_2 - m_1)} \cos\big((m_2 - m_1)x + (d_2 - d_1)\big)\,. \end{aligned} \tag{5.75}$$

The parameters f_0, f_1, f_2, f_3 specify the Fourier mode $k = m_1$ as before, whereas the new parameters g_0, g_1, g_2, g_3 are chosen to specify the second mode with $k = m_2$. Notice the appearance of mixed modes with $k = m_2 \pm m_1$ in (5.75); their amplitude is quadratically suppressed initially, just like the double wavenumber modes with $k = 2m_1$ and $2m_2$.

In our numerical computation, starting from the initial values (5.61 - 5.70), Eqs. (5.40 - 5.45) are evolved until one of the grid points first reaches future infinity. This is possible because the physical time $\tau = +\infty$ is compactified to a finite harmonic time t; indeed, for a homogeneous expansion with $a \sim \tau^{2/3(1+w)}$ and $w < 1$, the integral $t = \int a^{-3} d\tau$ converges at $\tau = +\infty$. The dynamical equations are evolved by using the iterated Crank-Nicholson method, with spatial derivatives evaluated by using standard second-order-accurate centered finite difference. The numerical convergence is tested by repeating the computation at successively higher resolutions and computing the left hand side of the constraint equation (5.38); the numerical residues vanish quadratically with the resolution, confirming second order

convergence. The results presented below are computed at a baseline resolution with 128 grid points, and a CFL factor of 0.5. Typical errors of the numerical solutions calculated from convergence studies are less than $\sim 0.1\%$.

To observe the nonsingular bounce, we calculate the volume expansion θ at every spatial point, which represents three times the local Hubble expansion rate. The expansion θ satisfies the generalized Friedmann equation (3.26),

$$(\tfrac{1}{3}\theta)^2 = \tfrac{1}{3}\big(E_\phi + E_\chi - \tfrac{1}{2}{}^{(3)}R + \sigma^2\big), \tag{5.76}$$

where E_ϕ and E_χ are the energy density of the scalar fields,

$$E_\phi = \tfrac{1}{2}\big(\dot\phi^2 + D^i\phi\, D_i\phi\big) + V(\phi)\,, \tag{5.77}$$

$$E_\chi = -\tfrac{1}{2}\big(\dot\chi^2 + D^i\chi\, D_i\chi\big)\,, \tag{5.78}$$

${}^{(3)}R$ is the spatial curvature, and σ^2 measures the amount of anisotropy,

$$\sigma^2 \equiv \tfrac{1}{2}\sigma^{ij}\sigma_{ij} = \tfrac{1}{2}\big(K^{ij} - \tfrac{1}{3}K\delta^{ij}\big)\big(K_{ij} - \tfrac{1}{3}K\delta_{ij}\big)\,. \tag{5.79}$$

The terms in Eq. (5.76) are used to compare the amount of curvature and anisotropy with the energy density of the scalar fields.

As an example, consider the case with parameters

$$\begin{aligned} &m = 0.01, && \lambda = -0.3. \\ &f_0 = -0.003, && f_1 = 0.001, \\ &f_2 = 0.002, && f_3 = -0.005. \end{aligned} \tag{5.80}$$

The numerical result for the local expansion rate θ at select times is plotted in Fig. 5.3. The nonsingular bounce happens when the expansion θ crosses zero from below. Note that, due to inhomogeneities, the bounce happens at different times for different spatial points. In this example the inhomogeneities are relatively small, and the universe undergoes a smooth nonsingular bounce as expected. Fig. 5.4 shows the ratio of E_ϕ to $|E_\chi|$, $|\frac{1}{2}{}^{(3)}R|$ to $|E_\chi|$, and σ^2 to $|E_\chi|$, as defined in Eq. (5.76). It can be seen that the magnitude of curvature and anisotropy remain small compared to the energy density of the scalar fields. Note that the ratio between σ^2 and $|E_\chi|$ stays constant over time, just like in the homogeneous case where they have the same equation of state $w = 1$. The ratio between E_ϕ and $|E_\chi|$ shows that the χ field energy density starts small and becomes substantial near the bounce, as in the homogeneous case shown in Fig. 5.2.

For large inhomogeneities, consider an example with different parameters

$$\begin{aligned} &f_0 = -0.03, && f_1 = 0.01, \\ &f_2 = 0.018, && f_3 = -0.05. \end{aligned} \tag{5.81}$$

As shown in Fig. 5.5, the expansion θ remains negative in the middle range of the coordinate x, indicating that this part of the universe keeps contracting and never

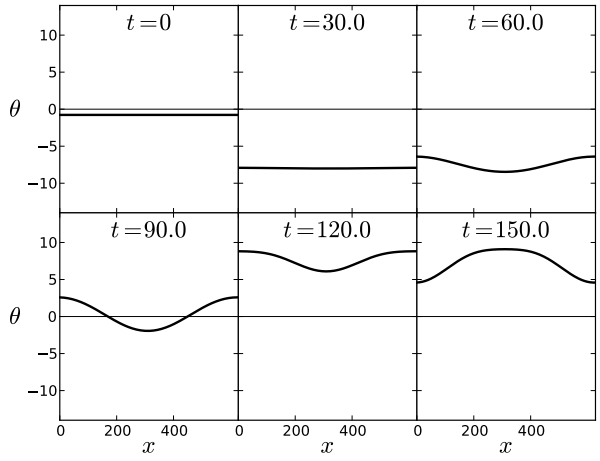

Figure 5.3: Local expansion θ as a function of the coordinate x at select times, computed with parameters in (5.80). The nonsingular bounce is achieved at a spatial point when the expansion θ crosses zero from below.

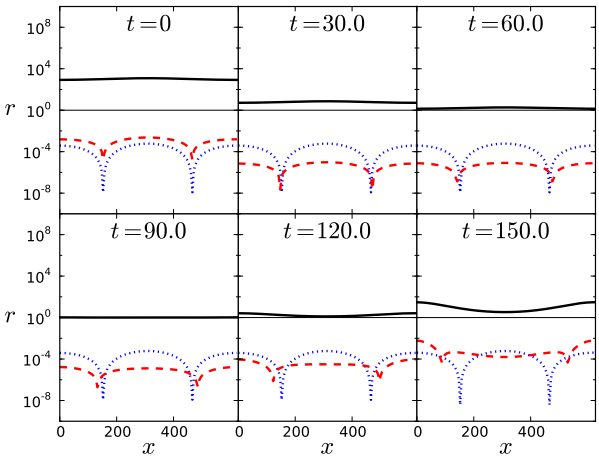

Figure 5.4: $|E_\phi/E_\chi|$ (black continuous), $|\frac{1}{2}{}^{(3)}R/E_\chi|$ (red dashed), and $|\sigma^2/E_\chi|$ (blue dotted) as a function of the coordinate x at select times, computed with parameters in (5.80). In this example, curvature and anisotropy are negligible compared to the energy density of the scalar fields.

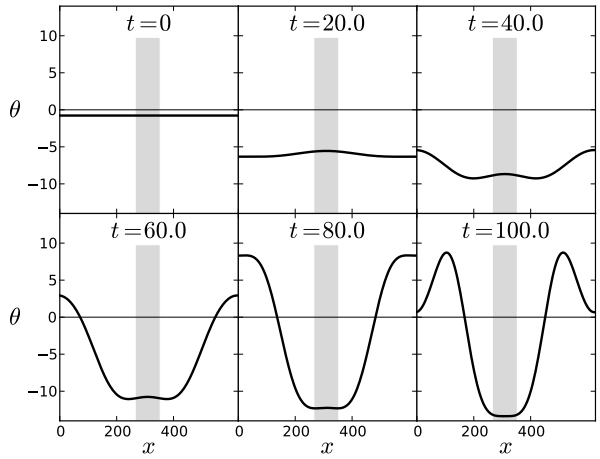

Figure 5.5: Local expansion θ as a function of the coordinate x at select times, computed with parameters in (5.81). The nonsingular bounce does not occur in the shaded region.

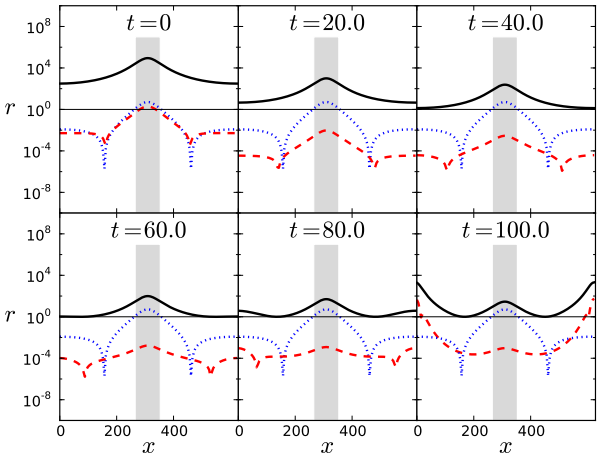

Figure 5.6: $|E_\phi/E_\chi|$ (black continuous), $|\frac{1}{2}{}^{(3)}R/E_\chi|$ (red dashed), and $|\sigma^2/E_\chi|$ (blue dotted) as a function of the coordinate x at select times, computed with parameters in (5.81). In this example, $|\sigma^2/E_\chi| > 1$ in the shaded region, preventing a nonsingular bounce.

bounces. The reason is that in this region the negative energy density of the χ field, which is supposed to induce the bounce, is overtaken by the amount of anisotropy. As shown in Fig. 5.6, the ratio of σ^2 to $|E_\chi|$ is greater than 1 in the shaded region. Since anisotropy grows at the same rate as the χ field energy density, the χ field will never catch up again to induce the bounce. Hence this part of the universe will collapse into a singularity, in contrast to the rest of the places that will pass through a nonsingular bounce.

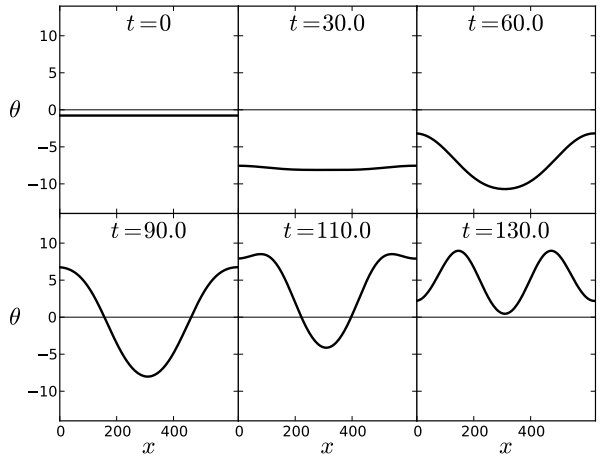

Figure 5.7: Local expansion θ as a function of the coordinate x at select times, computed with parameters in (5.82). The middle region bounces at a much later time compared to the other regions, causing large inhomogeneity and nonlinearity.

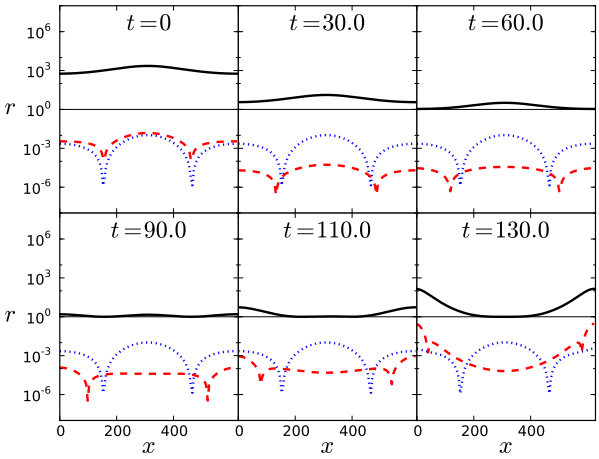

Figure 5.8: $|E_\phi/E_\chi|$ (black continuous), $|\frac{1}{2}{}^{(3)}R/E_\chi|$ (red dashed), and $|\sigma^2/E_\chi|$ (blue dotted) as a function of the coordinate x at select times, computed with parameters in (5.82). In this marginal case, the relative amount of anisotropy reaches as high as 10^{-2}, causing significant nonlinearity.

This example presents a new scenario of nonsingular bouncing cosmology, in which the nonsingular bounce does not occur everywhere in the universe, but only in separate regions that are relatively homogeneous and isotropic. The different future of separate regions is caused by large inhomogeneities that can only be calculated by a nonperturbative approach such as the one presented here. Indeed, in perturbative analysis of nonsingular bounces, the bouncing process is described by a background solution that takes place everywhere in the universe.

To have a criterion for whether certain part of the universe would undergo a nonsingular bounce, consider the ratio between the amount of anisotropy and the energy density of the χ field. Since this ratio remains constant during the cosmic evolution in our model, it is possible to determine whether certain region of the universe would undergo a nonsingular bounce just by analyzing the initial data. In particular, regions where this ratio is initially less than 1 would eventually reach a nonsingular bounce, whereas regions with a ratio greater than 1 would not make it.

This criterion also helps to estimate the size of inhomogeneity and nonlinearity during the bounce. For a ratio of σ^2 to $|E_\chi|$ less than but close to 1, the substantial amount of anisotropy would largely affect the bouncing process. A marginal case is given by the parameters

$$\begin{aligned} f_0 &= -0.01, \quad f_1 = 0.003, \\ f_2 &= 0.007, \quad f_3 = -0.015. \end{aligned} \tag{5.82}$$

Fig. 5.7 shows the local expansion θ at select times, and Fig. 5.8 shows the ratios between E_ϕ, $|\frac{1}{2}{}^{(3)}R|$, σ^2 and $|E_\chi|$. In this example, the ratio $\sigma^2/|E_\chi|$ reaches a maximum of $\sim 10^{-2}$ near the middle of the x range. Accordingly, the bouncing process in this region is much delayed relative to the other regions, making the universe highly inhomogeneous in space. The large amount of anisotropy also implies that perturbative analysis would not be accurate, since in linear perturbation theory anisotropy is a second order effect that must be negligible. Therefore in this case we also expect significant nonlinear effects in the evolution of adiabatic perturbations, to be discussed in Section 5.3.

Our computation shows that the presence of large inhomogeneities before the bouncing phase results in nonlinear growth of curvature and anisotropy that can disrupt the nonsingular bounce. On the other hand, sufficiently small perturbations can pass through the nonsingular bounce without affecting it. Nevertheless, these adiabatic modes may suffer from strong coupling during the bouncing phase that can alter the power spectrum and induce large non-Gaussianity. We will study the evolution of such small adiabatic perturbations in the next section.

5.3 Nonlinearity and strong coupling

To calculate the amplitude of the adiabatic perturbations, we use the covariant formalism presented in Section 3.3. Recall that the covariant and nonlinear generalization of the curvature perturbation is the integrated expansion $\mathcal{N}$, which can be solved from Eq. (3.106). As stated before, the value of $\mathcal{N}$ depends on the time slicing and its normal vector n_μ. In harmonic coordinates, the normal vector to the harmonic time slicing is simply given by

$$n_\mu^{(\mathrm{h})} = \Big(-1/\sqrt{-g^{00}}, 0, 0, 0 \Big). \tag{5.83}$$

This vector will be used in Eq. (3.106) to compute $\mathcal{N}^{(\mathrm{h})}$ in the harmonic gauge. The initial value is set to be $\mathcal{N}^{(\mathrm{h})}(0,x) = 2\log\Psi(x)$, so that $g_{ij}(0,x) = e^{2\mathcal{N}(0,x)}\delta_{ij}$ by Eq. (5.63).

Ideally, we would also like to calculate the integrated expansion $\mathcal{N}^{(\phi)}$ on the constant ϕ hypersurface, which is the generalization of the curvature perturbation $-\mathcal{R}_\phi$ in the comoving ϕ gauge. $\mathcal{N}^{(\phi)}$ should be calculated by using $n_\mu^{(\phi)} = \partial_\mu\phi/\sqrt{-(\partial\phi)^2}$, which is the normal vector to the constant ϕ hypersurfaces. However, the comoving ϕ gauge is not well-defined in the bouncing phase when there is inhomogeneity. Near the bounce the ϕ field switches from decreasing to increasing, causing $\partial_0\phi$ to vanish at certain point along the worldline. As a result, the normal vector $n_\mu^{(\phi)}$ stops being timelike near that point, and the constant ϕ hypersurface fails to be a spatial slicing. (The same problem happens in other commonly used gauges as well, including the uniform density gauge, constant mean curvature gauge, and uniform integrated expansion gauge.) Therefore we cannot calculate $\mathcal{N}^{(\phi)}$ directly in the numerical computation.

In the following, we compute $\mathcal{N}^{(\mathrm{h})}$ in the harmonic gauge (from here on we omit the superscript $^{(\mathrm{h})}$). Our purpose is to check whether its evolution becomes nonlinear, in which case the adiabatic perturbation would no longer remain scale invariant after the bounce. Otherwise, if nonlinearity remains small during the bouncing phase, then the curvature perturbation can be reliably calculated by linear perturbation theory.

To quantify the size of nonlinearity, we decompose $\mathcal{N}$ into various Fourier modes at each time step,

$$\mathcal{N}(\tau,x) = \mathcal{N}^{(0)}(\tau) + \mathcal{N}^{(1)}(\tau)\cos(mx) + \mathcal{N}^{(2)}(\tau)\cos(2mx) + \cdots . \tag{5.84}$$

The zeroth mode gives the homogeneous part of $\mathcal{N}$, which corresponds to the background solution N. The first Fourier mode $\mathcal{N}^{(1)}$ with $k = m$ corresponds to the linear perturbation given in Eq. (3.110), which can be compared to the curvature perturbation $-\psi^{(\mathrm{h})}$ in the harmonic gauge. The second Fourier mode $\mathcal{N}^{(2)}$ can only arise from nonlinearities in either the initial data or the evolution equations. For small perturbations, quadratic terms would be the dominant nonlinear contribution in a perturbative expansion. Therefore, the amplitude of $\mathcal{N}^{(2)}$ with double wavenumber $k = 2m$ represents the leading order nonlinearity in the curvature perturbation.

Consider the previous example with parameters given in (5.82). The first few Fourier modes of the integrated expansion $\mathcal{N}$ are plotted as a function of the harmonic time t in Fig. 5.9. It can be seen from the figure that nonlinearity is relatively large in this example. In particular, the amplitude of $\mathcal{N}^{(2)}$ is initially suppressed with respect to $\mathcal{N}^{(1)}$ by 2 orders of magnitude, but their difference quickly decreases to less than 1 order of magnitude, indicating that nonlinearity is no longer negligible. Similar behavior can also be observed for higher Fourier modes. Fig. 5.10 gives a direct comparison between the amplitude of $\mathcal{N}^{(1)}$ and $\mathcal{N}^{(2)}$, showing that the latter rapidly grows in the bouncing phase.

In addition, Fig. 5.11 shows the homogeneous part of $\mathcal{N}$, which is compared to the background solution $N = \ln a$ from Section 5.1. The substantial amount of anisotropy present in this example clearly changes the bouncing process of the universe. Fig. 5.12

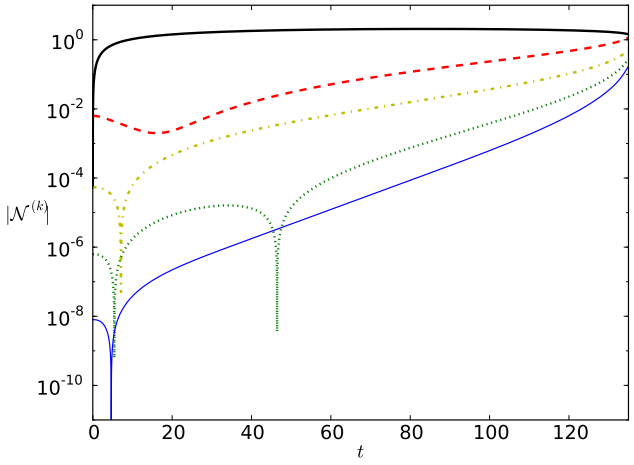

Figure 5.9: Amplitude of the first few Fourier modes of the integrated expansion $\mathcal{N}$, computed with parameters in (5.82): $|\mathcal{N}^{(0)}|$ (black thick), $|\mathcal{N}^{(1)}|$ (red dashed), $|\mathcal{N}^{(2)}|$ (yellow dash-dotted), $|\mathcal{N}^{(3)}|$ (green dotted), $|\mathcal{N}^{(4)}|$ (blue thin). In this example, the amplitude of the higher Fourier modes, especially $\mathcal{N}^{(2)}$, is separated by less than 1 order of magnitude from the linear mode $\mathcal{N}^{(1)}$, indicating that nonlinearity becomes significant during the bouncing phase.

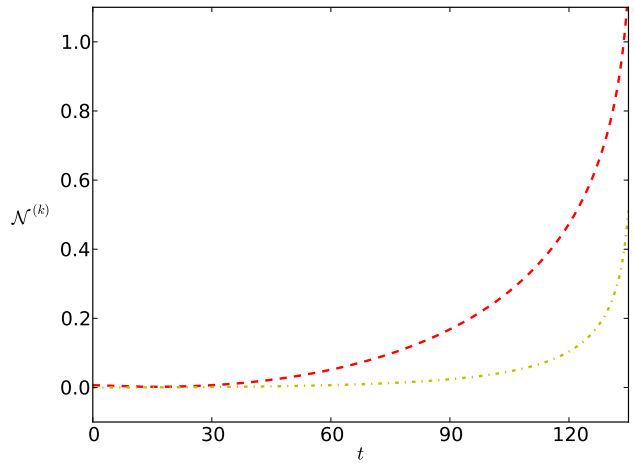

Figure 5.10: Comparison of the Fourier modes $\mathcal{N}^{(1)}$ (red dashed) and $\mathcal{N}^{(2)}$ (yellow dash-dotted). The amplitude of $\mathcal{N}^{(2)}$ becomes substantial during the bounce as compared to $\mathcal{N}^{(1)}$.

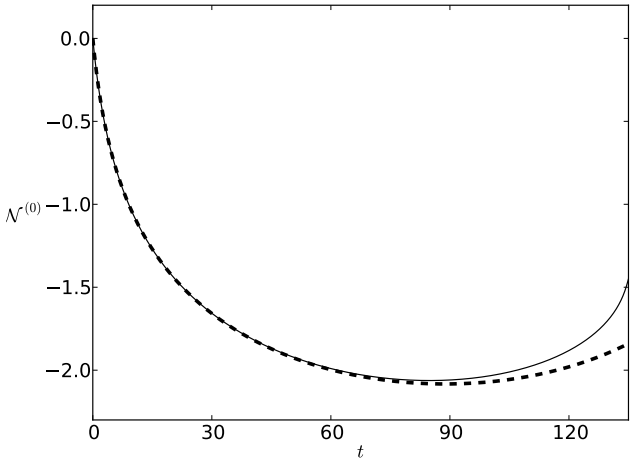

Figure 5.11: The homogeneous part of the integrated expansion, $\mathcal{N}^{(0)}$ (continuous), as compared to the background solution N (dashed). The bouncing process in the inhomogeneous case deviates from the background solution due to the substantial amount of anisotropy.

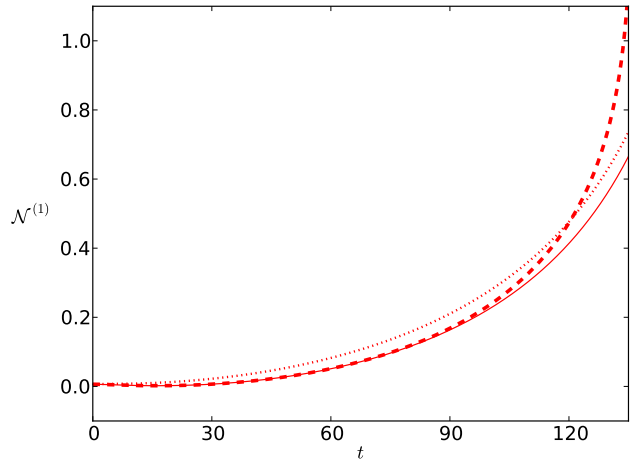

Figure 5.12: The first Fourier mode of the integrated expansion, $\mathcal{N}^{(1)}$ (dashed), as compared to the curvature perturbation $-\psi_{\mathrm{h}}$ (dotted) and lapse perturbation $\frac{1}{3}A_{\mathrm{h}}$ (continuous) calculated by linear perturbation theory. The clear disagreements indicate the inaccuracy of linear perturbative calculations due to the substantial amount of inhomogeneity and anisotropy.

shows the amplitude of the first Fourier mode $\mathcal{N}^{(1)}$, as compared to the linear harmonic curvature perturbation $-\psi^{(\mathrm{h})}$ calculated in Section 5.1. Also shown in this figure is $\frac{1}{3}A^{(\mathrm{h})}$, where $A^{(\mathrm{h})}$ is the lapse perturbation in the linear harmonic gauge, which should agree with $\mathcal{N}^{(1)}$ at linear order due to the particular gauge condition (5.10). The disagreement between those curves indicates that calculations by linear perturbation theory is far from accurate in this case, as a result of the substantial amount of inhomogeneity and anisotropy. Note that for both perturbative and non-perturbative calculations presented in this and other figures, the numerical error is much smaller than the width of the curves, so the disagreements here represent real deviations.

On the other hand, for sufficiently small perturbations, anisotropy is negligible compared to the energy density of the scalar fields ϕ and χ. In that case, the presence of nonlinearity would be an indicator for the strong coupling problem. Specifically, if the perturbations become strongly coupled, then nonlinear terms in their equations of motion are no longer negligible. Such terms would result in higher order perturbations in the solution, which would show as higher Fourier modes such as $\mathcal{N}^{(2)}$. We will check the amplitude of those higher Fourier modes and assess the validity of linear perturbation theory.

Consider very small perturbations with parameters

$$\begin{aligned} &m = 0.01, && \lambda = -0.3, \\ &f_0 = -0.00003, && f_1 = 0.00001, \\ &f_2 = 0.00002, && f_3 = -0.00005. \end{aligned} \tag{5.85}$$

The first few Fourier modes of the integrated expansion $\mathcal{N}$ are shown in Fig. 5.13. It can be seen that the higher order Fourier modes are successively suppressed by many orders of magnitude, suggesting that nonlinearity is negligible. Note that the common increase of their amplitude near the end is an artifact of the harmonic slicing – as noted in Section 5.2, the future infinity in physical time is compactified to a finite harmonic time, which appears to amplify the inhomogeneities. Fig. 5.14 compares the amplitude of the second Fourier mode $\mathcal{N}^{(2)}$ to the first Fourier mode $\mathcal{N}^{(1)}$. The fact that $\mathcal{N}^{(2)}$ remains small compared to $\mathcal{N}^{(1)}$ throughout the bounce implies that nonlinearity is truly insignificant in this example.

For this same example, the value of $\mathcal{N}^{(0)}$ is shown separately in Fig. 5.15, which agrees perfectly with the background solution $N = \ln a$ from Section 5.1. The amplitude of $\mathcal{N}^{(1)}$ is shown in Fig. 5.16, together with the linear harmonic curvature perturbation $-\psi^{(\mathrm{h})}$ calculated in Section 5.1. The small discrepancy between $\mathcal{N}^{(1)}$ and $-\psi^{(\mathrm{h})}$ is due to the gradient term in Eq. (3.110). A better agreement is shown between $\mathcal{N}^{(1)}$ and $\frac{1}{3}A^{(\mathrm{h})}$, which illustrates that linear perturbation theory gives a quite accurate result for the curvature perturbation.

We have shown that, for small perturbations, the evolution of a single Fourier mode does not suffer from nonlinearity during the bounce. It suggests that each mode evolves independently, and the total curvature perturbation is a superposition of different modes. In particular, there should be no mixing between various modes.

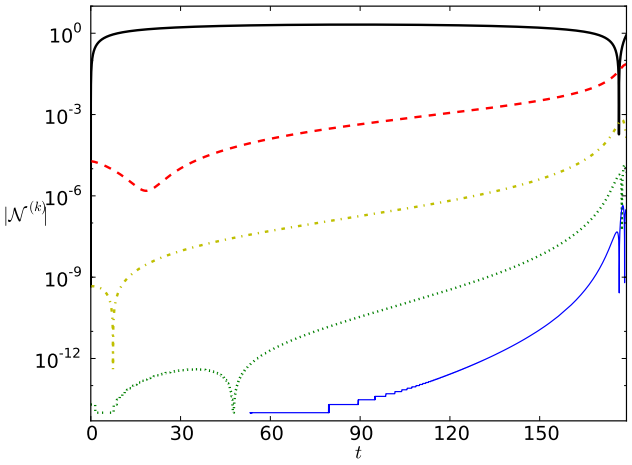

Figure 5.13: Amplitude of the first few Fourier modes of the integrated expansion $\mathcal{N}$, computed with parameters in (5.85): $|\mathcal{N}^{(0)}|$ (black thick), $|\mathcal{N}^{(1)}|$ (red dashed), $|\mathcal{N}^{(2)}|$ (yellow dash-dotted), $|\mathcal{N}^{(3)}|$ (green dotted), $|\mathcal{N}^{(4)}|$ (blue thin). In this example, the amplitude of higher Fourier modes are clearly suppressed with respect to the linear mode, indicating that nonlinearity is negligible.

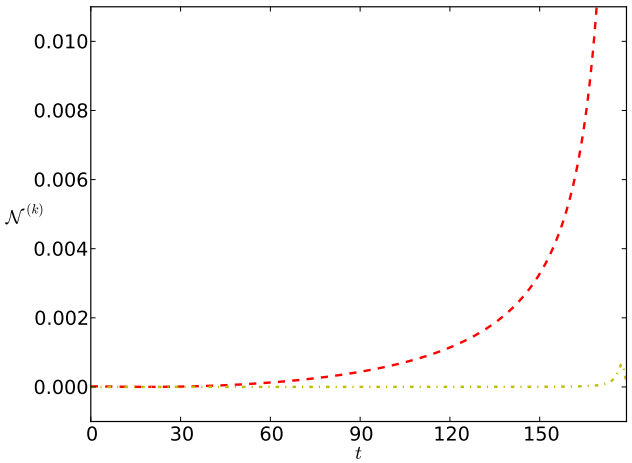

Figure 5.14: Comparison of the Fourier modes $\mathcal{N}^{(1)}$ (red dashed) and $\mathcal{N}^{(2)}$ (yellow dash-dotted). The amplitude of $\mathcal{N}^{(2)}$ stays negligible as compared to $\mathcal{N}^{(1)}$.

We verify this statement by studying the evolution of multiple modes, using the ansatz (5.71 - 5.75). Similar to the above analysis where we follow the amplitude of double wavenumber modes to check for nonlinearity, below we focus on the amplitude of the mixed modes to address the validity of superposition.

As an example, consider the parameters in (5.85) plus

$$m_1 = 0.01. \qquad m_2 = 0.03.$$

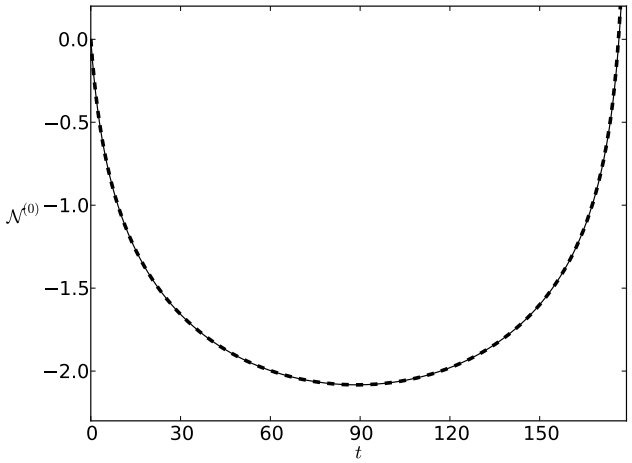

Figure 5.15: The homogeneous part of the integrated expansion, $\mathcal{N}^{(0)}$ (continuous), as compared to the background solution N (dashed). The perfect agreement shows that the background solution is a good approximation.

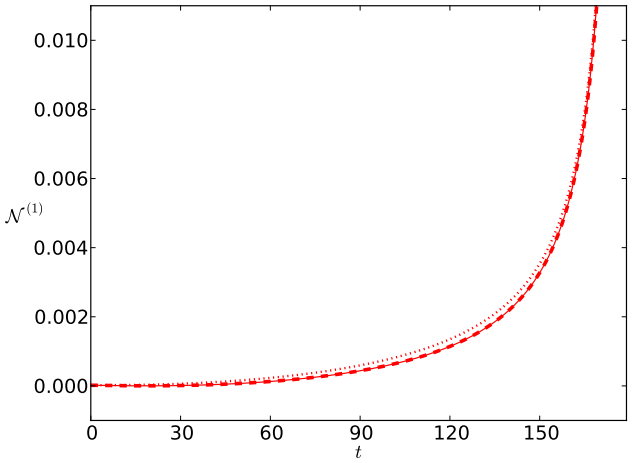

Figure 5.16: The first Fourier mode of the integrated expansion, $\mathcal{N}^{(1)}$ (dashed), as compared to the curvature perturbation $-\psi_{\mathrm{h}}$ (dotted) and lapse perturbation $\frac{1}{3}A_{\mathrm{h}}$ (continuous) calculated by linear perturbation theory. All three curves agree, showing that linear perturbation theory works as a good approximation.

$$\begin{aligned} g_0 &= 0.00002, \qquad & g_1 &= -0.00001, \\ g_2 &= -0.00002, \qquad & g_3 &= 0.00001, \end{aligned} \tag{5.86}$$

Here, since $m_1 = m$ as in (5.85) and $m_2 = 3m$, the mixed modes would have wavenumbers $k = 2m$ and $4m$. Following Eq. (5.84), we decompose the integrated expansion $\mathcal{N}$ into Fourier modes with wavenumbers equal to multiples of m. Fig. 5.17 shows the amplitude of the first few modes during the bounce. The principal modes with

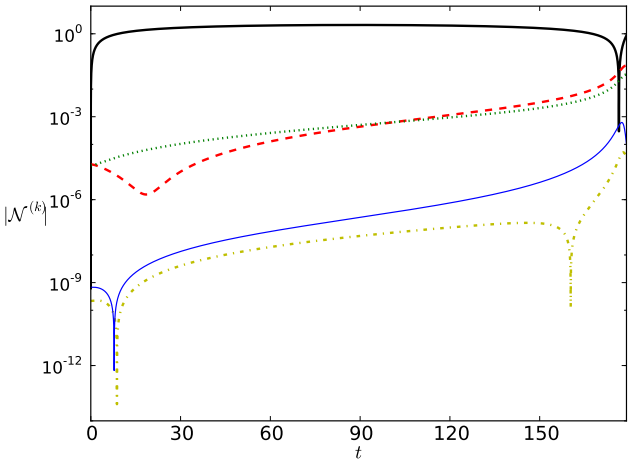

Figure 5.17: Amplitude of the first few Fourier modes of the integrated expansion $\mathcal{N}$, computed with parameters in (5.86): $|\mathcal{N}^{(0)}|$ (black thick), $|\mathcal{N}^{(1)}|$ (red dashed), $|\mathcal{N}^{(2)}|$ (yellow dash-dotted), $|\mathcal{N}^{(3)}|$ (green dotted), $|\mathcal{N}^{(4)}|$ (blue thin). In this example, the amplitude of the two input modes $\mathcal{N}^{(1)}$ and $\mathcal{N}^{(3)}$ are comparable to each other, whereas the mixed modes $\mathcal{N}^{(2)}$ and $\mathcal{N}^{(4)}$ are suppressed, indicating that mode mixing is negligible.

$k = m$ and $3m$ have comparable amplitudes, as set by the initial values, whereas the mixed modes with $k = 2m$ and $4m$ are clearly suppressed. This verifies that there is little mixing between different modes, consistent with the absence of nonlinearity.

Moreover, we compare the evolution of each principal mode in cases with and without the presence of the other. In Fig. 5.18, the $k = m$ mode in the current example is compared to the result in the previous example where it is the only mode in the input. Alternatively, the $k = 3m$ mode in the current example is compared to the case with g_i's given by (5.86) but f_i's set to zero. In both comparisons the amplitude from single and double mode computations agree perfectly, confirming that different modes evolve independently regardless of one another.

Let us comment on the apparent contradiction with the expectation of the strong coupling problem. The strong coupling argument states that, in the effective action for the curvature perturbation derived from a perturbative expansion of the Einstein action, the cubic Lagrangian becomes comparable in size to the quadratic Lagrangian when the parameter $\epsilon \equiv -\dot{H}/H^2$ is large [16]. Such strong coupling can arise either at the classical or the quantum level, depending on whether the modes have exited the horizon. For superhorizon modes that evolve classically, strong coupling implies that the linearized equations given by the quadratic Lagrangian would receive corrections from quadratic terms given by the cubic Lagrangian; these quadratic terms become comparable to the linear terms when ϵ is large, causing the evolution to become nonlinear. In that case, solving the linearized equations would not give the correct result for the curvature perturbation, hence linear perturbation theory would fail.

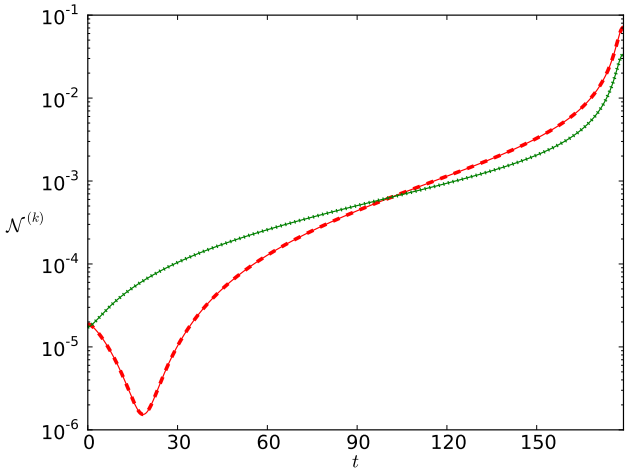

Figure 5.18: $k = m$ mode in the two-mode computation (red dashed) and the single-mode computation (red continuous), $k = 3m$ mode in the two-mode computation (green dotted) and the single-mode computation (green continuous). The agreement of two-mode and single-mode computations in each case shows that different Fourier modes evolve independently.

In particular, near a nonsingular bounce, ϵ diverges as $H \to 0$, implying that the quadratic terms become singular.

To disprove this argument, we first note that the full equations of motion (5.33, 5.34) and (5.36) remain regular during the bounce. Therefore a perturbative expansion in a well-defined gauge would not introduce singular terms. In fact, the anticipated singular terms would only arise in the cubic Lagrangian that is obtained by first eliminating the lapse and shift variables through the Hamiltonian and momentum constraints [110, 129, 31]. In the same way, one may choose to eliminate the lapse and shift variables in the equations of motion. For example, the momentum constraint (5.15) allows one to replace the lapse A with $(-\psi' + \frac{1}{2}\phi'\delta\phi - \frac{1}{2}\chi'\delta\chi)/\mathcal{H}$, incurring a factor $1/\mathcal{H}$ that is singular at $\mathcal{H} = 0$. However, the classical equations of motion would ensure that $(-\psi' + \frac{1}{2}\phi'\delta\phi - \frac{1}{2}\chi'\delta\chi)$ and $\mathcal{H}$ vanish proportionally so as to keep the lapse A finite at the bounce. Hence the quadratic terms in the equations of motion involving ψ' after the substitution would remain small at the bounce, despite the singular coefficient. This explains why at the classical level the nonlinearity is small even though the cubic Lagrangian exhibits strong coupling. Note that the situation is different at the quantum level where the perturbations can fluctuate independently of the fixed background $\mathcal{H}$. In this study we will not consider the quantum strong coupling as we focus on the classical evolution of adiabatic perturbations.

5.4 Power spectrum

Next we would like to study the power spectrum of the adiabatic modes, given by the dependence of their amplitude on the wavenumber k. Instead of the perturbations in the harmonic gauge, we shall calculate the comoving curvature perturbation $\mathcal{R}$ which becomes nearly constant on superhorizon scales in the expansion phase and determines the power spectrum of primordial fluctuations. With two scalar fields, the comoving curvature perturbation $\mathcal{R}$ at linear order is defined as in Eq. (3.138),

$$\mathcal{R} \equiv \psi + \mathcal{H}\frac{\phi'\delta\phi - \chi'\delta\chi}{\phi'^2 - \chi'^2}\,,$$

where ϕ' and χ' are given by the background solution. This quantity $\mathcal{R}$ does not have a covariant generalization. However, shortly before and after the bounce, since χ' is negligible compared to ϕ', the value of $\mathcal{R}$ can be well approximated by the curvature perturbation $\mathcal{R}_\phi$ in the comoving ϕ gauge, given by Eq. (3.60). Therefore we can use $\mathcal{R}_\phi$ to study the power spectrum of the adiabatic perturbations.

The covariant generalization of $\mathcal{R}_\phi$ is the integrated expansion $\mathcal{N}^{(\phi)}$ on the constant ϕ slices. As discussed in Section 5.3, $\mathcal{N}^{(\phi)}$ cannot be calculated directly in the numerical computation. Nevertheless, since for small amplitudes the linear perturbation theory is shown to work throughout the bounce, we will adopt the definition from there and use Eq. (3.60) to reconstruct $\mathcal{R}_\phi$. At linear order,

$$\mathcal{R}_\phi = -\mathcal{N}^{(1)} + \frac{\dot{\mathcal{N}}^{(0)}}{\dot{\phi}^{(0)}}\,\phi^{(1)}, \tag{5.87}$$

where the quantities on the right hand side are calculated in the harmonic gauge, and the superscript (k) denotes the kth Fourier mode in an expansion like (5.84).

To calculate the power spectrum, the initial values for the perturbations are no longer chosen arbitrarily. Instead, the adiabatic perturbations that arise from quantum fluctuations deep inside the horizon in the early contraction phase are determined by the Bunch-Davies vacuum state. Recall that during the contraction phase the universe is dominated by the ϕ field following the scaling solution (2.24) with a matter-like equation of state $w = 0$. For such background evolution, the scalar field perturbations in the *flat gauge* are given in Section 3.4.2. In particular, for $w = 0$ and hence $a \sim (-\eta)^2$, Eq. (3.137) gives

$$\delta\phi_\psi \sim \frac{1}{3\sqrt{2}}k^{3/2} - \frac{i}{8\sqrt{2}}k^{-3/2}(-\eta)^{-3}\,, \tag{5.88}$$

and the same for $\delta\chi_\psi$, where η is the conformal time given by $dt = a\,d\eta$.

Switching to the harmonic time τ, using the relation $d\tau = d\eta/a^2$ and hence $(\tau - \tau_{-\infty}) \sim (-\eta)^{-3}$, we can write

$$\delta\phi_\psi = -iC_1(k)(\tau - \tau_{-\infty}) + C_2(k), \tag{5.89}$$

where $\tau_{-\infty}$ corresponds to the time when $\eta \to -\infty$. The constants C_1, C_2 scale as

$$C_1(k) \sim k^{-3/2}, \quad C_2(k) \sim k^{3/2}, \tag{5.90}$$

and their relative size is fixed by Eq. (5.88),

$$\frac{C_2}{C_1} = \frac{8}{3}(-k\eta)^3(\tau - \tau_{-\infty}) = \frac{8}{3}\Big|\frac{k}{aH}\Big|^3\Big(\frac{-2}{3\mathcal{H}}\Big)\,. \tag{5.91}$$

For superhorizon modes with $k \ll aH$, the C_1 term in Eq. (5.89) dominates and gives rise to a scale invariant power spectrum, whereas the C_2 term is constant and subdominant. The value for C_1 should be normalized such that the final amplitude of the adiabatic perturbation matches the observed power spectrum of the primordial fluctuations (see Eq. (3.132)). For now, we take

$$C_1(k) \sim \frac{3.5 \times 10^{-5}}{(kL)^{3/2}}\,, \tag{5.92}$$

and bear in mind that it should be rescaled to the proper value in the end.

Thus, for our simulation that starts in the late contraction phase, the initial values for the scalar field perturbations in the flat gauge are

$$\delta\phi_\psi(0) = \delta\chi_\psi(0) = -iC_1(k)\Big(\frac{-2}{3\mathcal{H}_0}\Big) + C_2(k)\,, \tag{5.93}$$

$$\delta\phi'_\psi(0) = \delta\chi'_\psi(0) = -iC_1(k)\,. \tag{5.94}$$

Then the initial values for $\delta\phi$, $\delta\phi'$, $\delta\chi$, and $\delta\chi'$ in the harmonic gauge are obtained through a linear transformation

$$\delta\phi_\psi(0) = \delta\phi(0) + \frac{\phi'_0}{\mathcal{H}_0}\psi(0)\,, \tag{5.95}$$

$$\delta\phi'_\psi(0) = \delta\phi'(0) - \left(\frac{a_0^6 V_0\phi'_0 - ca_0^6 V_0\mathcal{H}_0}{\mathcal{H}_0^2}\right)\psi(0) + \frac{\phi'_0}{2\mathcal{H}_0}\big(\phi'_0\delta\phi(0) - \chi'_0\delta\chi(0)\big)\,, \tag{5.96}$$

$$\delta\chi_\psi(0) = \delta\chi(0) + \frac{\chi'_0}{\mathcal{H}_0}\psi(0)\,, \tag{5.97}$$

$$\delta\chi'_\psi(0) = \delta\chi'(0) - \left(\frac{a_0^6 V_0\chi'_0}{\mathcal{H}_0^2}\right)\psi(0) + \frac{\chi'_0}{2\mathcal{H}_0}\big(\phi'_0\delta\phi(0) - \chi'_0\delta\chi(0)\big)\,, \tag{5.98}$$

where $\psi(0)$ is given in terms of $\delta\phi'(0)$, $\delta\chi'(0)$, and $\delta\phi(0)$ by Eq. (5.32).

To account for the two modes C_1 and C_2, we use the ansatz (5.71 - 5.75) with the same wavenumber $m_1 = m_2 = m$, but different phases $d_1 = -\frac{\pi}{2}$ (corresponding to the factor $-i$) and $d_2 = 0$. The C_2 mode corresponds to the amplitude of $\cos(mx)$ in a Fourier expansion as before, whereas the C_1 mode corresponds to the amplitude of $\sin(mx)$. The parameters f_0 - f_3 are inferred from the C_1 term in $\delta\phi(0)$, $\delta\phi'(0)$, $\delta\chi(0)$, and $\delta\chi'(0)$ by using Eqs. (5.29, 5.30) and (5.31) in Section 5.1, and similarly

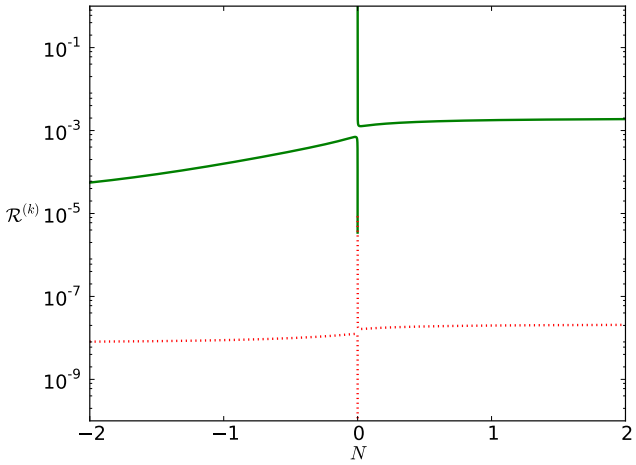

Figure 5.19: Amplitude of the growing mode (green continuous) and the constant mode (red dotted) with Bunch-Davies initial values for $m = 0.01$. The growing mode gives the dominant contribution to the amplitude after the bounce.

for g_0 - g_3 from the C_2 term. Note that the last term in Eq. (5.75) vanishes because the Bunch-Davies initial values ensure that the coefficient $f_0 g_1 - f_1 g_0 - f_2 g_3 + f_3 g_2$ equals 0 identically.

As an example, we calculate the growing (C_1) mode and the constant (C_2) mode for $m = 0.01$. The comoving curvature perturbation $\mathcal{R}_\phi$ for each mode is extracted from the integrated expansion $\mathcal{N}$ and the scalar field ϕ according to Eq. (5.87). Their amplitudes are shown in Fig. 5.19 as a function of the number of e-folds N, which is shifted such that the bounce occurs at $N = 0$, and the sign is chosen so that N is negative before and positive after the bounce. Note that the spikes near the bounce are due to the moment when $\dot{\phi}^{(0)} = 0$ in Eq. (5.87), which again shows that $\mathcal{N}^{(\phi)}$ cannot be evolved directly through the bounce.

The result shows that the growing mode in the contraction phase becomes a constant quickly after the bounce, and remains dominant in the expansion phase. Meanwhile the constant mode in the contraction phase also contributes to the constant mode in the expansion phase, but is negligible compared to the contribution from the growing mode. This matching condition implies that the power spectrum of primordial fluctuations in the expansion phase is primarily determined by the growing mode in the contraction phase, in agreement with [48, 4]. Note that the perturbation amplitude grows even after horizon crossing because the matter-like contraction phase is *not* an attractor. In addition, the asymmetry of the evolution before and after the bounce is due to the entropic perturbations between the two scalar fields. Such entropic perturbations source the adiabatic perturbations near the bounce when the χ field is significant. After the bounce, the χ field energy quickly diminishes, and the adiabatic perturbation approaches a constant.

To check the scale invariance of the power spectrum, we analyze the dependence of the perturbation amplitude on the wavenumber k. In the matter-like contraction

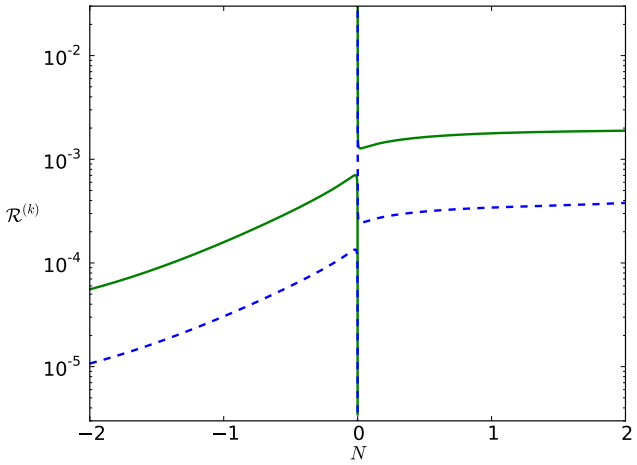

Figure 5.20: Amplitude of the comoving curvature perturbation $\mathcal{R}_\phi$ for wavenumbers $m_1 = 0.01$ (green continuous) and $m_2 = 0.03$ (blue dashed). Their relative amplitude, given by the vertical distance, stays approximately the same after the bounce, showing that the scale dependence of the evolution of the perturbation amplitudes during the bounce is weak.

phase after horizon crossing, the growing mode (C_1) has the correct k-dependence, $C_1 \sim k^{-3/2}$. To maintain the scale invariance into the expansion phase, modes with different wavenumbers must have the same factor of amplification during the bounce. Otherwise, a slight change in the scale dependence would induce a small tilt or running in the power spectrum.

As a case study, we calculate the comoving curvature perturbation $\mathcal{R}_\phi$ for wavenumbers $k = m$ and $3m$, where $m = 0.01$. Since the amplitude is dominated by the growing mode for each k, in the ansatz (5.71 - 5.75) we include only the C_1 term for each of the two wavenumbers $m_1 = 0.01$ and $m_2 = 0.03$, with $d_1 = d_2 = -\frac{\pi}{2}$. Fig. 5.20 shows their amplitude on a logarithmic scale; their relative amplitude, given by the vertical distance between the curves, stays approximately the same before and after the bounce. This suggests that the amplification factor for the perturbation amplitude depends very weakly on the wavenumber k, hence the power spectrum remains nearly scale invariant after the bounce. Fig. 5.21 shows the ratio between the amplitude of the two modes. The slight increase of this ratio after the bounce indicates a slightly larger amplitude at long wavelengths, hence a red tilt. However, as shown below, the amount of tilt turns out to be negligible on observable scales.

In order to quantify the deviation from scale invariance, we calculate the amplitude of the comoving curvature perturbation for a number of k modes ranging over ~ 10 e-folds. Since their evolution is well in the linear regime, we simply use the perturbative calculation presented in Section 5.1. The power spectrum is given by Eq. (3.132), $\Delta^2_{\mathcal{R}} \sim k^3|\mathcal{R}|^2$, as shown in Fig. 5.22. The amplitude has been rescaled to match the observed value $\Delta^2_{\mathcal{R}} \approx 2.4 \times 10^{-9}$ in the limit $k \to 0$. The absolute value of the numbers on the $\log k$ axis represents the number of e-folds after the mode exits the

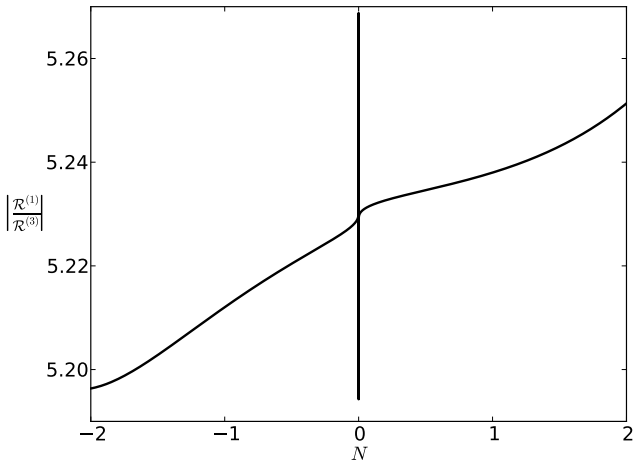

Figure 5.21: The ratio between the amplitude of the Fourier modes with $k = m$ and $k = 3m$. The increase of the ratio after the bounce implies a small red tilt.

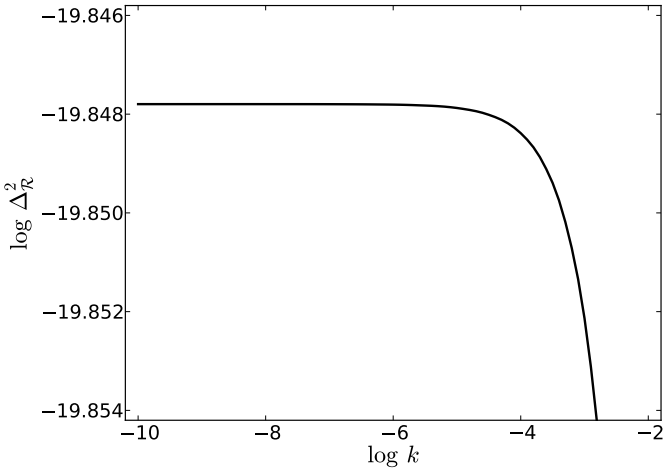

Figure 5.22: The power spectrum of the comoving curvature perturbation $\mathcal{R}_\phi$ after the bounce. The change in the amplitude over ~ 10 e-folds of wavenumbers is as small as 10^{-3}, and becomes negligible for even smaller k that corresponds to observable modes.

horizon and before the bouncing phase. The deviation of the power spectrum from a straight line indicates that there is a running of the spectral index on top of a tilt. However, the change in the amplitude is as small as $\sim 10^{-3}$ over ~ 10 e-folds that are shown in the figure. Such changes become negligible for even smaller k, especially the modes with $|\log k| \sim 50$ - 60 that are measured in the CMB. Therefore, in practice, there is no observable spectral tilt or running.

The conservation of the power spectrum across the bounce can be understood from the smooth evolution of the long wavelength modes through the bounce. If the long wavelength modes stay outside the "horizon" during the bounce, then their dynamics barely depends on their wavenumbers. Here the "horizon" scale is not simply $1/aH$, which becomes infinite at a nonsingular bounce. Instead, it should represent the length scale at which the spatial gradient terms in the equations of motion become negligible compared to the time derivatives. A good estimate may come from the evolution equation for linear perturbations, e.g. Eq. (3.135) in Section 3.4.2, in which k^2 should be compared to $a''/a = a^2(\dot{H} + 2H^2)$. This last quantity does not vanish near the bounce since $\dot{H}$ is positive during the bouncing phase. It can be checked that the modes k we considered in our computations are indeed much smaller than $a(\dot{H} + 2H^2)^{1/2}$ throughout the bounce.

5.5 Discussions

We have obtained the first nonperturbative calculation of a nonsingular bounce. Our computation is based on a bouncing model with one canonical scalar field that drives a matter-like contraction phase and another ghost field that induces a nonsingular bounce. We have shown that large inhomogeneity and anisotropy would disrupt the bounce, as predicted by our perturbative analysis in Chapter 4. Such nonlinear effects become substantial when the amount of anisotropy is close to or larger than the ghost field energy density that is responsible for inducing the bounce. For smaller perturbations the anisotropy remains subdominant and does not affect the nonsingular bounce. In that case, nonlinearities are insignificant during the bounce and the strong coupling problem does not occur for superhorizon modes, indicating that the nonsingular bounce does not cause large non-Gaussianity. We have further analyzed the scale dependence of the amplitude of the adiabatic perturbations and showed that, given scale invariant amplitudes generated in the matter-like contraction phase, the power spectrum remains scale invariant in the expansion phase without observable deviations.

A new picture that emerges from our study is that the nonsingular bounce could happen in separate parts of the universe. Specifically, regions of the universe that are overwhelmed by inhomogeneity and anisotropy would collapse into singularities, whereas regions with relatively smooth and isotropic conditions would pass through a nonsingular bounce. This gives a completely different global picture of a nonsingular bouncing universe from what has been expected by linear perturbative analysis. The new scenario resembles the "phoenix universe" model [99] in which a contracting universe collapses in certain regions and bounces in the others, except that here the

bounce is nonsingular. Since the inhomogeneous regions of the universe terminate in singularities, the volume of the universe would be dominated by the desirable regions that pass through the bounce and expand. One can further imagine that the local amplitude of the primordial fluctuations within an expanding region that bounced successfully would evolve indifferently to the existence of collapsed regions that are way beyond the horizon. Since the evolution of different regions of the universe can be followed through the bounce by directly solving classical equations of motion, it may be possible to find a definite probability measure for various observables over all bounced regions.

There are some drawbacks in the specific model considered in this paper, especially that the matter-like contraction is not an attractor solution. Consequently, a sufficiently long period of matter-like contraction phase requires fine-tuning of initial values for the background solution. Moreover, classical inhomogeneity and anisotropy grow faster than the background energy density with a matter-like equation of state, so it requires further fine-tuning to suppress inhomogeneities during the contraction phase. Besides, although the matter-like contraction phase can create scale invariant adiabatic perturbations, the dominant mode of these perturbations that carries the scale invariant power spectrum is not conserved even on superhorizon scales; hence the amplitude of the adiabatic perturbations in the expansion phase is different from that at the horizon crossing.

These problems can be avoided if the contraction phase is ekpyrotic instead of matter-like. Yet the ghost field model used here can only support a nonsingular bounce with a non-ekpyrotic contraction phase; otherwise, as discussed in Section 4.1, the energy density of the ghost field would be diluted away before it can induce a bounce. To resolve the above problems, we will need a modification to the bouncing mechanism that can endure an ekpyrotic contraction phase as well as produce a nonsingular bounce.

Chapter 6

An Ekpyrotic Nonsingular Bounce

Based on the results of Chapters 4 and 5, we would like to construct a nonsingular bounce that is stable and does not require fine-tuning. Such conditions can be achieved if the contraction phase is ekpyrotic and the bouncing phase suppresses the growth of curvature and anisotropy. In light of the problems found in Chapter 4 with a single scalar field driving both phases, here we will use separate scalar fields to drive the ekpyrotic phase and induce the bounce. Unlike in Chapter 5 where the "bounce field" χ has $w = 1$ that forces the contraction to be non-ekpyrotic, here we will have a bounce field φ that is ekpyrotic itself, with $w > 1$, so that its energy density is not diluted away during the ekpyrotic contraction. To violate the NEC and induce a nonsingular bounce, this field must satisfy $\rho + p = \rho(1 + w) < 0$. Therefore it needs to have a negative energy density, $\rho < 0$; it must also have a noncanonical Lagrangian $P(X, \varphi)$ to satisfy $\rho + p \propto P_{,X} < 0$. To make the equation of motion well-defined and free of gradient instability, we require that the speed of sound satisfies $c_s^2 = P_{,X}/\rho_{,X} > 0$. Hence the bounce field must have $\rho_{,X} < 0$, that is, it has to be a ghost field, like in Chapter 5.

Our plan is as follows: The universe first undergoes an ekpyrotic contraction phase driven by a canonical scalar field ϕ. During the ekpyrotic contraction, the ghost field φ *tracks* the equation of state of the canonical field, so that the ratio of their energy densities remains constant, whereas any amount of curvature and anisotropy would be suppressed exponentially. The ekpyrotic phase ends when the potential energy of the canonical field vanishes and converts to kinetic energy, reducing the equation of state to $w = 1$. Meanwhile, the ghost field stops tracking the canonical field and maintains an equation of state $w > 1$. Therefore its negative energy density grows faster than that of the canonical field, and eventually catches up with the latter to cause a nonsingular bounce. Because the equation of state of the ghost field remains greater than 1 throughout the bouncing phase, curvature and anisotropy continue to be highly suppressed. Note that the overall equation of state of the universe, given by $\frac{3}{2}(1 + w) \equiv -\dot{H}/H^2$, necessarily becomes $w < -1$ when $\dot{H} > 0$ during the bouncing phase, so curvature and anisotropy do grow relative to the *total* energy density which decreases to zero at the bounce; but they are always suppressed relative to the energy density of each scalar field, hence are never significant during the entire evolution.

6.1 Ekpyrotic tracker

The first step in the above setup is to have the ghost field track the equation of state of the canonical field during an ekpyrotic contraction. The ekpyrotic phase is driven as before by a canonical scalar field ϕ described in Section 2.2; the energy density and pressure of the ϕ field are

$$\rho_\phi = \tfrac{1}{2}\dot{\phi}^2 + V(\phi)\,, \quad p_\phi = \tfrac{1}{2}\dot{\phi}^2 - V(\phi)\,, \tag{6.1}$$

and the potential $V(\phi)$ can be written as (see Fig. 2.1) [132]

$$V(\phi) = V_0\, e^{-c\,\phi}\, \exp\big\{ -\tfrac{1}{g_0} e^{-\gamma\phi} \big\}\,, \tag{6.2}$$

which vanishes as $\phi \to -\infty$. For the ghost field φ, we consider a noncanonical Lagrangian,

$$\mathcal{L}[\varphi] = K(\varphi)\tilde{P}(X)\,, \quad X \equiv -\tfrac{1}{2}(\partial\varphi)^2\,, \tag{6.3}$$

where the functions $K(\varphi)$ and $\tilde{P}(X)$ will be specified below. The energy density and pressure of the φ field are given by

$$\rho_\varphi = K(\varphi)\tilde{\rho}(X) \equiv K(\varphi)\big(2X\tilde{P}_{,X} - \tilde{P}\big)\,, \quad p_\varphi = K(\varphi)\tilde{P}(X)\,. \tag{6.4}$$

Hence the equation of state and the speed of sound are given by

$$w_\varphi = \frac{\tilde{P}}{\tilde{\rho}} = \frac{\tilde{P}}{2X\tilde{P}_{,X} - \tilde{P}}\,, \tag{6.5}$$

$$c_s^2 = \frac{\tilde{P}_{,X}}{\tilde{\rho}_{,X}} = \frac{\tilde{P}_{,X}}{2X\tilde{P}_{,XX} + \tilde{P}_{,X}}\,. \tag{6.6}$$

For the ghost field to be ekpyrotic and free of gradient instability, the function $\tilde{P}(X)$ should be such that $w_\varphi > 1$ and $c_s^2 > 0$; requiring $\rho_\varphi < 0$ also imposes $\tilde{\rho} < 0$ and $\tilde{P} < 0$, if we assume $K(\varphi) > 0$ without loss of generality. The Friedmann equations are given by

$$H^2 = \tfrac{1}{3}\big(\rho_\phi + \rho_\varphi\big)\,, \tag{6.7}$$

$$\dot{H} = -\tfrac{1}{2}\dot{\phi}^2 - K(\varphi)XP_{,X}\,, \tag{6.8}$$

Let r be the ratio between the energy density of the φ and ϕ fields,

$$r \equiv \frac{\rho_\varphi}{\rho_\phi}\,. \tag{6.9}$$

The value of r lies within $0 > r \geq -1$ since $\rho_\phi > 0$ and $\rho_\varphi < 0$, and the total energy density $\rho_\phi + \rho_\varphi$ should be non-negative, vanishing only at the bounce.

During the ekpyrotic phase, the potential is approximately $V(\phi) = V_0 e^{-c\phi}$ with $V_0 < 0$, and the equation of state of the ϕ field evolves according to [147]

$$\frac{dw_\phi}{dN} = (1 - w_\phi)\sqrt{3(1 + w_\phi)}\left(\sqrt{3(1 + w_\phi)} - \frac{c}{\sqrt{1 + r}}\right) , \tag{6.10}$$

where we use $N \equiv \log(a_0/a)$ as the time variable, $dN = -H\, dt$. By using the stress-energy conservation (2.5) for each scalar field, one derives an equation for the energy ratio r,

$$\frac{dr}{dN} = 3(w_\varphi - w_\phi)r\,. \tag{6.11}$$

Then, for the ghost field φ, the equation of motion is, similar to (4.4),

$$\frac{d\log X}{dN} = 6c_s^2\left(1 + \frac{1}{3(1 + w_\varphi)}\frac{K_{,\varphi}}{K}\sqrt{\frac{2X}{H^2}}\right) . \tag{6.12}$$

By Eq. (6.7), $H^2 = \frac{1}{3}K(\varphi)\tilde{\rho}(1 + 1/r)$, so the last term in the above equation can be expressed in terms of X and r only, provided that $K(\varphi) \propto \varphi^{-2}$ [8]. Without loss of generality, we choose the function

$$K(\varphi) = \frac{1}{\varphi^2}\,. \tag{6.13}$$

Then Eq. (6.12) becomes

$$\frac{d\log X}{dN} = -6c_s^2\left(1 - \frac{2}{3(w_\varphi + 1)}\sqrt{\frac{6X}{-\tilde{\rho}}}\sqrt{\frac{-r}{1 + r}}\right) . \tag{6.14}$$

An ekpyrotic "tracker" solution is such that both ϕ and φ fields have the same constant equation of state, $w_\phi = w_\varphi > 1$, and the ratio r of their energy densities remains constant, according to Eq. (6.11). By Eq. (6.10), w_ϕ is constant if it takes the value (cf. Eq. (2.25))

$$w_\phi = \frac{c^2}{3(1 + r)} - 1\,. \tag{6.15}$$

In order for w_φ to take the same constant value, Eq. (6.14) requires X to be given by

$$\frac{6X}{\tilde{\rho}} = \frac{9(w_\varphi + 1)^2(1 + r)}{4r}\,. \tag{6.16}$$

The tracker solution is stable only if it is also an attractor [7, 8]. Consider small deviations from the tracker solution. Perturbing Eqs. (6.10, 6.11, 6.14) and using the equilibrium conditions (6.15, 6.16), one obtains

$$\frac{d\delta w_\phi}{dN} = \frac{3}{2}(1 - w)\delta w_\phi + \frac{3(1 - w^2)}{2(1 + r)}\,\delta r\,, \tag{6.17}$$

$$\frac{d\delta r}{dN} = \frac{3(1+w)(c_s^2-w)r}{2c_s^2(1+r)^2}\,\delta\log X - \frac{3r}{(1+r)^2}\,\delta w_\phi\,, \tag{6.18}$$

$$\frac{d\,\delta\log X}{dN} = \frac{3}{2}(1-w)\,\delta\log X - \frac{3c_s^2}{r(1+r)}\,\delta r\,. \tag{6.19}$$

Here w is the common value of w_ϕ and w_φ at the equilibrium. The three eigenvalues to the above linear system are given by

$$\lambda_1 = \lambda_2 + \lambda_3 = \frac{3}{2}(1-w)\,,$$
$$\lambda_2\lambda_3 = \frac{9}{2}(1+w)\Big[(c_s^2-w) - \frac{r}{1+r}(c_s^2-1)\Big]\,.$$

For the tracker solution to be stable against small perturbations, we require all eigenvalues to be negative, obtaining the condition

$$\frac{c_s^2+r}{1+r} > w > 1\,. \tag{6.20}$$

Note that for $0 > r \geq -1$, this condition always implies *superluminality*, $c_s^2 > 1$. In the following, we will use a stronger condition,

$$c_s^2 > w > 1\,, \tag{6.21}$$

which is sufficient for (6.20) regardless of the value of r.

6.2 Nonsingular bounce

The ekpyrotic phase ends when the ϕ field passes the bottom of the potential $V(\phi)$ and quickly becomes kinetic energy dominated, with an equation of state $w_\phi \to 1$. Since the φ field tracks the equation of state of the ϕ field, w_φ starts to decrease as well. But the function $\tilde{P}(X)$ can be arranged such that w_φ is always greater than 1. In that case, the negative energy density of the φ field would increase faster than the ϕ field, and eventually bring the total energy density to zero, creating a nonsingular bounce.

The "ghost tracker" field can be realized by constructing a function $\tilde{P}(X)$ that satisfies the condition (6.21), i.e.

$$\frac{\tilde{P}_{,X}}{2X\tilde{P}_{,XX}+\tilde{P}_{,X}} > \frac{\tilde{P}}{2X\tilde{P}_{,X}-\tilde{P}} > 1\,, \quad \tilde{P}, \tilde{P}_{,X} < 0\,. \tag{6.22}$$

Define the variables

$$f \equiv \log(-\tilde{P})\,, \quad y \equiv \log X\,, \tag{6.23}$$

then Eqs. (6.5, 6.6) become

$$w_\varphi = \frac{1}{2f'(y)-1}\,, \quad c_s^2 = \frac{\frac{1}{2}f'(y)}{f''(y)+f'(y)^2-\frac{1}{2}f'(y)}\,. \tag{6.24}$$

The inequalities in (6.21), or (6.22), simplify to

$$\tfrac{1}{2} < f'(y) < 1\,, \tag{6.25}$$

$$-f'(y)^2 + \tfrac{1}{2}f'(y) < f''(y) < 0\,. \tag{6.26}$$

As an example, let

$$f(y) = b_1 \log\Big(\big(1+e^y\big)^{b_2/b_1} - 1\Big) \approx \begin{cases} b_2 y\,, & y \gg 1\,, \\ b_1 y\,, & y \ll -1\,, \end{cases} \tag{6.27}$$

where the constants b_1, b_2 satisfy $\frac{1}{2} \le b_2 < b_1 \le 1$. Accordingly, the function $\tilde{P}(X)$ is given by

$$\tilde{P}(X) = -\Big((1+X)^{b_2/b_1} - 1\Big)^{b_1}. \tag{6.28}$$

As X varies from 0 to $+\infty$, w_φ increases monotonically from $w_1 = 1/(2b_1-1)$ to $w_2 = 1/(2b_2-1)$. It can be checked that the condition (6.26) is satisfied for parameters in the range $1 < w_1 < w_2 \lesssim 130$.

Given the functions $K(\varphi)$ from (6.13) and $\tilde{P}(X)$ from (6.28), we can solve the equations of motion,

$$\phi'' - \Big(3 - \frac{H'}{H}\Big)\phi' + \frac{V_{,\phi}}{H^2} = 0\,, \tag{6.29}$$

$$\varphi'' - \Big(3c_s^2 - \frac{H'}{H}\Big)\varphi' - \frac{2c_s^2}{(1+w_\varphi)}\frac{\varphi'^2}{\varphi} = 0\,, \tag{6.30}$$

$$H' - \frac{1}{2}H\phi'^2 - \frac{X\tilde{P}_{,X}}{H\varphi^2} = 0\,, \tag{6.31}$$

where the prime denotes $\frac{d}{dN}$, and w_φ, c_s^2 are given by (6.5, 6.6) in terms of $X = \frac{1}{2}H^2\varphi'^2$. Note that, compared to Eq. (6.10) which is valid only for $V(\phi) \sim e^{-c\,\phi}$ during the ekpyrotic phase, here in Eq. (6.29) the potential $V(\phi)$ is given by the full function (6.2) that is bounded from below, as shown in Fig. 2.1. Eqs. (6.29 - 6.31) are supplemented by a constraint equation coming from (6.7),

$$3H^2 = \frac{1}{2}H^2\phi'^2 + V(\phi) + \frac{1}{\varphi^2}\,\tilde{\rho}(X). \tag{6.32}$$

Fig. 6.1 - 6.3 show an example obtained by numerically solving the equations (6.29 - 6.31) with $w_1 = 3$ and $w_2 = 100$. The equation of state w for the ϕ and φ fields are shown in Fig. 6.1; the ratio r of their energy densities is shown in Fig. 6.2. It can be seen that w_ϕ and w_φ start from different values, then quickly converge to the

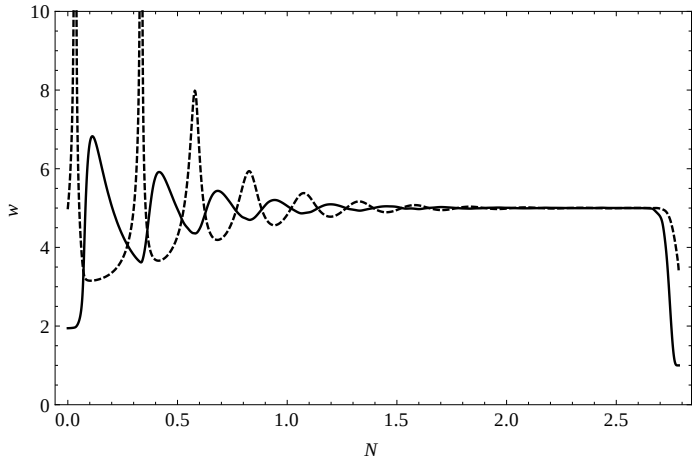

Figure 6.1: The equation of state w for the ϕ field (solid) and the φ field (dashed).

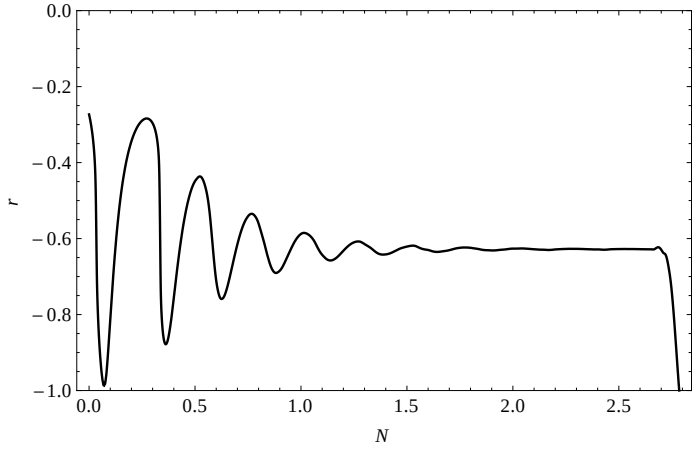

Figure 6.2: The ratio between the energy density of the φ field and the ϕ field.

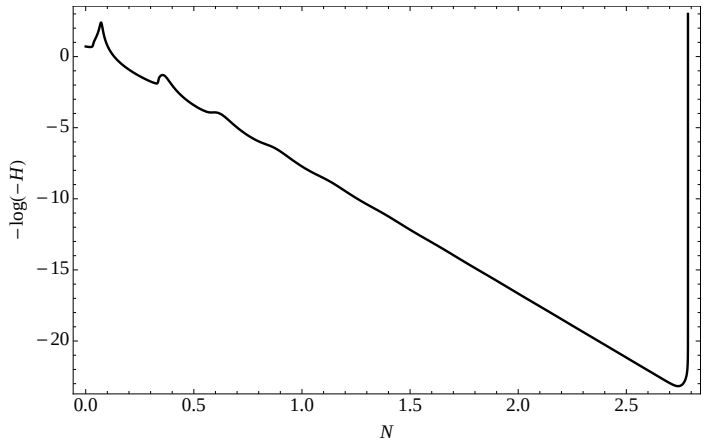

Figure 6.3: $-\log(-H)$ as a function of N.

same constant value during the ekpyrotic phase, proving that the tracker solution is an attractor. Note that since a contracts slowly in the ekpyrotic phase, the number $N = \log(a_0/a)$ does not change very much; however, the Hubble parameter H changes over a large number of e-folds, as shown in Fig. 6.3. In this figure, the curve rises steeply near the bounce because $-\log(-H) \to \infty$ as $H \to 0^-$. The bounce occurs when the ratio r reaches -1, as shown in Fig. 6.2.

6.3 Entropic perturbations

As discussed in Chapter 4, the adiabatic perturbations produced in an ekpyrotic contraction phase do not carry a scale-invariant power spectrum. On the other hand, for a matter-like contraction as in Chapter 5, although the adiabatic perturbations are nearly scale-invariant, the amplitude is not conserved outside the horizon. In the current ekpyrotic nonsingular bouncing model with two scalar fields, there is yet another way of generating scale-invariant perturbations that are conserved – converting entropic perturbations into adiabatic perturbations after horizon crossing [88, 98, 26].

The adiabatic and entropic perturbations can be defined through a decomposition of the scalar field perturbations $\delta\phi$ and $\delta\varphi$,

$$\delta\sigma \equiv \cos\theta\,\delta\phi + \sin\theta\,\delta\varphi\,, \tag{6.33}$$

$$\delta s \equiv -\sin\theta\,\delta\phi + \cos\theta\,\delta\varphi\,, \tag{6.34}$$

where θ is the angle of the trajectory given by $\tan\theta \equiv P_{,X}\dot{\varphi}/\dot{\phi}$ (as a generalization of the definition in [59]). It is known that during the ekpyrotic contraction phase, the scalar field perturbations $\delta\phi$ and $\delta\varphi$ would acquire a nearly scale-invariant power spectrum [97]; so do both $\delta\sigma$ and δs. But the adiabatic perturbation $\delta\sigma$ and the entropic perturbation δs source the curvature perturbation $\mathcal{R}$ differently [59, 93], through the equation

$$\dot{\mathcal{R}} = \frac{H}{\dot{H}}\frac{c_s^2 k^2}{a^2}\Psi - (1+c_s^2)H\frac{\dot{\theta}}{\dot{\sigma}}\,\delta s\,. \tag{6.35}$$

The first term represents the adiabatic contribution that is the same as in the single-field case (cf. Eq. (3.74)), resulting in a blue spectrum due to the factor k^2; the second term represents the entropic contribution that remains scale-invariant. The entropic perturbation is converted into the curvature perturbation whenever the trajectory bends and $\dot{\theta}$ is nonzero. After the conversion the curvature perturbation $\mathcal{R}$ is dominated by the scale-invariant entropic contribution and remains constant on superhorizon scales.

6.4 Discussions

We have presented an ekpyrotic nonsingular bouncing model that can suppress the growth of curvature and anisotropy during the entire contraction phase, as well as produce nearly scale-invariant curvature perturbations. Several problems with the

bouncing models studied in Chapters 4 and 5 are resolved here by using the tracker solution for maintaining an ekpyrotic equation of state and the entropic mechanism for generating scale-invariant curvature perturbations. From our previous results, we expect the power spectrum of the curvature perturbation on superhorizon scales to be conserved across the bounce. Since there is no gradient instability in the model, the results can be verified by numerical computations.

The remaining problem with this model is the ghost instability, which we ignored in our analysis by considering only the classical evolution of superhorizon modes, as argued in Chapter 5. Another new issue is the requirement of superluminality, as found in Section 6.1. Nevertheless, a superluminal speed of sound does not necessarily violate the causal structure of spacetime [24, 44, 11]. Despite these issues, the ghost tracker model works as an effective description of a successful nonsingular bounce.

Chapter 7

Conclusion

7.1 Summary

In this thesis we developed the theory of bouncing cosmology in which the universe undergoes a preceding contraction phase and transitions into the current expansion phase through a big bounce. This scenario stands as the alternative to the big bang theory in which the universe begins with an initial singularity and continues to expand ever since. Compared to the big bang theory, the primordial fluctuations that seed structure formation in the bouncing cosmology are produced in the contraction phase before the bounce. This approach is meant to avoid the problems created by the inflation process that has trouble producing consistent primordial fluctuations in the expansion phase.

In particular, we studied the nonsingular bounce scenario in which the transition from contraction to expansion occurs at a finite size of the universe, without reaching a classical singularity. We considered several implementations of such a nonsingular bounce and analyzed two major aspects: the stability against the growth of curvature and anisotropy, and the conservation of the power spectrum of primordial fluctuations.

In the ghost condensation model studied in Chapter 4, the bounce is induced by the same scalar field that drives an ekpyrotic contraction phase beforehand. We showed that, in this setup, there is an inevitable large gap between the energy scales of the ekpyrotic phase and the ghost condensation, which leads to unstable growth of curvature and anisotropy that spoils the power spectrum and disrupts the bounce altogether.

To resolve the conflict between the contraction phase and the bouncing phase, we studied an alternative model in which the nonsingular bounce is induced by a separate scalar field with negative kinetic energy. As a result, the growth of curvature and anisotropy in the bouncing phase is limited, but the contraction phase has to be non-ekpyrotic and requires fine-tuning. We used numerical methods to compute the classical evolution of adiabatic perturbations in this model, and showed that sufficiently small perturbations can pass through the bounce without altering the power spectrum. However, the amplitude of the adiabatic perturbations is not conserved even on superhorizon scales.

Inspired by the successes and problems of the above models, we proposed an ekpyrotic nonsingular bouncing model that combines the desirable features and overcomes the major difficulties. This new model includes an ekpyrotic contraction phase and a stable bouncing phase, during which curvature and anisotropy are both highly suppressed; nearly scale-invariant primordial fluctuations are produced during the contraction phase, and stay constant outside the horizon during the bounce. This model gives a good example of a nonsingular bounce that meets our expectations.

7.2 Outlook

In some of our models we used a ghost field as an effective mechanism for violating the NEC to create a nonsingular bounce. To have a UV-complete theory, the quantum instability associated with the ghost field has to be stabilized. There may be other bouncing mechanisms that are free of both ghost and gradient instability, perhaps by using more general effective field theories such as a Galileon field [116, 124, 40, 27]. It will be interesting to check if our results continue to hold in the more general case.

A nonsingular bounce can also be thought of as an effective description of a singular bounce. Indeed, a singular bounce can be regularized provided that the bouncing solution satisfies certain analyticity conditions [17, 145]. We conjecture that, under such conditions, the outcome of a singular bounce may be captured by a nonsingular regularization of the bouncing process. Hence our results would have implications on bouncing cosmology in general.

Our results suggest that the bouncing cosmology is a plausible scenario for the early Universe. We have accounted for the observed homogeneity, flatness, and isotropy on large scales, as well as the nearly scale-invariant primordial fluctuations. To further test the model, it remains to study predictions for the other aspects of the universe, such as more detailed statistical properties of the primordial fluctuations including non-Gaussianity, polarization, and tensor modes. The careful exploration of the bouncing cosmology has merely started and deserves further consideration.

Appendix A

Scale-invariant Single-field Models

In this Appendix we present a general scheme to describe single-field cosmological models by a set of flow parameters [144]. Any single-field model can be represented by a point or a trajectory in the flow parameter space. The requirement of a scale-invariant power spectrum constrains the dynamics of the flow parameters and determines particular classes of trajectories. We show that all existing models correspond to nearly constant values of the flow parameters. By looking for fixed points in the parameter space, we find four types of models that generalize inflation, adiabatic ekpyrosis, apex, and tachyacoustic models respectively. Furthermore, we analyze the flow lines near the fixed points in different cross-sections of the parameter space to find new cosmological models that can produce scale-invariant perturbations equally well.

Our approach is very different from the conventional way of starting from a particular scalar field Lagrangian and studing its cosmological solutions. In that approach, generally speaking, only solutions in a limited region of field phase space would yield scale-invariant perturbations, corresponding to a particular type of mechanism represented by some part of the flow parameter space. In our approach, however, by tracing the flow lines in the whole parameter space, we obtain all possible cosmic evolutions that can create a scale-invariant power spectrum. Each and every flow line leads to scale-invariant perturbations, but different trajectories may correspond to very different scalar field models. This approach effectively avoids the limitations of particular scalar field models.

A.1 Flow parameters

Consider a single scalar degree of freedom evolving on a flat FLRW background. Generalizing the derivation in Section 3.4 to allow a noncanonical speed of sound c_s, the power spectrum of curvature perturbations can be studied by using the Mukhanov variable $v \equiv q\,\mathcal{R}$, where $q^2 \equiv a^2\epsilon/c_s$ [81, 16]. As before, the Fourier mode v_k should satisfy the equation of motion

$$v_k'' + \Big(k^2 - \frac{q''}{q}\Big)v_k = 0, \tag{A.1}$$

where $'$ denotes the derivative with respect to the "sound horizon time" y, related to the physical time t by $dy = (c_s/a)dt$. In comparison to the comoving length scale $1/k$, $|q''/q|^{-1/2}$ represents the *freeze-out horizon* scale.

Consider the background evolution of the universe given by a power-law $q \propto y^n$, then $q''/q = n(n-1)/y^2$, and the horizon size is roughly $\sim |y|$. The time variable y runs from $-\infty$ to 0, so that the Fourier modes arise from deep inside the horizon and later exit the horizon. As in Section 3.4, the solution to eq. (A.1) that matches the Bunch-Davies vacuum state in the asymptotic past is given by

$$v_k(y) = \sqrt{\frac{\pi y}{4}}\, H_\nu^{(1)}(-ky), \tag{A.2}$$

where $\nu = |n - \frac{1}{2}|$. After horizon crossing when $k(-y) \ll 1$, the curvature perturbation $\mathcal{R}_k = v_k/\sqrt{2}q$ becomes

$$\mathcal{R}_k = C_1 k^{-\nu}(-y)^{\frac{1}{2}-n-\nu} + C_2 k^{\nu}(-y)^{\frac{1}{2}-n+\nu} + \mathcal{O}(k^{2+\nu}), \tag{A.3}$$

where C_1, C_2 are dimensionless Taylor coefficients. Note that for $n < \frac{1}{2}$, the leading term in eq. (A.3) is time independent while the second and higher terms are decaying at late times, hence $\mathcal{R}_k$ approaches constant values on large scales outside the horizon. But for $n > \frac{1}{2}$, however, the leading term keeps growing even after crossing the horizon, indicating that the homogeneous background is unstable.

The power spectrum of the curvature perturbation $\mathcal{R}$ should be evaluated at horizon crossing or when the super-horizon modes stop growing [81]. In either cases, the spectral tilt is given by the leading term in (A.3),

$$n_s - 1 = 3 - 2\nu = 3 - |2n - 1|. \tag{A.4}$$

For the power spectrum to be scale-invariant, one needs $n = -1$ or 2. The latter case with $n > \frac{1}{2}$ is subject to unstable growths of curvature perturbation on large scales; hence we focus on the former case with $n = -1$.

In general, the relation $q \propto (-y)^n$ can be written as

$$n = \frac{d\log q}{d\log(-y)}\,. \tag{A.5}$$

Define the following flow parameters in a similar way,

$$p \equiv \frac{d\log a}{d\log(-y)} = \frac{aHy}{c_s}, \tag{A.6}$$

$$\tilde{s} \equiv \frac{d\log c_s}{d\log(-y)}, \tag{A.7}$$

$$r \equiv \frac{d\log|aH|}{d\log(-y)} = \frac{d\log|p|}{d\log(-y)} + \tilde{s} - 1. \tag{A.8}$$

The parameter p measures the expansion or contraction rate of the universe. Since y goes from $-\infty$ to 0, $p < 0$ corresponds to an expanding universe, whereas $p > 0$ corresponds to a contracting universe. The parameter $\tilde{s}$ measures the time dependence of the speed of sound c_s. $c_s = 1$ corresponds to $\tilde{s} = 0$; for $\tilde{s} < 0$ the speed of sound c_s increases with time, whereas for $\tilde{s} > 0$ it decreases with time. Note that the more commonly defined parameter $s \equiv \dot{c_s}/Hc_s$ can be expressed as $s = \tilde{s}/p$. The parameter r measures how the comoving Hubble horizon $1/|aH|$ scale with the freeze-out horizon $\sqrt{|q/q''|} \sim (-y)$. When ϵ or c_s varies with time, these two horizon scales do not coincide. Note that p also measures the ratio between the freeze-out horizon $(-y)$ and the "comoving sound horizon" $|c_s/aH|$.

In terms of these flow parameters, the parameter $\epsilon = \frac{3}{2}(1 + w)$ is given by

$$\epsilon \equiv \frac{-\dot{H}}{H^2} = \frac{p - r}{p}. \tag{A.9}$$

Here the NEC is assumed, which implies $\epsilon \geq 0$. To compute n, define the parameter

$$\tilde{\eta} \equiv \frac{d\log\epsilon}{d\log(-y)} = \frac{1}{p-r}\left[r(r - \tilde{s} + 1) - \frac{dr}{d\log(-y)}\right]. \tag{A.10}$$

It is related to the usual slow-roll parameter $\eta \equiv \dot{\epsilon}/H\epsilon$ by $\eta = \tilde{\eta}/p$. With these parameters, it is straightforward to write n in eq. (A.5) as

$$n = p + \frac{1}{2}(\tilde{\eta} - \tilde{s}). \tag{A.11}$$

To have a constant n, equations (A.8) and (A.10) imply the following equations,

$$-\frac{dp}{d\log(-y)} = -p(r - \tilde{s} + 1), \tag{A.12}$$

$$-\frac{dr}{d\log(-y)} = -p(2p - \tilde{s} - 2n) + 2pr - r(r + 2n + 1). \tag{A.13}$$

On the left hand side, the derivative is with respect to the "log time" $-\log(-y)$, which runs from $-\infty$ to ∞. Given the value of $\tilde{s}$, these two equations determine the flow in the parameter space $(p, r, \tilde{s})$.

For example, in the case where $c_s = $ const, the parameter $\tilde{s}$ vanishes. In the $p\,r$-plane with $\tilde{s} = 0$, the flow lines according to eqs. (A.12, A.13) for $n = -1$ are shown in figure A.1. The shaded region corresponds to $\epsilon = (p - r)/p < 0$, which is forbidden by the NEC. There are three fixed points at $(p, r) = (-1, -1)$, $(0, 0)$, and $(0, 1)$ respectively. The one at $(0, 1)$ behaves as a sink where nearby trajectories converge. The one at $(0, 0)$ is a saddle point where trajectories approach from both sides but eventually move away. The other saddle point at $(-1, -1)$ is attached to a separatrix which, together with the shaded region, divides the plane into three sectors.

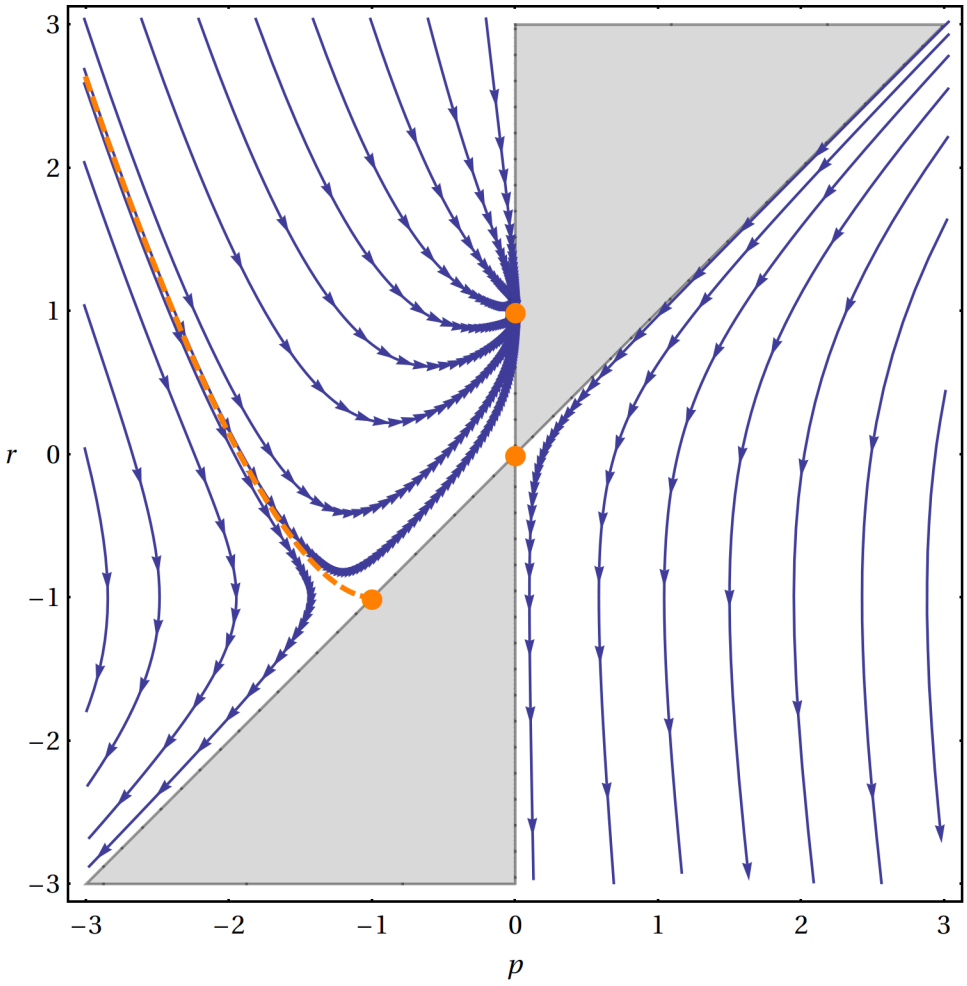

Figure A.1: Flow lines for $n = -1$ in the $p\,r$-plane with $\tilde{s} = 0$. The three solid circles are the fixed points representing inflation $(-1, -1)$, adiabatic ekpyrosis $(0, 0)$, and apex $(0, 1)$ respectively; the dashed line is a separatrix. Each line segment between adjacent arrowheads on the flow lines represents 0.1 log time interval, or 0.1 e-fold of scale-invariant modes.

Every flow line in the figure corresponds to a cosmological model that yields scale-invariant perturbations. The time interval along each flow line measures the number of scale-invariant modes, since $-\log(-y) \sim \log k$ when the modes exit the horizon. In the bulk of each sector away from the fixed points, the flow lines are qualitatively similar to each other. Typically the time dependence of the flow parameters is very complicated, preventing analytic descriptions of the corresponding cosmological models.

The more distinctive flow lines are the trajectories near the fixed points. There the flow velocities given by eqs. (A.12, A.13) approach zero, so the flow parameters stay near those points for a sustained period. During that period a large number of modes exit the horizon with a scale-invariant spectrum. The corresponding cosmological models can be characterized by nearly constant values of the flow parameters, which allows simple descriptions of the cosmic evolutions. Indeed, the three fixed points in figure A.1 precisely correspond to the three types of scale-invariant cosmological models with $c_s = 1$. Let us identify each of them.

The fixed point at $(-1, -1)$ corresponds to *inflation* [62, 104, 3]. On the point $(-1, -1)$ the parameter $\epsilon = 0$, which corresponds to the false vacuum inflation where $H = \text{const}$ until the universe tunnels to the true vacuum. In that case $aH = 1/(-\tau)$, where τ is the conformal time that equals the sound horizon time y for $c_s = 1$, hence $p = aH\tau = -1$ and $r = aH\tau(1-\epsilon) = -1$. In slow-roll inflation, however, ϵ is small but nonzero; the energy of the inflaton field ϕ is dominated by a nearly flat potential $V(\phi)$. The slow-roll approximation implies $\dot\phi \approx -V_{,\phi}/3H \approx (-V_{,\phi}/V)\sqrt{V/3}$, and $\epsilon \approx \frac{1}{2}(\frac{-V_{,\phi}}{V})^2 \ll 1$ which is assumed to vary only slowly. Therefore

$$\log a = \int H\, dt \approx \int \sqrt{\frac{V}{3}}\, \frac{d\phi}{(\frac{-V_{,\phi}}{V})\sqrt{V/3}} \approx \big(\tfrac{V}{-V_{,\phi}}\big) \int d\phi, \tag{A.14}$$

hence $a \approx e^{(-V/V_{,\phi})\phi}$ and

$$\tau = \int \frac{dt}{a} \approx \int \frac{e^{(V/V_{,\phi})\phi}\, d\phi}{(\frac{-V_{,\phi}}{V})\sqrt{V/3}} \approx -\frac{e^{(V/V_{,\phi})\phi}}{\sqrt{V/3}} + \int e^{(V/V_{,\phi})\phi}\Big(\frac{-V_{,\phi}}{2V}\Big)\frac{d\phi}{\sqrt{V/3}} \approx -\frac{1}{aH} + \epsilon\,\tau, \tag{A.15}$$

where an integration by parts is performed and the integration constant is chosen to be zero. Consequently, $p = aH\tau \approx -1 - \epsilon$ and $r = aH\tau(1-\epsilon) \approx -1 + \mathcal{O}(\epsilon^2)$, indeed close to the fixed point. Inflation ends when the potential becomes steep and the field speeds up, which lead the flow parameters to move up across the $r = 0$ ($\epsilon = 1$) line and stop producing scale-invariant modes.

The fixed point at $(0, 0)$ corresponds to the *adiabatic ekpyrotic* model [82, 83]. This model relies on a slow contraction phase with $H \approx H_0 + c/t$, where $H_0 < 0$ and $c \ll 1$. During the period between $t_{\rm beg} \approx 1/H_0$ and $t_{\rm end} \approx c/H_0$, $H \approx H_0$ but $\dot H \sim -1/t^2$, hence ϵ increases rapidly as $\sim 1/t^2$. Also within this one Hubble time $a \approx \text{const}$, hence the conformal time $\tau \sim t$. Therefore $q^2 \sim \epsilon \sim 1/\tau^2$, which guarantees a scale-invariant power spectrum. The number of scale-invariant modes is given by $N \approx \log|t_{\rm beg}/t_{\rm end}| \approx \log(1/c)$. To see that during this period the flow

parameters stay near the saddle point, note that $p = aH\tau \approx H_0 t$, and $p - r = aH\tau\epsilon \approx -t\dot{H}/H \approx c/H_0 t$. Hence for $t_{\rm beg} \ll t \ll t_{\rm end}$ we find $0 < p \ll 1$ and $|r| \ll 1$. Note that $(p-r)$ corresponds to a growing eigenmode of eqs. (A.12, A.13) near the saddle point $(0,0)$; it starts extremely small at $t_{\rm beg} = 1/H_0$, $(p-r)_{\rm beg} \approx c \sim e^{-N} \ll 1$, and becomes $(p-r)_{\rm end} \sim \mathcal{O}(1)$ at $t_{\rm end} \approx c/H_0$. We have shown that the adiabatic ekpyrotic mechanism takes place near the point $(0,0)$ on the $p > 0$ side. Notably, this fixed point may also be approached from the $p < 0$ side, which corresponds to a *slow expansion* [79, 77] that produces scale-invariant perturations in a similar way.

Finally, the fixed point at $(0,1)$ corresponds to the *apex* model, first discussed in [79]. In this model the universe slowly transitions from expansion to contraction. When the universe gradually stops expansion to reach an apex, the scale factor a slowly comes to a halt, and the Hubble parameter H has to drop from positive to zero. Therefore, near the apex we may assume that $H \approx \dot{H}_0 t$, where the constant $\dot{H}_0 < 0$ and t goes from negative to 0. During the last Hubble time when $t > t_{\rm beg} = -1/\sqrt{-\dot{H}_0}$, the scale factor $a \approx$ const, hence $\tau \sim t$. The scale-invariant perturbations are produced by $q^2 \sim \epsilon \approx -\dot{H}_0/H^2 \sim 1/\tau^2$. The flow parameters are given by $p = aH\tau \approx \dot{H}_0 t^2$, and $r = aH\tau(1-\epsilon) \approx 1 + \dot{H}_0 t^2$. They approach the sink point $(0,1)$ asymptotically as $t \to 0^-$. It seems that, as the log time $-\log(-\tau) \to \infty$, an infinite number of scale-invariant modes would be produced. Nevertheless, before reaching the point $(0,1)$ at which $\epsilon \to \infty$, our analysis based on linear perturbation theory should be expected to break down due to strong coupling [16]. Therefore the number of scale-invariant modes would be finite. It is also important to have an asymmetry in the cosmic evolution before and after the apex, so that the scale-invariant modes are not undone in the subsequent contraction phase.

We have represented all scale-invariant cosmological models with $c_s = 1$ by the flow lines on the $\tilde{s} = 0$ plane in the parameter space. Our diagrammatic representation provides a clear way of classifying models by the flow lines and searching for simple analytic solutions near the fixed points. To look for new types of scale-invariant cosmological models with a time-varying speed of sound, we shall generalize our analysis to the whole parameter space $(p, r, \tilde{s})$.

A.2 Fixed points

Despite the unknown dynamics of $\tilde{s}$, the fixed points of the flow equations (A.12, A.13) must satisfy

$$\begin{cases} -p(r - \tilde{s} + 1) = 0, \\ -p(2p - 2n - \tilde{s}) + 2pr - r(r + 2n + 1) = 0. \end{cases} \tag{A.16}$$

For each value of $\tilde{s}$, there are four solutions to these equations, namely $(p, r) = (0, 0)$, $(0, -2n-1)$, $(\tilde{s}-1, \tilde{s}-1)$, and $(\tilde{s}/2 + n, \tilde{s} - 1)$. Each solution draws a fixed point in the parameter space, which traces out a line as $\tilde{s}$ varies; their positions projected on the $p\,r$-plane are shown in figure A.2 for $n = -1$. The first three fixed points are generalizations of the ones in the $c_s = 1$ ($\tilde{s} = 0$) case to models with time varying

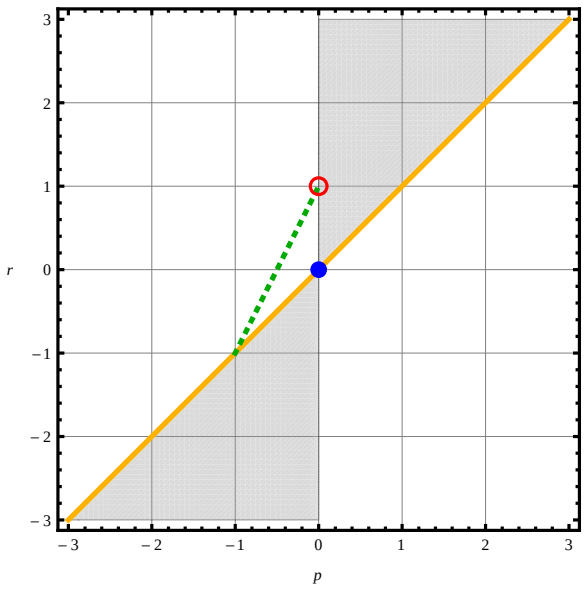

Figure A.2: Positions of the four fixed points in scale-invariant models ($n = -1$), projected on the $p\,r$-plane for different values of $\tilde{s}$: the adiabatic ekpyrosis (solid blue circle) at $(0, 0)$ for all $\tilde{s}$, the decelerated expansion (red circle) at $(0, 1)$ for all $\tilde{s}$, the inflation/deflation point (thick orange line) at $(\tilde{s} - 1, \tilde{s} - 1)$, and the tachyacoustic expansion (dashed green line) at $(\frac{\tilde{s}}{2} - 1, \tilde{s} - 1)$ for $0 < \tilde{s} < 2$.

c_s ($\tilde{s} \neq 0$). They will be referred to as the *adiabatic ekpyrosis* point $(0, 0)$, the *decelerated expansion* point $(0, 1)$, and the *inflation/deflation* point $(\tilde{s} - 1, \tilde{s} - 1)$. The fourth fixed point $(\tilde{s}/2 - 1, \tilde{s} - 1)$ corresponds to the *tachyacoustic expansion* scenario [9, 120, 109, 19]. It is degenerate with inflation at $\tilde{s} = 0$, but otherwise is a distinct scenario that can generate scale-invariant curvature perturbations in an expanding universe with a decreasing speed of sound.

Incidentally, cosmological models that correspond to the $n = 2$ fixed points have also been considered in the literature. For example, the second fixed point with $n = 2$ is at $(0, -5)$, which represents the slowly evolving universe described in [121]. The fourth fixed point with $n = 2$, located at $(\tilde{s}/2+2, \tilde{s}-1)$, corresponds to a contracting universe with a growing speed of sound presented in [81]. The latter scenario includes the matter dominated contraction model [141, 48, 23] as its $\tilde{s} = 0$ (constant c_s) limit. The third fixed point stays in the same position $(\tilde{s}-1, \tilde{s}-1)$ for $n = 2$; it corresponds to the "ultra slow-roll" inflation [74, 139, 86, 115, 111] for unit speed of sound $c_s = 1$ ($\tilde{s} = 0$). Despite their instability against the growth of curvature perturbation on large scales, these models can be discussed in similar ways to the $n = -1$ models that we consider below.

To learn the properties of the fixed points, we shall analyze the flow lines near those points, as in the $\tilde{s} = 0$ case. In the more general case, the parameter $\tilde{s}$ may be nonzero and even time dependent. However, in the larger parameter space $(p, r, \tilde{s})$, the dynamics of the parameter $\tilde{s}$ is not constrained by the requirement of a scale-invariant power spectrum that led to eqs. (A.12, A.13). For a practical model such as a scalar

field with a particular Lagrangian, the speed of sound c_s is determined by the field configuration. Hence generally there is a relation between the parameters $\tilde{s}$ and p, r. Here, without being constrained by the underlying model, we will phenomenologically explore different situations in which $\tilde{s}$ can vary with respect to p and r.

In particular, consider flow lines on a surface $\tilde{s}(p, r)$ in the parameter space that goes through one fixed point. Then near that point a small deviation in $\tilde{s}$ is given by

$$\delta\tilde{s} \approx \frac{\partial\tilde{s}}{\partial p}\,\delta p + \frac{\partial\tilde{s}}{\partial r}\,\delta r \equiv \alpha\,\delta p + \beta\,\delta r, \tag{A.17}$$

where (α, β) is the gradient of the function $\tilde{s}(p, r)$ at the fixed point. The flow equations (A.12, A.13) can be expanded to linear order in $\delta p, \delta r$ near that point, setting $n = -1$,

$$-\frac{d\,\delta p}{d\log(-y)} = -(-\alpha p + r - \tilde{s} + 1)\,\delta p - (1-\beta)p\,\delta r, \tag{A.18}$$

$$-\frac{d\,\delta r}{d\log(-y)} = -((4-\alpha)p - 2r - \tilde{s} + 2)\,\delta p - (-(2+\beta)p + 2r - 1)\,\delta r. \tag{A.19}$$

The eigenvalues to this linear system are given by

$$\lambda_1 + \lambda_2 = (2 + \alpha + \beta)p - 3r + \tilde{s}, \tag{A.20}$$

$$\lambda_1\lambda_2 = (3\alpha + 4\beta - 4)p^2 + (3\tilde{s} + \alpha + \beta - 4)p - (2\alpha + 3\beta)pr + (2r-1)(r - \tilde{s} + 1). \tag{A.21}$$

These eigenvalues determine whether a fixed point is a source, a sink, or a saddle point.

In the following we analyze each of the four fixed points and derive approximate solutions of the nearby flow lines. The corresponding types of cosmological models are described and verified to create scale-invariant curvature perturbations. These models rely on having a manifestly time dependent speed of sound; constraints from the strong coupling problem and superluminality are discussed in section A.3.

A.2.1 adiabatic ekpyrosis: $(p, r) = (0, 0)$

This fixed point stays in the same position for any value of $\tilde{s}$. Like in the $\tilde{s} = 0$ case, the corresponding cosmological model is either a slow contraction if $0 < p \ll 1$ or a slow expansion if $-1 \ll p < 0$. The eigenvalues from eqs. (A.20) can be explicitly found to be $\lambda_1 = 1$, $\lambda_2 = \tilde{s} - 1$. Because the first eigenvalue is positive, this fixed point can be either a saddle point or a source of flow depending on the value of the second eigenvalue. Specifically, it is a saddle point if $\tilde{s} < 1$, which is qualitatively the same as in the case $\tilde{s} = 0$ discussed in section A.1. However, for $\tilde{s} > 1$ we find a new situation where this point behaves like a source.

In this new situation with $\tilde{s} > 1$, the flow lines emerge from the point $(0, 0)$ in the asymptotic past $y \to -\infty$. In that limit, since $p, r \to 0$, both a and H approach

constant values, $a \approx a_{-\infty}$ and $H \approx H_{-\infty}$. Take $\alpha = \beta = 0$ for simplicity, so that $c_s \sim (-y)^{\tilde{s}}$. Then in the asymptotic past,

$$t = \int \frac{a}{c_s} dy \sim \int_{-\infty}^{y} \frac{a_{-\infty}}{(-y)^{\tilde{s}}} dy \sim \frac{1}{(-y)^{\tilde{s}-1}}, \tag{A.22}$$

which goes from 0 to ∞. That is, the asymptotic past corresponds to finite physical time t.

To see the cosmic evolution in this situation, it is better to solve the flow equations and express a and H in terms of t. Near $(p, r) = (0, 0)$, the eigenmodes of eqs. (A.18, A.19) are given by $p \propto 1/(-y)^{\tilde{s}-1}$ and $r - p \propto 1/(-y)$. Using the definitions of p and r, one finds

$$\log\left(\frac{a}{a_{-\infty}}\right) \sim \frac{1}{(-y)^{\tilde{s}-1}} \sim t, \tag{A.23}$$

$$\log\left(\frac{H}{H_{-\infty}}\right) \sim \frac{1}{(-y)} \sim t^{1/(\tilde{s}-1)}. \tag{A.24}$$

Therefore, in the limit $t \to 0$,

$$a \approx a_{-\infty}(1 + H_{-\infty} t), \tag{A.25}$$

$$H \approx H_{-\infty}\Big(1 - C(H_{-\infty} t)^{1/(\tilde{s}-1)}\Big), \tag{A.26}$$

$$c_s \sim (-y)^{\tilde{s}} \sim t^{-\tilde{s}/(\tilde{s}-1)}, \tag{A.27}$$

where we assume $C \sim \mathcal{O}(1) > 0$. For $t \ll 1/|H_{-\infty}|$ it is approximately true that $a \approx a_{-\infty}$ and $H \approx H_{-\infty}$. Under this approximation,

$$\epsilon \approx \frac{-\dot{H}}{H_{-\infty}^2} \approx \frac{C}{\tilde{s}-1}(H_{-\infty} t)^{(2-\tilde{s})/(\tilde{s}-1)} \sim (-y)^{\tilde{s}-2}, \tag{A.28}$$

which guarantees the condition $q^2 \sim \epsilon/c_s \sim 1/(-y)^2$ for generating scale-invariant curvature perturbations.

A particularly interesting example is when $\tilde{s} = 2$. This corresponds to a cosmological model in which $H \approx H_{-\infty} - C H_{-\infty}^2 t$. For $0 < t \ll 1/|H_{-\infty}|$, it gives $a \approx a_{-\infty}$ and $\epsilon \approx C = \text{const}$. If the speed of sound satisfies $c_s \sim 1/t^2$, then one finds $(-y) \sim 1/t$, hence $q^2 \sim 1/c_s \sim 1/(-y)^2$. That is, the scale invariance of the power spectrum is achieved by having a uniquely time dependent speed of sound. This model can be considered as dual to either inflation or adiabatic ekpyrosis in which the $1/(-y)^2$ dependence of $q^2 = a^2\epsilon/c_s$ comes solely from either a or ϵ. Like in adiabatic ekpyrosis, this mechanism works in either a contracting or an expanding universe according to whether $H_{-\infty}$ is negative or positive.

A.2.2 decelerated expansion: $(p, r) = (0, 1)$

This fixed point represents a decelerated cosmic expansion, since near this point $p < 0$ and $\epsilon = (p - r)/p \gg 1$. The eigenvalues from eqs. (A.20) are $\lambda_1 = -1$, $\lambda_2 = \tilde{s} - 2$, which again do not depend on α, β. For $\tilde{s} < 2$ this fixed point is a sink, the same as the apex model in the $\tilde{s} = 0$ case. But for $\tilde{s} > 2$ it becomes a saddle point, which gives rise to a new scenario.

In this new scenario with $\tilde{s} > 2$, the flow lines do not asymptote towards $p = 0$ but move away from it instead. Hence the universe does not approach an apex. Indeed, near the point $(0, 1)$, $a \approx$ const and $H \sim (-y)$; but unlike in the apex model where $H \to 0$ as $y \to 0^-$, here the flow line passes by the saddle point while y remains finite. The unstable eigenmode of eqs. (A.18, A.19) is given by $p \propto -1/(-y)^{\tilde{s}-2}$, which implies $\epsilon \approx -1/p \propto (-y)^{\tilde{s}-2}$. For $\tilde{s} > 2$, ϵ decreases with time rather than increases.

To see the cosmic evolution in physical time t, assume again $\alpha = \beta = 0$ so that $c_s \sim (-y)^{\tilde{s}}$. Then for $a \approx$ const one obtains $t \sim 1/(-y)^{\tilde{s}-1}$ as in eq. (A.22), where $t > 0$ and increases. Thus the cosmological model can be described by a decelerated expansion with

$$H \sim t^{-1/(\tilde{s}-1)}, \quad c_s \sim t^{-\tilde{s}/(\tilde{s}-1)}. \tag{A.29}$$

We can check that $\dot{H} \sim -t^{-\tilde{s}/(\tilde{s}-1)}$ and hence $\epsilon \sim t^{-(\tilde{s}-2)/(\tilde{s}-1)} \sim (-y)^{\tilde{s}-2}$, ensuring $q^2 \sim \epsilon/c_s \sim 1/(-y)^2$. To be consistent, since by eq. (A.29),

$$\log\left(\frac{a}{a_0}\right) \sim t^{(\tilde{s}-2)/(\tilde{s}-1)}, \tag{A.30}$$

the approximation $a \approx$ const holds for sufficiently small t. This approximation breaks down at finite time before H reaches 0, showing again that it is different from an apex model.

There is a marginal case where $\tilde{s} = 2 + 2p_0$ with $-1 \ll p_0 < 0$. In that case $p \approx p_0 =$ const, hence $a \sim (-y)^{p_0}$. Since $c_s \sim (-y)^{2+2p_0}$, the physical time $t \sim 1/(-y)^{1+p_0} > 0$. The cosmic evolution is given by

$$a \sim t^{-p_0/(1+p_0)}, \quad H \approx \frac{(-p_0)}{(1+p_0)t}, \quad c_s \sim \frac{1}{t^2}. \tag{A.31}$$

This is a slow expansion with constant $\epsilon = -(1+p_0)/p_0 \gg 1$. Therefore $q^2 \sim a^2/c_s \sim 1/(-y)^2$, which produces scale-invariant curvature perturbations. This model describes an extremely decelerated expansion with a rapidly decreasing speed of sound, which is the $\epsilon \gg 1$ limit of the tachyacoustic model to be discussed in section A.2.4.

A.2.3 inflation/deflation: $(p, r) = (\tilde{s} - 1, \tilde{s} - 1)$

This fixed point describes a de Sitter universe with $\epsilon = (p - r)/p = 0$. The position of this fixed point depends on $\tilde{s}$. For $\tilde{s} < 1$ it lies on the border $p = r < 0$ in the left half plane, the same as inflation; but for $\tilde{s} > 1$ it moves to the right half plane with $p = r > 0$ (the case $\tilde{s} = 0$ coincides with adiabatic ekpyrosis). The eigenvalues from

eqs. (A.20) are $\lambda_1 = \tilde{s}$, $\lambda_2 = (\alpha+\beta-1)(\tilde{s}-1)$. Depending on the value of $\alpha+\beta$, this point can be a saddle, a source, or a sink, as listed in table A.1.

Here we consider the new situation when $\tilde{s} > 1$ and $p = r > 0$, which corresponds to an extremely rapid cosmic contraction, or "deflation". Specifically, near this fixed point, $p \approx \tilde{s}-1$ and $r-p \approx 0$, hence $a \sim (-y)^{\tilde{s}-1}$ and $H \approx$ const. The eigenmode that corresponds to the first eigenvalue is $(p-r) \propto 1/(-y)^{\tilde{s}}$. Therefore $\epsilon \approx (p-r)/(\tilde{s}-1) \sim 1/(-y)^{\tilde{s}}$, which is crucial to ensure $q^2 = a^2\epsilon/c_s \sim 1/(-y)^2$. Now that ϵ is rapidly increasing, it is clear that the flow parameters can only stay near the deflation point for a finite time.

For $a \sim (-y)^{\tilde{s}-1}$ and $c_s \sim (-y)^{\tilde{s}}$, the physical time t is given by

$$t = \int \frac{a}{c_s} dy \sim \int \frac{(-y)^{\tilde{s}-1}}{(-y)^{\tilde{s}}} dy = -\log(-y), \tag{A.32}$$

i.e. proportional to the number of scale-invariant modes. In physical time t, if $H \approx H_0 < 0$, then $a \sim e^{H_0 t}$. Comparing that to $a \sim (-y)^{\tilde{s}-1}$, one finds

$$t \approx \frac{\tilde{s}-1}{H_0} \log(-y), \quad \text{or} \quad (-y) \approx e^{H_0 t/(\tilde{s}-1)}. \tag{A.33}$$

The crucial part of this model is to have a rapidly growing ϵ and a rapidly decreasing c_s,

$$\epsilon \approx \frac{\epsilon_0}{(-y)^{\tilde{s}}} \approx \epsilon_0\, e^{-\frac{\tilde{s}}{\tilde{s}-1} H_0 t}, \quad c_s \sim (-y)^{\tilde{s}} \sim e^{\frac{\tilde{s}}{\tilde{s}-1} H_0 t}. \tag{A.34}$$

The de Sitter approximation $\epsilon \ll 1$ is valid until $t_{\rm end} \approx \frac{(\tilde{s}-1)/\tilde{s}}{(-H_0)} \log(\frac{1}{\epsilon_0})$. If we assume that $\epsilon_0 \ll 1$, then there can be many numbers of Hubble times before $t_{\rm end}$.

Therefore, this deflation model is described by a rapid cosmic contraction with

$$H \approx H_0 \Big(1 + \tfrac{\tilde{s}-1}{\tilde{s}}\, \epsilon_0\, e^{-\frac{\tilde{s}}{\tilde{s}-1} H_0 t}\Big), \tag{A.35}$$

which satisfies $H \approx H_0$ for $t \ll t_{\rm end}$. The scale invariance of the power spectrum is achieved by an interplay between

$$a \sim e^{H_0 t}, \quad \epsilon \approx \epsilon_0\, e^{-\frac{\tilde{s}}{\tilde{s}-1} H_0 t}, \quad c_s \sim e^{\frac{\tilde{s}}{\tilde{s}-1} H_0 t}. \tag{A.36}$$

So far the dependence of the model on α, β has been neglected as we implicitly assumed a nearly constant $\tilde{s}$. For $\alpha+\beta > 1$ the fixed point is actually a source where the flow line emerges in the asymptotic past, so the above description works even better at early times $t \to -\infty$. However, for $\alpha+\beta < 1$ the fixed point is a saddle point instead. In that case, when extrapolating backwards in time, the flow parameters would deviate from the saddle point at certain time $t_{\rm beg}$. This time is controlled by the second eigenvalue, $t_{\rm beg} \approx \frac{1}{(1-\alpha-\beta)H_0} \log(\frac{1}{\epsilon_0})$. The model described above is valid between $t_{\rm beg}$ and $t_{\rm end}$ to produce roughly $N \sim \log(\frac{1}{\epsilon_0})$ scale-invariant modes.

Note that eqs. (A.35, A.36) also apply for $\tilde{s} < 1$ and $H_0 > 0$, in which case they describe an exponentially expanding universe with a time varying speed of sound, or "acoustic inflation". This model is less interesting since inflation with $\epsilon \ll 1$ and a constant c_s can already produce scale-invariant perturbations. In contrast, the deflation model relies on having a rapidly decreasing c_s as well as a small but increasing ϵ.

A.2.4 tachyacoustic expansion: $(p, r) = (\tilde{s}/2 - 1, \tilde{s} - 1)$

The position of this fixed point also depends on $\tilde{s}$. Moreover, since $\epsilon = (p - r)/p = \tilde{s}/(2 - \tilde{s})$, the null energy condition $\epsilon \geq 0$ requires $0 < \tilde{s} < 2$ (the cases $\tilde{s} = 0, 2$ coincide with inflation and apex respectively). Thus in the $p\,r$-plane, this fixed point lies on the line segment $r = 2p + 1$ for $-1 < p < 0$, as shown in figure A.2. Since $p < 0$ and $\tilde{s} > 0$, it describes an expanding universe with a decreasing speed of sound.

Here we show that this model precisely corresponds to the *tachyacoustic expansion* scenario [9, 120, 109, 19]. Specifically, at the point $(p, r) = (\tilde{s}/2 - 1, \tilde{s} - 1)$ for certain value of $\tilde{s}$, the model is described by $a \sim (-y)^{\tilde{s}/2-1}$, $H \sim (-y)^{\tilde{s}/2}$, and $c_s \sim (-y)^{\tilde{s}}$. From eq. (A.11) one finds $\tilde{\eta} = 0$, consistent with $\epsilon = \tilde{s}/(2 - \tilde{s}) = \text{const}$. Therefore $q^2 \sim a^2/c_s \sim 1/(-y)^2$, ensuring a scale-invariant power spectrum.

In this model, the physical time t is given by

$$t = \int \frac{a}{c_s} dy \sim \int \frac{dy}{(-y)^{\tilde{s}/2+1}} \sim \frac{1}{(-y)^{\tilde{s}/2}}. \tag{A.37}$$

Thus in physical time t, $a \sim t^{(2-\tilde{s})/\tilde{s}}$, $H = (2 - \tilde{s})/(\tilde{s}\,t)$, and $c_s \sim 1/t^2$. We can check that $\epsilon = -\dot{H}/H^2 = \tilde{s}/(2 - \tilde{s})$ as expected. In terms of the parameter $s \equiv \dot{c}_s/Hc_s = \tilde{s}/p$, this relation can be expressed as $s = -2\epsilon$, which agrees perfectly with the tachyacoustic scenario [9, 120, 109, 19, 81]. This scenario is emphatically different from inflation since here ϵ need not be small at all. In particular, the limit $\epsilon \gg 1$ corresponds precisely to the marginal case in section A.2.2.

For flow lines near this fixed point, the eigenvalues in eq. (A.20) become

$$\begin{cases} \lambda_1 + \lambda_2 = \big(\frac{\alpha+\beta}{2} - 1\big)\tilde{s} - (\alpha + \beta - 1), \\ \lambda_1\lambda_2 = \frac{1}{2}\big(\frac{\alpha}{2} + \beta - 1\big)\tilde{s}(2 - \tilde{s}). \end{cases} \tag{A.38}$$

Therefore this point is a saddle point if $\frac{\alpha}{2} + \beta < 1$, otherwise a source or a sink depending on whether $\big(\frac{\alpha+\beta}{2} - 1\big)\tilde{s} - (\alpha + \beta - 1) > 0$ or < 0, as listed in table A.1.

A.3 Physical constraints

In the simplistic analysis above, each model can potentially produce a large number of exactly scale-invariant modes. In practice, some physical constraints should be considered that could affect the stability of the models and limit the range of scale-invariant modes [56, 16].

fixed points	adia ekpy $(0,0)$	decel exp $(0,1)$	inf / def $(\tilde{s}-1,\tilde{s}-1)$	tachyacoustic $(\frac{\tilde{s}}{2}-1,\tilde{s}-1)$
source	$\tilde{s}>1$	／	$0<\tilde{s}<1,\alpha+\beta<1$	$\frac{\alpha}{2}+\beta>1,$
			$\tilde{s}>1,\alpha+\beta>1$	$\big(\frac{\alpha+\beta}{2}-1\big)\tilde{s}>(\alpha+\beta-1)$
saddle	$\tilde{s}\leq 1$	$\tilde{s}>2$	$\tilde{s}\leq 0,\alpha+\beta<1$	$\frac{\alpha}{2}+\beta<1$
			$0<\tilde{s}<1,\alpha+\beta>1$	
			$\tilde{s}>1,\alpha+\beta<1$	
sink	／	$\tilde{s}\leq 2$	$\tilde{s}\leq 0,\alpha+\beta>1$	$\frac{\alpha}{2}+\beta>1,$
				$\big(\frac{\alpha+\beta}{2}-1\big)\tilde{s}<(\alpha+\beta-1)$

Table A.1: Positions and properties of the fixed points for flow lines on a constrained surface $\tilde{s}(p,r)$ with local gradient (α,β).

First of all, the period during which the scale-invariant modes are created should be stable against the growth of spatial curvature and anisotropy. The effective densities of these two components scale as $1/a^2$ and $1/a^6$ respectively [47], whereas the dominant energy density of the universe scales as $1/a^{2\epsilon}$. Therefore an expansion phase with $\epsilon<1$ can efficiently dilute away spatial curvature and anisotropy, leading to a flat, homogeneous and isotropic universe as observed today. Hence accelerated expansion models like inflation (with $\epsilon\ll 1$) and tachyacoustic expansion (with $\epsilon\lesssim 1$) can solve the horizon problem as well as provide a scale-invariant power spectrum; but decelerated expansion models including adiabatic ekpyrotic expansion and apex (with $\epsilon\gg 1$) must be supplemented by additional mechanisms, e.g. an ekpyrotic contraction phase, to suppress inhomogeneity and anisotropy [77]. Similarly, a slow contraction phase with $\epsilon>3$, such as adiabatic ekpyrosis, can automatically beat curvature and anisotropy; but a rapid contraction such as deflation ($\epsilon\ll 1$) would require an extra stabilization phase, just like in the matter-like contraction model [27].

Besides, for models where the comoving Hubble horizon $1/aH$ does not coincide with the freeze-out horizon, the scale-invariant modes that have left the freeze-out horizon must also exit the Hubble horizon before the standard expansion phase. In models including adiabatic ekpyrosis, decelerated expansion, and deflation, this can be done by having a subsequent ekpyrotic phase to push the modes outside the Hubble horizon, such as in [82, 83, 78].

Moreover, since the cosmological models assume classical general relativity, for consistency the energy density of the universe should remain sub-Planckian, $H^2/M_{\rm Pl}^2\lesssim 1$. To estimate the size of the Hubble parameter when the scale-invariant modes are generated, taking $n=-1$ in eq. (A.2) to fix the coefficients in eq. (A.3),

one finds that the power spectrum is given by

$$P_{\mathcal{R}} \equiv \frac{k^3}{2\pi^2}\frac{|v_k|^2}{q^2} = \frac{1}{8\pi^2 M_{\rm Pl}^2 q^2 y^2} = \frac{1}{8\pi^2 M_{\rm Pl}^2}\frac{c_s}{\epsilon\, a^2 y^2}. \tag{A.39}$$

From the measured amplitude of the power spectrum, $P_{\mathcal{R}} \approx 2.4 \times 10^{-9}$, the sub-Planckian energy density criterion can be expressed as

$$\frac{H^2}{M_{\rm Pl}^2} \approx \frac{8\pi^2}{4\times 10^8}\frac{\epsilon\, a^2 H^2 y^2}{c_s} \approx \frac{p^2 \epsilon\, c_s}{5\times 10^6} \lesssim 1. \tag{A.40}$$

For models with time varying ϵ and c_s, it is also important to avoid strong coupling in generating scale-invariant perturbations. A simple estimate and often reliable criterion is that the magnitude of the third order action for $\mathcal{R}$, $S_3 \sim \int \mathcal{O}(\mathcal{R}^3)$, should be smaller than the quadratic action S_2 (cf. (3.113)) [96, 16]. For a rapidly growing ϵ or a rapidly decreasing c_s, the dominant contribution to the ratio S_3/S_2 can be estimated by the term [78]

$$\frac{S_3}{S_2} \sim \mathcal{R}\,\frac{\epsilon^2}{c_s^2}. \tag{A.41}$$

This term results in a non-Gaussianity that peaks at small scales where the observational bound on $f_{NL} \sim S_3/\mathcal{R}\,S_2$ is weak. Demanding that $S_3/S_2 \lesssim 1$ when the scale-invariant modes crosses the horizon, the weak coupling criterion can be written as

$$\frac{\epsilon^2}{c_s^2} \lesssim \frac{1}{\mathcal{R}} \sim \frac{1}{5\times 10^{-5}}. \tag{A.42}$$

The above two constraints can quantitatively limit the number of scale-invariant modes generated in certain types of models. For example, in the tachyacoustic model with a constant $\epsilon \sim \mathcal{O}(1)$, using $p = \tilde{s}/2 - 1 = -1/(\epsilon+1)$ from section A.2.4, eq. (A.40) becomes $c_s\epsilon/(\epsilon+1)^2 \lesssim 5\times 10^6$. Combining that with eq. (A.41), one obtains

$$7\times 10^{-3}\,\epsilon \lesssim c_s \lesssim 5\times 10^6\,\frac{(\epsilon+1)^2}{\epsilon}. \tag{A.43}$$

Since $c_s \sim (-y)^{\tilde{s}} \sim k^{-2\epsilon/(\epsilon+1)}$ at horizon crossing, the number of scale-invariant modes is bounded by [78]

$$N \lesssim \frac{\epsilon+1}{2\epsilon}\log\left(\frac{5\times 10^6}{7\times 10^{-3}}\Big(\frac{\epsilon+1}{\epsilon}\Big)^2\right) \approx 22. \tag{A.44}$$

Similarly, in the decelerated expansion model described in section A.2.2, using $\epsilon \approx -1/p$, eqs. (A.40) and (A.41) imply $7\times 10^{-3} \lesssim c_s/\epsilon \lesssim 5\times 10^6$. Since in this model $c_s/\epsilon \sim y^2 \sim 1/k^2$ at horizon crossing, the number of scale-invariant modes is bound by $N \lesssim \frac{1}{2}\log(5\times 10^6/7\times 10^{-3}) \approx 10$, just enough to encompass the observed 10 e-folds of primordial density fluctuations. This result is the same as for the apex model [79].

Finally, models with a time varying c_s often run into a superluminal speed of sound, $c_s > 1$. Such a superluminal speed of sound does not necessarily violate the causal structure of spacetime [24, 44, 11]. Nevertheless, it is important to understand how constrained the cosmological models become if $c_s \leq 1$. It is can be seen from eq. (A.43) that the tachyacoustic model requires superluminality (hence the name) for generating a wide range of scale-invariant modes; otherwise this constraint becomes $7 \times 10^{-3}\,\epsilon \lesssim c_s \leq 1$, allowing only $N \lesssim \frac{1}{2}\log(10^3/7\epsilon) \approx 3$ e-folds of scale-invariant modes for $\epsilon \sim \mathcal{O}(1)$. The same bound also applies to the particular adiabatic ekpyrotic model described in section A.2.1. Similarly, for the decelerated expansion model discussed above, since $\epsilon \gg 1$, one finds $7 \times 10^{-3} \lesssim c_s/\epsilon \ll 1$, posing an even tighter bound on N. Hence these models all rely on having a superluminal speed of sound for generating a sufficient number of scale-invariant modes, in the same spirit as the tachyacoustic model.

Bibliography

[1] P.A.R. Ade et al. Planck 2013 results. XVI. Cosmological parameters. *arXiv:1303.5076*, 2013.

[2] Nishant Agarwal, Rachel Bean, Liam McAllister, and Gang Xu. Universality in D-brane Inflation. *JCAP*, 1109:002, 2011.

[3] Andreas Albrecht and Paul J. Steinhardt. Cosmology for Grand Unified Theories with Radiatively Induced Symmetry Breaking. *Phys.Rev.Lett.*, 48:1220–1223, 1982.

[4] Laura E. Allen and David Wands. Cosmological perturbations through a simple bounce. *Phys.Rev.*, D70:063515, 2004.

[5] Alexey Anisimov and Alexander Vikman. Classical stability of the ghost condensate. *JCAP*, 0504:009, 2005.

[6] Nima Arkani-Hamed, Hsin-Chia Cheng, Markus A. Luty, and Shinji Mukohyama. Ghost condensation and a consistent infrared modification of gravity. *JHEP*, 0405:074, 2004.

[7] C. Armendariz-Picon, Viatcheslav F. Mukhanov, and Paul J. Steinhardt. A Dynamical solution to the problem of a small cosmological constant and late time cosmic acceleration. *Phys.Rev.Lett.*, 85:4438–4441, 2000.

[8] C. Armendariz-Picon, Viatcheslav F. Mukhanov, and Paul J. Steinhardt. Essentials of k essence. *Phys.Rev.*, D63:103510, 2001.

[9] Cristian Armendariz-Picon. Near Scale Invariance with Modified Dispersion Relations. *JCAP*, 0610:010, 2006.

[10] Abhay Ashtekar and Parampreet Singh. Loop Quantum Cosmology: A Status Report. *Class.Quant.Grav.*, 28:213001, 2011.

[11] Eugeny Babichev, Viatcheslav Mukhanov, and Alexander Vikman. k-Essence, superluminal propagation, causality and emergent geometry. *JHEP*, 0802:101, 2008.

[12] James M. Bardeen. Gauge Invariant Cosmological Perturbations. *Phys.Rev.*, D22:1882–1905, 1980.

[13] James M. Bardeen, Paul J. Steinhardt, and Michael S. Turner. Spontaneous Creation of Almost Scale - Free Density Perturbations in an Inflationary Universe. *Phys.Rev.*, D28:679, 1983.

[14] Itzhak Bars, Shih-Hung Chen, Paul J. Steinhardt, and Neil Turok. Antigravity and the Big Crunch/Big Bang Transition. *Phys.Lett.*, B715:278–281, 2012.

[15] Daniel Baumann. TASI Lectures on Inflation. *arXiv:0907.5424*, 2009.

[16] Daniel Baumann, Leonardo Senatore, and Matias Zaldarriaga. Scale-Invariance and the Strong Coupling Problem. *JCAP*, 1105:004, 2011.

[17] Edward Belbruno. On the regularizability of the big bang singularity. *Celestial Mechanics and Dynamical Astronomy*, 115(1):21–34, 2013.

[18] V.A. Belinsky, I.M. Khalatnikov, and E.M. Lifshitz. Oscillatory approach to a singular point in the relativistic cosmology. *Adv.Phys.*, 19:525–573, 1970.

[19] Dennis Bessada, William H. Kinney, Dejan Stojkovic, and John Wang. Tachyacoustic Cosmology: An Alternative to Inflation. *Phys.Rev.*, D81:043510, 2010.

[20] N.D. Birrell and P.C.W. Davies. *Quantum Fields in Curved Space*. Cambridge University Press, 1982.

[21] Martin Bojowald. Quantum Cosmology: Effective Theory. *Class.Quant.Grav.*, 29:213001, 2012.

[22] Arvind Borde, Alan H. Guth, and Alexander Vilenkin. Inflationary space-times are incomplete in past directions. *Phys.Rev.Lett.*, 90:151301, 2003.

[23] Robert H. Brandenberger. The Matter Bounce Alternative to Inflationary Cosmology. *arXiv:1206.4196*, 2012.

[24] Jean-Philippe Bruneton. On causality and superluminal behavior in classical field theories: Applications to k-essence theories and MOND-like theories of gravity. *Phys.Rev.*, D75:085013, 2007.

[25] Marco Bruni, George F.R. Ellis, and Peter K.S. Dunsby. Gauge invariant perturbations in a scalar field dominated universe. *Class.Quant.Grav.*, 9:921–946, 1992.

[26] Evgeny I. Buchbinder, Justin Khoury, and Burt A. Ovrut. New Ekpyrotic cosmology. *Phys.Rev.*, D76:123503, 2007.

[27] Yi-Fu Cai, Damien A. Easson, and Robert Brandenberger. Towards a Nonsingular Bouncing Cosmology. *JCAP*, 1208:020, 2012.

[28] Yi-Fu Cai, Taotao Qiu, Robert Brandenberger, Yun-Song Piao, and Xinmin Zhang. On Perturbations of Quintom Bounce. *JCAP*, 0803:013, 2008.

[29] Yi-Fu Cai, Taotao Qiu, Yun-Song Piao, Mingzhe Li, and Xinmin Zhang. Bouncing universe with quintom matter. *JHEP*, 0710:071, 2007.

[30] Sean M. Carroll. *Spacetime and Geometry: An Introduction to General Relativity*. Addison-Wesley, 2004.

[31] Xingang Chen, Min-xin Huang, Shamit Kachru, and Gary Shiu. Observational signatures and non-Gaussianities of general single field inflation. *JCAP*, 0701:002, 2007.

[32] Paolo Creminelli, Markus A. Luty, Alberto Nicolis, and Leonardo Senatore. Starting the Universe: Stable Violation of the Null Energy Condition and Non-standard Cosmologies. *JHEP*, 0612:080, 2006.

[33] Paolo Creminelli, Alberto Nicolis, and Matias Zaldarriaga. Perturbations in bouncing cosmologies: Dynamical attractor versus scale invariance. *Phys.Rev.*, D71:063505, 2005.

[34] Paolo Creminelli and Leonardo Senatore. A Smooth bouncing cosmology with scale invariant spectrum. *JCAP*, 0711:010, 2007.

[35] C. Deffayet, Gilles Esposito-Farese, and A. Vikman. Covariant Galileon. *Phys.Rev.*, D79:084003, 2009.

[36] Cedric Deffayet, Oriol Pujolas, Ignacy Sawicki, and Alexander Vikman. Imperfect Dark Energy from Kinetic Gravity Braiding. *JCAP*, 1010:026, 2010.

[37] Nathalie Deruelle and Viatcheslav F. Mukhanov. On matching conditions for cosmological perturbations. *Phys.Rev.*, D52:5549–5555, 1995.

[38] S. Dubovsky, T. Gregoire, A. Nicolis, and R. Rattazzi. Null energy condition and superluminal propagation. *JHEP*, 0603:025, 2006.

[39] Ruth Durrer and Filippo Vernizzi. Adiabatic perturbations in pre - big bang models: Matching conditions and scale invariance. *Phys.Rev.*, D66:083503, 2002.

[40] Damien A. Easson, Ignacy Sawicki, and Alexander Vikman. G-Bounce. *JCAP*, 1111:021, 2011.

[41] A. Einstein and W. de Sitter. On the Relation between the Expansion and the Mean Density of the Universe. *Proc.Nat.Acad.Sci.*, 18:213–214, 1932.

[42] Albert Einstein. Cosmological Considerations in the General Theory of Relativity. *Sitzungsber.Preuss.Akad.Wiss.Berlin (Math.Phys.)*, 1917:142–152, 1917.

[43] Albert Einstein. Zum Kosmologischen Problem der allgemeinen Relativitätstheorie. (German) [On the cosmological problem of the General Theory of Relativity]. *Ständiger Beobachter der Preussischen Akademie der Wissenschaften, Phys.-math. Klasse, Sitzungsberichte*, pages 235–237, 1931.

[44] George Ellis, Roy Maartens, and Malcolm A.H. MacCallum. Causality and the speed of sound. *Gen.Rel.Grav.*, 39:1651–1660, 2007.

[45] G.F.R. Ellis and M. Bruni. Covariant and gauge invariant approach to cosmological density fluctuations. *Phys.Rev.*, D40:1804–1818, 1989.

[46] Kari Enqvist and Martin S. Sloth. Adiabatic CMB perturbations in pre - big bang string cosmology. *Nucl.Phys.*, B626:395–409, 2002.

[47] Joel K. Erickson, Daniel H. Wesley, Paul J. Steinhardt, and Neil Turok. Kasner and mixmaster behavior in universes with equation of state $w \geq 1$. *Phys.Rev.*, D69:063514, 2004.

[48] Fabio Finelli and Robert Brandenberger. On the generation of a scale invariant spectrum of adiabatic fluctuations in cosmological models with a contracting phase. *Phys.Rev.*, D65:103522, 2002.

[49] Ben Freivogel. Making predictions in the multiverse. *Class.Quant.Grav.*, 28:204007, 2011.

[50] Ben Freivogel, Matthew Kleban, Maria Rodriguez Martinez, and Leonard Susskind. Observational consequences of a landscape. *JHEP*, 0603:039, 2006.

[51] A. Friedman. On the Curvature of space. *Z.Phys.*, 10:377–386, 1922.

[52] David Garfinkle. Harmonic coordinate method for simulating generic singularities. *Phys.Rev.*, D65:044029, 2002.

[53] David Garfinkle, Woei Chet Lim, Frans Pretorius, and Paul J. Steinhardt. Evolution to a smooth universe in an ekpyrotic contracting phase with $w > 1$. *Phys.Rev.*, D78:083537, 2008.

[54] M. Gasperini and G. Veneziano. Pre - big bang in string cosmology. *Astropart.Phys.*, 1:317–339, 1993.

[55] M. Gasperini and G. Veneziano. The Pre - big bang scenario in string cosmology. *Phys.Rept.*, 373:1–212, 2003.

[56] Ghazal Geshnizjani, William H. Kinney, and Azadeh Moradinezhad Dizgah. General conditions for scale-invariant perturbations in an expanding universe. *JCAP*, 1111:049, 2011.

[57] G.W. Gibbons and Neil Turok. The Measure Problem in Cosmology. *Phys.Rev.*, D77:063516, 2008.

[58] Dalia S. Goldwirth. On inhomogeneous initial conditions for inflation. *Phys.Rev.*, D43:3204–3213, 1991.

[59] Christopher Gordon, David Wands, Bruce A. Bassett, and Roy Maartens. Adiabatic and entropy perturbations from inflation. *Phys.Rev.*, D63:023506, 2001.

[60] Eric Gourgoulhon. Construction of initial data for 3+1 numerical relativity. *J.Phys.Conf.Ser.*, 91:012001, 2007.

[61] Eric Gourgoulhon. *3+1 Formalism in General Relativity: Bases of Numerical Relativity*. Springer, 2012.

[62] Alan H. Guth. The Inflationary Universe: A Possible Solution to the Horizon and Flatness Problems. *Phys.Rev.*, D23:347–356, 1981.

[63] Alan H. Guth. Eternal inflation and its implications. *J.Phys.*, A40:6811–6826, 2007.

[64] Alan H. Guth and S.Y. Pi. Fluctuations in the New Inflationary Universe. *Phys.Rev.Lett.*, 49:1110–1113, 1982.

[65] S.W. Hawking. Perturbations of an expanding universe. *Astrophys.J.*, 145:544–554, 1966.

[66] S.W. Hawking. The Development of Irregularities in a Single Bubble Inflationary Universe. *Phys.Lett.*, B115:295, 1982.

[67] S.W. Hawking and G.F.R. Ellis. *The Large Scale Structure of Space-Time*. Cambridge University Press, 1973.

[68] S.W. Hawking and R. Penrose. The Singularities of gravitational collapse and cosmology. *Proc.Roy.Soc.Lond.*, A314:529–548, 1970.

[69] G. Hinshaw et al. Nine-Year Wilkinson Microwave Anisotropy Probe (WMAP) Observations: Cosmological Parameter Results. *arXiv:1212.5226*, 2012.

[70] Stephen D.H. Hsu, Alejandro Jenkins, and Mark B. Wise. Gradient instability for w ¡ -1. *Phys.Lett.*, B597:270–274, 2004.

[71] Edwin Hubble. A relation between distance and radial velocity among extragalactic nebulae. *Proc.Nat.Acad.Sci.*, 15:168–173, 1929.

[72] Jai-chan Hwang and Ethan T. Vishniac. Gauge-invariant joining conditions for cosmological perturbations. *Astrophys.J.*, 382:363–368, 1991.

[73] Anna Ijjas, Paul J. Steinhardt, and Abraham Loeb. Inflationary paradigm in trouble after Planck2013. *Phys.Lett.*, B723:261–266, 2013.

[74] Shogo Inoue and Jun'ichi Yokoyama. Curvature perturbation at the local extremum of the inflaton's potential. *Phys.Lett.*, B524:15–20, 2002.

[75] W. Israel. Singular hypersurfaces and thin shells in general relativity. *Nuovo Cim.*, B44S10:1, 1966.

[76] Stanley L. Jaki. *Science and Creation: From Eternal Cycles to an Oscillating Universe*. Scottish Academic Press, 1986.

[77] Austin Joyce and Justin Khoury. Scale Invariance via a Phase of Slow Expansion. *Phys.Rev.*, D84:023508, 2011.

[78] Austin Joyce and Justin Khoury. Strong Coupling Problem with Time-Varying Sound Speed. *Phys.Rev.*, D84:083514, 2011.

[79] Justin Khoury and Godfrey E.J. Miller. Towards a Cosmological Dual to Inflation. *Phys.Rev.*, D84:023511, 2011.

[80] Justin Khoury, Burt A. Ovrut, Paul J. Steinhardt, and Neil Turok. The Ekpyrotic universe: Colliding branes and the origin of the hot big bang. *Phys.Rev.*, D64:123522, 2001.

[81] Justin Khoury and Federico Piazza. Rapidly-Varying Speed of Sound, Scale Invariance and Non-Gaussian Signatures. *JCAP*, 0907:026, 2009.

[82] Justin Khoury and Paul J. Steinhardt. Adiabatic Ekpyrosis: Scale-Invariant Curvature Perturbations from a Single Scalar Field in a Contracting Universe. *Phys.Rev.Lett.*, 104:091301, 2010.

[83] Justin Khoury and Paul J. Steinhardt. Generating Scale-Invariant Perturbations from Rapidly-Evolving Equation of State. *Phys.Rev.*, D83:123502, 2011.

[84] Justin Khoury, Paul J. Steinhardt, and Neil Turok. Inflation versus cyclic predictions for spectral tilt. *Phys.Rev.Lett.*, 91:161301, 2003.

[85] Justin Khoury, Paul J. Steinhardt, and Neil Turok. Designing cyclic universe models. *Phys.Rev.Lett.*, 92:031302, 2004.

[86] William H. Kinney. Horizon crossing and inflation with large eta. *Phys.Rev.*, D72:023515, 2005.

[87] Hideo Kodama and Misao Sasaki. Cosmological Perturbation Theory. *Prog.Theor.Phys.Suppl.*, 78:1–166, 1984.

[88] Kazuya Koyama and David Wands. Ekpyrotic collapse with multiple fields. *JCAP*, 0704:008, 2007.

[89] Helge Kragh. Continual fascination: The oscillating universe in modern cosmology. *Science in Context*, 22:587–612, 11 2009.

[90] Helge Kragh. *Higher Speculations: Grand Theories and Failed Revolutions in Physics and Cosmology*. Oxford University Press, 2011.

[91] D. Krotov, C. Rebbi, V.A. Rubakov, and V. Zakharov. Holes in the ghost condensate. *Phys.Rev.*, D71:045014, 2005.

[92] D. Langlois. Lectures on inflation and cosmological perturbations. *Lect.Notes Phys.*, 800:1–57, 2010.

[93] David Langlois and Sebastien Renaux-Petel. Perturbations in generalized multi-field inflation. *JCAP*, 0804:017, 2008.

[94] David Langlois and Filippo Vernizzi. Conserved non-linear quantities in cosmology. *Phys.Rev.*, D72:103501, 2005.

[95] David Langlois and Filippo Vernizzi. Nonlinear perturbations of cosmological scalar fields. *JCAP*, 0702:017, 2007.

[96] Louis Leblond and Sarah Shandera. Simple Bounds from the Perturbative Regime of Inflation. *JCAP*, 0808:007, 2008.

[97] Jean-Luc Lehners. Ekpyrotic and Cyclic Cosmology. *Phys.Rept.*, 465:223–263, 2008.

[98] Jean-Luc Lehners, Paul McFadden, Neil Turok, and Paul J. Steinhardt. Generating ekpyrotic curvature perturbations before the big bang. *Phys.Rev.*, D76:103501, 2007.

[99] Jean-Luc Lehners, Paul J. Steinhardt, and Neil Turok. The Return of the Phoenix Universe. *Int.J.Mod.Phys.*, D18:2231–2235, 2009.

[100] Georges Lemaitre. A homogeneous Universe of constant mass and growing radius accounting for the radial velocity of extragalactic nebulae. *Annales Soc.Sci.Brux.Ser.I Sci.Math.Astron.Phys.*, A47:49–59, 1927.

[101] E.M. Lifshitz and I.M. Khalatnikov. Investigations in relativistic cosmology. *Adv.Phys.*, 12:185–249, 1963.

[102] Chunshan Lin, Robert H. Brandenberger, and Laurence Levasseur Perreault. A Matter Bounce By Means of Ghost Condensation. *JCAP*, 1104:019, 2011.

[103] Lee Lindblom, Mark A. Scheel, Lawrence E. Kidder, Robert Owen, and Oliver Rinne. A New generalized harmonic evolution system. *Class.Quant.Grav.*, 23:S447–S462, 2006.

[104] Andrei D. Linde. A New Inflationary Universe Scenario: A Possible Solution of the Horizon, Flatness, Homogeneity, Isotropy and Primordial Monopole Problems. *Phys.Lett.*, B108:389–393, 1982.

[105] Andrei D. Linde. INITIAL CONDITIONS FOR INFLATION. *Phys.Lett.*, B162:281–286, 1985.

[106] David H. Lyth, Karim A. Malik, and Misao Sasaki. A General proof of the conservation of the curvature perturbation. *JCAP*, 0505:004, 2005.

[107] David H. Lyth and Yeinzon Rodriguez. The Inflationary prediction for primordial non-Gaussianity. *Phys.Rev.Lett.*, 95:121302, 2005.

[108] David H. Lyth and David Wands. Generating the curvature perturbation without an inflaton. *Phys.Lett.*, B524:5–14, 2002.

[109] Joao Magueijo. Speedy sound and cosmic structure. *Phys.Rev.Lett.*, 100:231302, 2008.

[110] Juan Martin Maldacena. Non-Gaussian features of primordial fluctuations in single field inflationary models. *JHEP*, 0305:013, 2003.

[111] Jerome Martin, Hayato Motohashi, and Teruaki Suyama. Ultra Slow-Roll Inflation and the non-Gaussianity Consistency Relation. *Phys.Rev.*, D87:023514, 2013.

[112] Charles W. Misner. Mixmaster universe. *Phys.Rev.Lett.*, 22:1071–1074, 1969.

[113] Charles W. Misner, K.S. Thorne, and J.A. Wheeler. *Gravitation*. Freeman, 1973.

[114] Viatcheslav F. Mukhanov, H.A. Feldman, and Robert H. Brandenberger. Theory of cosmological perturbations. Part 1. Classical perturbations. Part 2. Quantum theory of perturbations. Part 3. Extensions. *Phys.Rept.*, 215:203–333, 1992.

[115] Mohammad Hossein Namjoo, Hassan Firouzjahi, and Misao Sasaki. Violation of non-Gaussianity consistency relation in a single field inflationary model. *Europhys.Lett.*, 101:39001, 2013.

[116] Alberto Nicolis, Riccardo Rattazzi, and Enrico Trincherini. The Galileon as a local modification of gravity. *Phys.Rev.*, D79:064036, 2009.

[117] Roger Penrose. The basic ideas of conformal cyclic cosmology. *AIP Conf.Proc.*, 1446:233–243, 2010.

[118] Patrick Peter, Emanuel J.C. Pinho, and Nelson Pinto-Neto. A Non inflationary model with scale invariant cosmological perturbations. *Phys.Rev.*, D75:023516, 2007.

[119] Patrick Peter and Nelson Pinto-Neto. Primordial perturbations in a non singular bouncing universe model. *Phys.Rev.*, D66:063509, 2002.

[120] Yun-Song Piao. Seeding Primordial Perturbations During a Decelerated Expansion. *Phys.Rev.*, D75:063517, 2007.

[121] Yun-Song Piao. Adiabatic Spectra During Slowly Evolving. *Phys.Lett.*, B701:526–529, 2011.

[122] N. Pinto-Neto and J.C. Fabris. Quantum cosmology from the de Broglie-Bohm perspective. *Class.Quant.Grav.*, 30:143001, 2013.

[123] Frans Pretorius. Numerical relativity using a generalized harmonic decomposition. *Class.Quant.Grav.*, 22:425–452, 2005.

[124] Taotao Qiu, Jarah Evslin, Yi-Fu Cai, Mingzhe Li, and Xinmin Zhang. Bouncing Galileon Cosmologies. *JCAP*, 1110:036, 2011.

[125] G.I. Rigopoulos and E.P.S. Shellard. The separate universe approach and the evolution of nonlinear superhorizon cosmological perturbations. *Phys.Rev.*, D68:123518, 2003.

[126] W. Rindler. Visual horizons in world-models. *Gen.Rel.Grav.*, 34:133–153, 2002.

[127] D.S. Salopek and J.R. Bond. Nonlinear evolution of long wavelength metric fluctuations in inflationary models. *Phys.Rev.*, D42:3936–3962, 1990.

[128] Misao Sasaki and Ewan D. Stewart. A General analytic formula for the spectral index of the density perturbations produced during inflation. *Prog.Theor.Phys.*, 95:71–78, 1996.

[129] David Seery and James E. Lidsey. Primordial non-Gaussianities in single field inflation. *JCAP*, 0506:003, 2005.

[130] Alexei A. Starobinsky. Dynamics of Phase Transition in the New Inflationary Universe Scenario and Generation of Perturbations. *Phys.Lett.*, B117:175–178, 1982.

[131] Alexei A. Starobinsky. Multicomponent de Sitter (Inflationary) Stages and the Generation of Perturbations. *JETP Lett.*, 42:152–155, 1985.

[132] Paul J. Steinhardt and Neil Turok. Cosmic evolution in a cyclic universe. *Phys.Rev.*, D65:126003, 2002.

[133] Paul J. Steinhardt and Neil Turok. *Endless Universe: Beyond the Big Bang*. Broadway Books, 2007.

[134] Paul Joseph Steinhardt. NATURAL INFLATION. *in The Very Early Universe, edited by Gibbons, Hawking, and Siklos (Cambridge University Press, 1983)*, pages 251–266.

[135] P.J. Steinhardt and N. Turok. A cyclic model of the universe. *Science*, 296:1436–1439, 2002.

[136] Andrew J. Tolley, Neil Turok, and Paul J. Steinhardt. Cosmological perturbations in a big crunch / big bang space-time. *Phys.Rev.*, D69:106005, 2004.

[137] R.C. Tolman. *Relativity, Thermodynamics, and Cosmology*. Dover books on physics. DOVER PUBN Incorporated, 1987.

[138] Richard C. Tolman. On the theoretical requirements for a periodic behaviour of the universe. *Phys. Rev.*, 38:1758–1771, Nov 1931.

[139] N.C. Tsamis and Richard P. Woodard. Improved estimates of cosmological perturbations. *Phys.Rev.*, D69:084005, 2004.

[140] Alexander Vilenkin. The Birth of Inflationary Universes. *Phys.Rev.*, D27:2848, 1983.

[141] David Wands. Duality invariance of cosmological perturbation spectra. *Phys.Rev.*, D60:023507, 1999.

[142] David Wands, Karim A. Malik, David H. Lyth, and Andrew R. Liddle. A New approach to the evolution of cosmological perturbations on large scales. *Phys.Rev.*, D62:043527, 2000.

[143] Steven Weinberg. *Gravitation and Cosmology*. John Wiley & Sons, 1972.

[144] BingKan Xue. The four fixed points of scale invariant single field cosmological models. *JCAP*, 1210:054, 2012.

[145] BingKan Xue and Edward Belbruno. Regularization of the big bang singularity in the ekpyrotic scenario. 2013.

[146] BingKan Xue, David Garfinkle, Frans Pretorius, and Paul J. Steinhardt. Nonperturbative analysis of cosmological perturbations in a nonsingular bounce. 2013.

[147] BingKan Xue and Paul J. Steinhardt. Unstable growth of curvature perturbation in non-singular bouncing cosmologies. *Phys.Rev.Lett.*, 105:261301, 2010.

[148] BingKan Xue and Paul J. Steinhardt. Evolution of curvature and anisotropy near a nonsingular bounce. *Phys.Rev.*, D84:083520, 2011.

[149] Jr. York, James W. Gravitational degrees of freedom and the initial-value problem. *Phys.Rev.Lett.*, 26:1656–1658, 1971.